Development of a robust NADPH regeneration system for enzyme-catalysed synthesis



Tianze Zhu

Jesus College

Trinity Term 2019

A Thesis submitted to the Board of the Faculty of Physical Sciences, for the degree of

Doctor of Philosophy, University of Oxford

Abstract

Development of a robust NADPH regeneration system for enzyme-catalysed synthesis

Tianze Zhu

Jesus College, University of Oxford

A Thesis submitted for the degree of Doctor of Philosophy, Trinity Term 2019

Cofactor NADH and NADPH regeneration is a crucial topic in the area of biotechnology, as many redox enzymes such as alcohol dehydrogenases, imine reductases, and P450 monooxgenases require cofactor to deliver their redox equivalent. However, as the cofactors are particularly expensive, it is not economically feasible to supply stoichiometric cofactor when these enzymes are used in chemical synthesis. Instead a number of cofactor regeneration systems have been developed to tackle this problem. Traditional regeneration systems for the reduced cofactors suffers from drawbacks, as most of them require carbon based sacrificial co-substrate reductant and produce a by-product which is likely to be burnt as waste, hindering the downstream product purification process and lowering atom economy. The Vincent group has successfully developed a modular H_2 driven NADH regeneration system, in which hydrogenase, NAD^+-reductase, and the cofactor dependent enzyme are co-immobilised on carbon particles. However, several enzymes require exclusively NADPH as their redox equivalent. Therefore, this thesis focuses on the development of a new H_2 driven NADPH regeneration system and coupling it with NADPH dependent enzymes to demonstrate its feasibility. To achieve a new NADPH regeneration, the NAD^+-reductase was targeted and several variants are produced. The most robust variant was then selected to be incorporated into the new NADPH regeneration system. The new

system was then coupled with NADPH dependent enzymes imine reductase and P450 monooxygenase to demonstrate its feasibility. Another approach to achieve NADPH regeneration is to introduce a fourth enzyme, soluble transhydrogenase into the NADH regeneration system. The soluble transhyrogenase was produced, isolated and partly characterised, but not yet incorporated to the regeneration system. This thesis also discusses the further development for a more robust and easy accessible H_2 driven NADH regeneration system, as the NAD^+-reductase currently used is not easy to produce, and not very efficient. A promising candidate to replace the NAD^+-reductase currently used in the system is the NAD^+-reductase part of respiratory Complex I subunit NuoF. The subunit was successfully isolated and characterised. However, it suffers from stability problem. Therefore, it is not ideal yet to be incorporated into the NADH regeneration system.

Acknowledgements

At first, I would like to express my sincere gratefulness to my supervisor Professor Kylie Vincent, without whom it was not possible for me to accomplish my D.Phil. Professor Vincent kindly provide me with a position at her research group, and provide tuition, supervision, and many other support for me during my studying here as a D.Phil student. Also I was very grateful for Professor Vincent to give me to support and encouragement during my darkest time when I was seriously ill and have to suspend my study in Oxford for a long period of time.

I would like to thank Dr. Holly Reeve, who carefully provided me with useful guidance and instructions for my project and experiments, especially helping me set up electrochemical equipment and carry out protein film electrochemistry in the glovebox. Also Dr. Reeve's daily hilarious amusement made not only me but also the whole group always immersed in a harmonious and happy environment.

My special thanks go to all other Vincent group current and past members. The four years of working together with them left me with a much cherished experience of my life. I still remembered each time my group member celebrate my birthday for me. And every Christmas we had a special Christmas dinner when every one of us brought our own dishes and shared with each other. I also want to thank my college, Jesus College and my benefactor Mr. Richard Paice for supporting my study and research financially.

At last, I would like to thank my wife, my parents, grandmother, and all my family members to give me support and encouragement. Also I am very grateful for having lots of lovely friends here in Oxford, who also gave me help and made my life extremely colourful here.

Collaborations and assistance

Much of the work done in this thesis involved collaborations, either external or internal. The Lenz Group and in particular Dr Lars Lauterbach and Ms Katja Karstens provided *Ralstonia eutropha* soluble hydrogenase samples and the variants of this enzyme (Chapter Three). They also carried out biochemical solution assays to characterise the kinetic properties of these enzyme samples. The Wong Group provided the NADPH dependent enzyme $P450_{BM3}$ monooxygenase. Dr. Holly Reeve in the Vincent Group and Dr. Koji Urata in the Wong group carried out experiments to demonstrate the feasibility of the new NADPH regeneration system was feasible by coupling it with P450 monooxygenase.

The imine reductase catalysis experiments were carried out under the guidance of Dr. Jack Rowbotham. Mr. Jake Nicholson also provided help with the NMR experiments on deuterated 2-methylpyrroline.

Dr. Miguel Ramirez provided general guidance and supervision for the molecular biological experiments. Ms. Claudia Orbegozo Rubio constructed the pETnuoEFG plasmid, and carried out the preliminary protein expression and characterisation experiments.

Abbreviations

ADH	Alcohol dehydrogenase
BP2000	Black pearls 2000
CE	Counter electrode
CV	Cyclic voltammogram
DMSO	Dimethyl sulfoxide
E	Electrode potential
e	electron
E. coli	*Escherichia coli*
ee	Enantiomeric excess
F	Faraday's constant
FAD	Flavin adenine dinucleotide
FDH	Formate dehydrogenase
FMN	Flavin mononucleotide
FNR	Ferredoxin $NADP^+$ reductase
GDH	Glucose dehydrogenase
GlyDH	Glycerol dehydrogenase
HoxHYFU	Soluble hydrogenase whole enzyme
HoxFU	NAD^+ reducing subunits of the soluble hydrogenase
HPLC	High performance liquid chromatography
Hyd-1	*Escherichia coli* Hydrogenase 1
Hyd-2	*Escherichia coli* Hydrogenase 2
K_I	Inhibition constant
K_M	Michaelis constant
LDH	Lactate dehydrogenase
MBH	Membrane bound hydrogenase
N_A	Avogadro constant
NAD^+	Nicotinamide adenine dinucleotide (oxidised)
NADH	Nicotinamide adenine dinucleotide hydride (reduced)
$NADP^+$	Nicotinamide adenine dinucleotide phosphate (oxidised)
NADPH	Nicotinamide adenine dinucleotide phosphate hydride (reduced)
P450	Cytochrome P450
PFE	Protein film electrochemistry
PGE	Pyrolytic graphite edge
Q	Charge
R	*The gas constant*
R.e	*Ralstonia eutropha* H16
RDE	Rotating disk electrode
RE	Reference electrode
RH	Regulatory hydrogenase
SCE	saturated calomel electrode
SH	Soluble hydrogenase
SHE	Standard hydrogen electrode
TOF	Turnover frequency
TN	Turnover number
TTN	Total turnover number

WE	Working electrode
WT	Wild type
ε	Extinction coefficient

Contents

1 Chapter One: Introduction 13

1.1 Biocatalysis 14

1.1.1 Advantages of biocatalysis over conventional organic synthesis 18

1.1.2 Usage of biocatalysis in the pharmaceutical industry 19

1.2 Cofactors 21

1.2.1 NADH and NADPH 22

1.2.2 FMN and iron-sulfur clusters 24

1.3 NAD(P)H-dependent enzymes 26

1.4 Cofactor regeneration system 27

1.5 Carbon particle based modular H_2-driven NAD(P)H recycling 32

1.5.1 Structure of the modular H_2-driven NADH regeneration system 32

1.5.2 Advantages of the modular H_2-driven NADH regeneration system 33

1.6 Further development of current H_2-driven NADH regeneration system 34

1.6.1 Development of more robust NADH regeneration system 35

1.6.2 Extend the current system to NADPH recycling 36

1.7 Enzymes involved in development of an NAD(P)H regeneration system in this study 36

1.7.1 Hydrogenase 2 from *E. coli* 36

1.7.2 Soluble Hydrogenase HoxHYFU from *Ralstonia eutropha* 38

1.7.3 Soluble Hydrogenase variants 40

1.7.4 NuoF subunit of respiratory Complex I 42

1.7.5 NuoF variants 47

1.7.6 Soluble transhydrogenase 49

1.8 Applications of a H_2-driven regeneration system 52

1.9 Structure of this thesis 52

2 Chapter Two: Methods and Theory 54

2.1 Gene cloning and protein expression 55

2.1.1 Protein expression and purification of *nuo* genes 55

2.1.2 Protein expression and purification of *udhA* gene 56

2.2 Protein film electrochemistry 57

2.2.1 Equipment and set-ups 59
2.2.2 Cyclic Voltammetry 62
2.2.3 Chronoamperometry 63
2.2.4 Experiment considerations 65
2.3 Other equipment 65
2.3.1 Ultraviolet-visible spectrometry 66
2.3.2 Gas chromatography 67
2.3.3 High-Performance Liquid Chromatography 68
2.4 Enzyme kinetics 69
2.4.1 Affinity constant 71
2.4.2 Inhibition constant 75
2.4.3 The relationship between enzyme kinetics and electrochemistry 79
3 Chapter Three Electrochemical characterisation of *Ralstonia eutropha* soluble hydrogenase and its variants 81
3.1 Electro-catalytic behaviour assays 83
3.1.1 Cyclic voltammetry of NAD^+ reduction 84
3.2 Cyclic voltammetry of $NADP^+$ reduction 87
3.3 Determination of affinity constants for the variants 93
3.3.1 Affinity constants for NAD^+ reduction 94
3.3.2 Affinity constants for NADH oxidation 102
3.3.3 Affinity constants for $NADP^+$ reduction 103
3.3.4 Affinity constants for NADPH oxidation 106
3.4 Determination of inhibition constants 107
3.4.1 Inhibition constant for NADH inhibition of NAD^+ reduction for the variant $HoxF^{D467S}$ 109
3.5 Electrochemical characterisation of *R.e* SH variant $HoxF^{E341A, S342R}$ 111
3.5.1 The electro-catalytic behaviour of $HoxF^{E341A, S342R}$ 111
3.5.2 The affinity constant of $HoxF^{E341A, S342R}$ 112
3.6 Summary of kinetic data for $NADP^+$ reductase variants 113
3.7 The Comparison of biochemical determined affinity constants and electrochemical determined affinity constants 115
4 Chapter Four: Demonstration of NADPH recycling coupled to NADPH dependent enzymes 116

4.1 Introduction to imine reductases 117
4.1.1 NADPH recycling system coupled with imine reductase 119
4.1.2 Substrate deuteration catalysed by IRED ..... **Error! Bookmark not defined.**
4.2 Introduction to Cytochrome P450 mono-oxygenase 126
4.2.1 An NADPH regeneration system coupled with a P450 BM3 variant 127
5 Chapter Five: Expression and application of soluble transhydrogenase UdhA 131
5.1 Introduction 132
5.2 Molecular cloning of soluble transhydrogenase UdhA 133
5.3 Expression and isolation of UdhA 134
5.4 Cofactor stability 135
5.4.1 Single cofactor stability 136
5.4.2 Cofactor mixture stability 138
5.5 Transhydrogenation using UdhA 139
5.6 Artificial transhydrogenation 141
5.7 Summary 145
6 Chapter Six: Other approaches for NADH and NADPH regeneration 147
6.1 NAD^+-reductase domain of respiratory Complex I from *E. coli* 149
6.1.1 Molecular cloning of NuoF and NuoEF from *E. coli* Complex I 149
6.2 Expression and purification of NuoF subunit of Complex I 150
6.2.1 Characterization of NuoF subunit 153
6.2.2 Discussion of NuoF 157
6.3 Overexpression, purification, and characterisation of NuoEF subcomplex 159
6.4 Overexpression, purification, and characterisation of NuoEFG subcomplex 161
6.5 Discussion of NAD^+ reducing subunits from Complex I 164
7 Chapter Seven: Conclusions and outlook 165
7.1 Conclusions 166
7.1.1 Development towards a more robust NADH regeneration system 166
7.1.2 Development towards NADPH regeneration system 167
7.2 Outlook 169
8 Appendix 171
9 Bibliography 176

Chapter One: Introduction

1.1 Biocatalysis

Biocatalysis, or biotransformation, describes the processes that use enzymes or other biological catalysts (whole cells, cell extracts, etc.) to perform chemical reactions[1]. In recent years, biocatalysis has gained more and more attention in both academia and industry[2,3]. Biocatalysis as a technique has been exploited by humans for thousands of years. In ancient times, our ancestors had already acquired the biocatalysis techniques to produce beer, cheese, and other kinds of food and beverages[4]. For instance, Sumerians utilised brewer's yeast to brew alcoholic beverages over 6000 years ago in Mesopotamia[5]. It was not until the 19th century that scientists realised that it was the components in living organisms which catalyse the chemical transformations we desire[6]. In 1814, Kirchhoff found that a glutinous component of wheat was able to convert starch to sugar[7]. Back then, people utilised extracts from plants or microorganisms to catalyse chemical reactions. In the early 20th century, scientists found out that it was one specific kind of protein, namely enzymes, responsible for the chemical conversions, and people began to use purified enzymes to catalyse reactions. There are in general six major categories of enzymes by their functions[8] (**Table 1-1**). Currently in biotechnological industry, hydrolases are most commonly used, and they account for 60% of total industrial biotransformations. Oxidoreductases come second, accounting for 20% of total biotransformations. The enzymes used in this thesis are mostly oxidoreductases.

Table 1-1: Summary of the six major categories of enzymes, example enzymes of each category, and their functions.

Type of enzyme	Examples	Function
Hydrolases	Lipase, protease, esterase, nitrilase, phosphatase	Hydrolysis reaction using H_2O
Oxidoreductases	Dehydrogenase, oxygenase, oxidase, peroxidase	Oxidation and reduction
Transferases	Transaminase, transaldolase	Transfer a group from one molecule to another
Lyases	Decarboxylase, aldehyde lyase	Nonhydrolytic bond cleavage
Isomerases	Xylose isomerase, phosphopentomutase	Intramolecular rearrangement
Ligases	DNA ligase, aminoacyl tRNA synthetase	Bond formations

For industrial and academic utilization, biocatalysts can be divided into three categories by the nature of the catalyst: isolated enzyme, cell extract, and whole cell catalyst[9] (**Figure 1-1A**). Isolated enzymes are purified target enzymes containing no other proteins or cell components, straightforward to be used to catalyse specific reactions, and often produce very pure products compared with other types of biocatalyst[10]. Nevertheless, isolated enzymes are difficult to purify and handle, greatly increasing the costs for producing and storing the biocatalyst. Therefore, in practical applications, cell extracts containing over-expressed target enzymes are preferred due to their low cost. Cell extracts used in biocatalysis can be divided into two types of biocatalyst: cell lysates, and crude purified enzymes. Cell lysates are direct lysed cells containing all the cellular components including target enzymes. Crude purified enzymes are crudely purified cell lysate. Cell extracts may have lower activity per unit weight, as extracts contain many other proteins and cell components, and useful enzymes are usually less than 50% of the weight. Other cell components in the cell may hamper or inhibit the desired enzymatic reactions[10]. Other enzymes in the extracts may also lead to side reactions and by-products, making it hard and costly for the downstream processing and purification. Recently, whole cell catalysis is also

gaining more and more attention, especially when a desired product molecule requires a series of complicated enzymatic cascade reactions. A lot of molecules, particularly active pharmaceutical ingredients (APIs) or drug precursors involve very complicated biosynthesis pathways, requiring a group of enzymes to be produced[11]. In this kind of circumstance, the entire target metabolic biosynthesis pathway is cloned into a host cell and expressed, and the entire host cell is used as catalyst to effect the reactions[12]. The whole cell catalysed production of biofuels[13,14] also takes advantage of the cell's native metabolic pathways, supplemented with heterologously expressed enzymes from other species[9]. However, whole cell catalysis also suffers from side reactions and by-products from other enzymes and components of the host cell. Some of the substrates or the products are not membrane permeable, diminishing the conversion rate, or requiring breaking of the cells to harvest the products[15]. The toxicity of the substrates, the solvent, or the products to the cell also decreases the efficiency of whole cell catalysis[16].

Biocatalysts can also be divided into two categories by the form of the catalyst: immobilised biocatalyst, and non-immobilised biocatalyst[17] (**Figure 1-1B**). Immobilised enzymes overcome some of the limitations of the catalysts described above. Immobilisation often makes enzymes more stable and able to be reused, by preventing enzyme denaturation caused by organic solvent or extreme conditions such as high temperature and extreme pH. Immobilisation also makes it more efficient for enzyme cascade reactions where multiple enzymes are immobilised together to carry out a series of reactions, because the intermediates do not need to diffuse into the bulk solution before they are used by the next enzyme. Immobilised biocatalysts can be further divided into three categories by the methods of immobilisation: binding to a support, entrapment and cross-linking. Biocatalysts can bind to a physical support via covalent bonds, ionic bonds, or van der Waals interactions. Entrapment is the inclusion of an enzyme in a polymer network, such as polyacrylamide,

silica sol–gel, or a membrane structure. Cross-linking means that enzymes are linked to each other to form carrierless macro-particles. In this study, most biocatalysts are isolated enzymes immobilised non-covalently on carbon based particles.

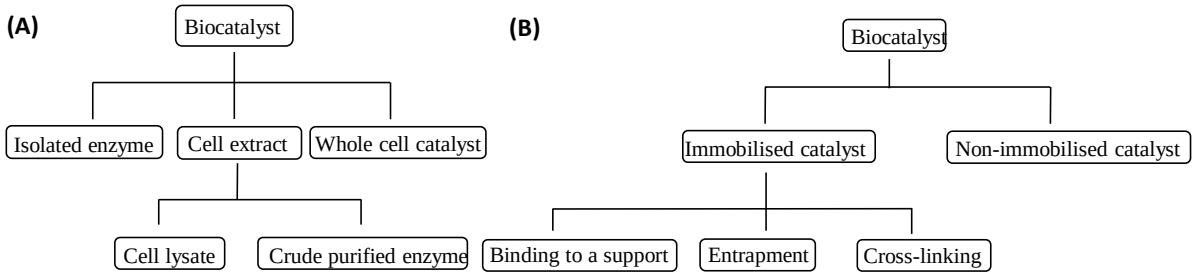


Figure 1-1 The classification of biocatalysts by the nature of the catalysts (A), or by the form of the catalysts (B).

Generally speaking, enzymes and other biological components are less stable compared with conventional chemical catalysts, especially in harsh conditions like extreme temperature or pH, organic solvent or high concentration of substrates or products which are usually organic compounds. In real chemical synthesis applications, enzymes usually do not act on their native substrates, so the activity of enzymes for the desired reactions may also be low. In recent years, as molecular biology techniques have developed, directed evolution has been applied in biocatalysis to overcome these limitations[18]. Directed evolution involves iterative cycles of random amino acid changes as well as rational designed mutagenesis in a protein, followed by selection or screening of the resulting libraries of variants to target a number of enzymatic characteristics, including activity, substrate specificity, thermal stability, tolerance for organic solvent and extreme conditions, as well as chiral selectivity[19].

Despite these limitations, enzymatic catalysis has its advantages over conventional organic synthesis approaches, making it useful and sometimes even irreplaceable in some areas especially in the pharmaceutical industry.

1.1.1 Advantages of biocatalysis over conventional organic synthesis

Biocatalysis has a number of advantages over traditional organic synthesis approaches. Enzymatic catalysis is more environmentally friendly, and requires no precious metal[20]. In conventional organic synthesis, reduction or oxidation reactions often require complicated catalysts which may contain a transition metal or a precious metal centre and several large complex ligands. For example, alcohol dehydrogenase 105 provided by Johnson Matthey catalyses the reduction of acetophenone to (*S*)-1-phenylethanol with over 99% *ee*, under ambient temperature and in an aqueous phase. While for the conventional approaches to stereo-selective hydrogenation, one popular option is to use Noyori's second generation catalyst, ruthenium-[(S)-PPhos $RuCl_2$ (S)-DAIPEN] complex[21,22], a ruthenium centre and complicated chiral ligands, which is difficult to synthesise[23–25] (**Figure 1-2**).

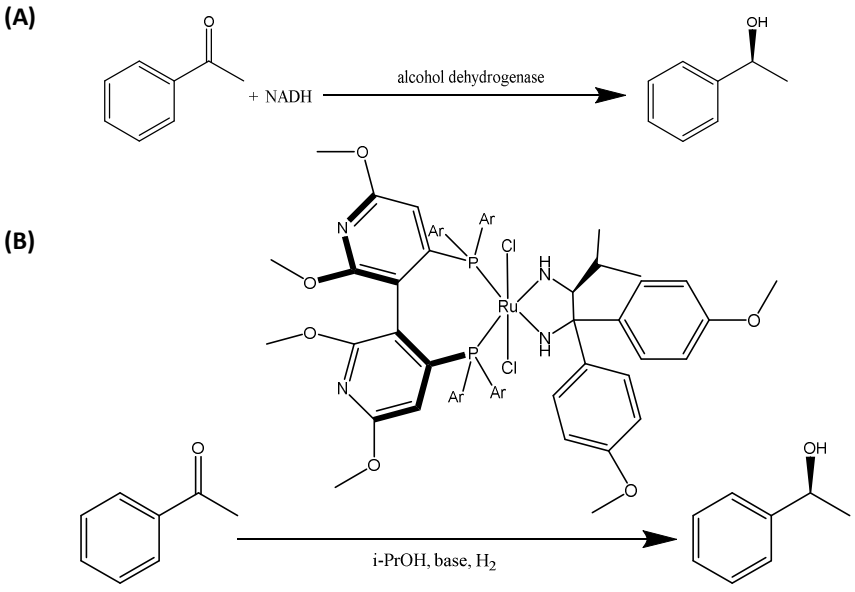


Figure 1-2: The reduction of acetophenone to *S*-phenylethanol. Alcohol dehydrogenase uses NADH as redox equivalent to carry out the reaction in Bis-Tris buffer (50mM, pH 6.0) at room temperature. In traditional organic synthesis approaches, one possible way is to use the second generation of Noyori's catalyst, (*S*)-PPhos $RuCl_2$ (*S*)-DAIPEN complex with a Ruthenium centre and several chiral ligands, in organic solvent isopropanol and strong base.

Organic approaches usually require organic solvents, and may need strong acid or base to facilitate the reactions. All of these are potentially hazardous to the environment. Biocatalysis, on the other hand, adopts a greener approach[26]. The catalysts are biological

materials expressed in living organisms, harmless to the environment. The reaction conditions for biocatalysis are often much milder: ambient temperature, neutral pH, around atmospheric pressure, and in aqueous phase. In this way, biocatalysis is not only more environmentally friendly, but energy efficient as well[27]. As environmental factors and carbon emission become a growing concern to the public, biocatalysis becomes more and more attractive to industry[28]. Moreover, enzymatic catalysis is highly stereo- and regio-selective compared to conventional methods, making it especially useful in the pharmaceutical industry, where most of the active compounds are chiral molecules. Enzymes can also distinguish the same functional groups in different positions of a complex molecule and specifically target the desired group, while conventional synthesis has to adopt multiple protection and de-protection steps to achieve chemo- or regio- selectivity.

Currently, conventional chemical methods are still used for producing bulk chemicals. However, enzymatic catalysis has been adopted by a variety of industries. Even in the bulk and fine chemical industry, there are already biocatalysis approaches to compete with the traditional organic synthesis approaches. For example, nitrile hydratase is applied to produce acrylamide, an important bulk commodity chemical. In the food industry, a lot of hydrolases are used for hydrolysis of biological macromolecules like starches, celluloses, and proteins. Biocatalysis gains most attention in the pharmaceutical industry. A number of pharmaceutical companies have already used enzymes or genetically engineered bacteria to produce novel antibiotics and other drugs. Most pharmaceutical companies are also creating enzyme libraries and biocatalysis is also widely used on R&D scale.

1.1.2 Usage of biocatalysis in the pharmaceutical industry

Pharmaceutical substances are mostly large complex organic molecules with multiple chiral centres, a large proportion of which are biological molecules or their derivatives[29]. This

means biocatalysis is greatly advantageous over conventional approaches for pharmaceutical compounds[11,30]. For example, Ajikumar and co-workers reported whole cell biosynthesis of the taxol precursor taxadiene[31], which is an anti-cancer compound first found from plant *Taxus brevifolia* Pacific yew tree, by genetically engineered *E. coli* cells (**Figure 1-3A)**. They took advantage of an *E. coli* native upstream methylerythritol-phosphate (MEP) pathway and reconstructed a heterologous downstream terpenoid–forming pathway. Another example of successful practical application of biocatalysis in the pharmaceutical industry is the enzymatic production of the anti-diabetic drug molecule sitagliptin developed by Merck (**Figure 1-3B**)[32]. Engineered *R*-selective ω-transaminase from *Arthrobacter* sp. is applied for the asymmetric amination of pro-sitagliptin ketone to form sitagliptin. As discussed before, pro-sitagliptin ketone has two carbonyl groups which are hard to selectively target using conventional methods, and it is also hard for the conventional methods to convert the pro-chiral ketone to a chiral product, but the engineered ω-transaminase can target the desired ketone group and make the desired product with high efficiency.

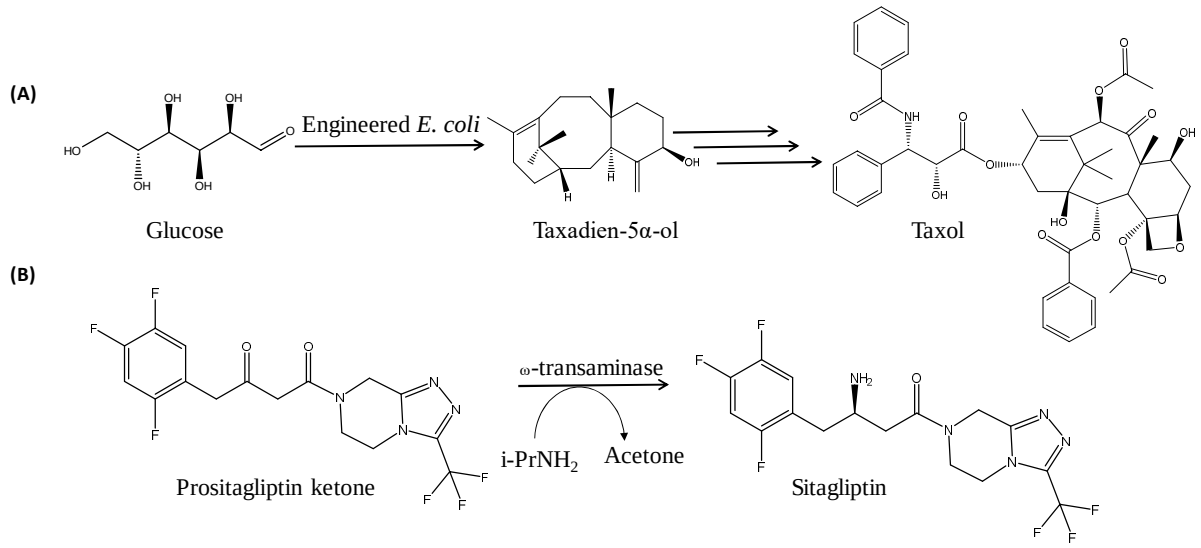


Figure 1-3: Examples of biocatalysis application in the pharmaceutical industry. A Synthetic biology technique is applied to genetically engineer *E. coli* metabolic pathway to allow it to produce taxadien-5α-ol, the precursor of anti-cancer drug taxol (A). Engineered ω-transaminase is used to convert prositagliptin ketone to antidiabetic drug sitagliptin (B).

There are other examples of successful applications of biocatalysis in the pharmaceutical industry, including biosynthesis of boceprevir[33], a clinical drug for chronic hepatitis C infections[34], developed by Merck, and multi-enzyme processing of hydroxynitrile[35], a key intermediate for atorvastatin[36], developed by Pfizer.

It has become common for pharmaceutical companies to use biocatalysis approaches to produce drug molecules. For large and complex molecules that require multiple steps to synthesise, a combined approach with both biotransformation and organic synthesis is usually adopted to keep the cost of the procedure as low as possible.

1.2 Cofactors

A lot of enzymatic reactions require the addition of cofactors. Cofactors are therefore very important in industrial biocatalysis. A cofactor, by definition, is a non-protein chemical compound that is required for the biological activities of protein. They are very important in biocatalysis, as most of the oxidoreductases used in this area require cofactors, which are crucial for the functionality of enzymes. Cofactors are either inorganic ions, such as Fe^{2+}, Mg^{2+}, Mn^{2+}, Zn^{2+}, iron-sulfur clusters, or complex organic or metallo-organic molecules called coenzymes[37]. Coenzymes are transient carriers of specific functional groups, most of which are derived from vitamins, organic nutrients required in small quantities in our diet. A cofactor very tightly or even covalently bound to the enzyme is called a prosthetic group[38]. Nicotinamide adenine dinucleotide (NAD), nicotinamide adenine dinucleotide phosphate (NADP), flavin mononucleotide (FMN), and flavin adenine dinucleotide (FAD) are cofactors that undergo reversible oxidation and reduction in a variety of electron-transfer reactions in living organisms. NAD and NADP are abundant and move freely in cells, while

FMN and FAD are usually prosthetic groups bound to enzymes. A number of cofactors are involved in this study, and they will be discussed in detail below.

1.2.1 NADH and NADPH

Nicotinamide adenine dinucleotide hydride (NADH) and Nicotinamide adenine dinucleotide phosphate hydride (NADPH) are composed of two nucleotides joined through their phosphate groups by a phosphoanhydride bond. Both cofactors undergo reversible redox reactions of the nicotinamide ring. In this reaction, NAD^+ or $NADP^+$ accepts one one proton and two electrons to form NADH or NADPH. Reduction of $NAD(P)^+$ converts the pyridinium ring of the nicotinamide group to a dihydronicotinamide (**Figure 1-4**).

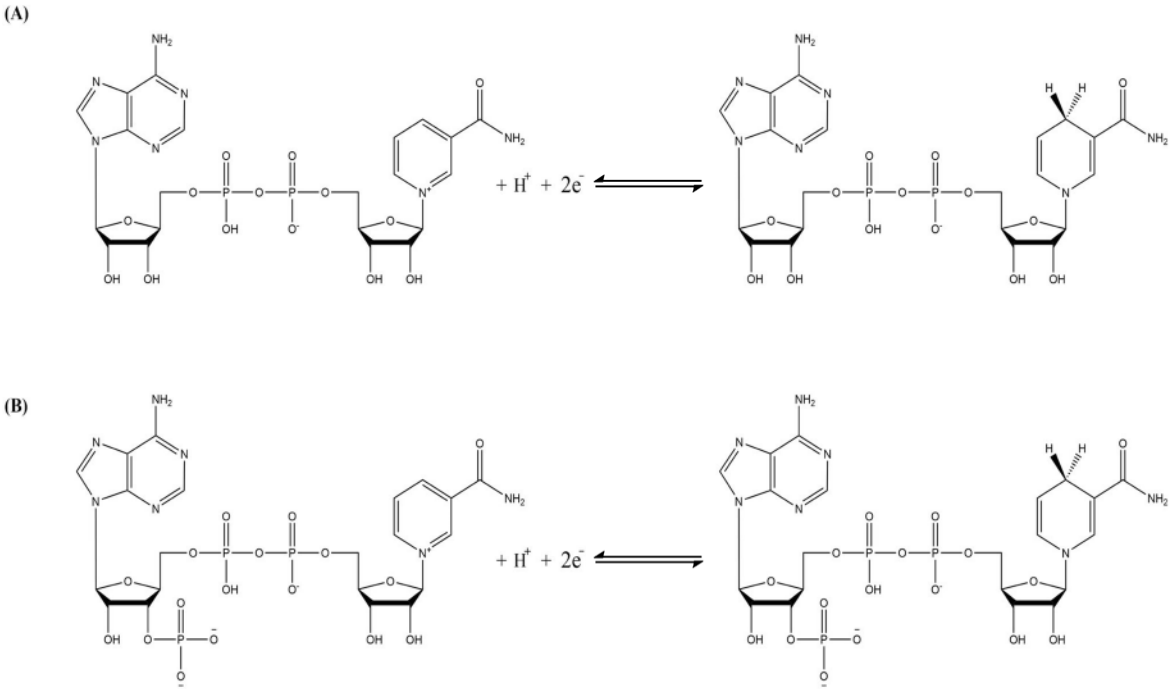


Figure 1-4: The structure of NAD^+ and its reduction to NADH by acquiring one proton and two electrons (A). The structure of $NADP^+$ has an additional phosphate group compared with NAD^+. $NADP^+$ also reduces to NADPH when acquiring one proton and two electrons (B).

NADH and NADPH are both key reducing equivalents and energy conversion intermediates in living organisms, but they are involved in different roles. The total concentration of NAD^+ and NADH in most cells is 10^{-5} M, while the total concentration of $NADP^+$ and NADPH is

10^{-6} M. Normally the ratio of NAD^+ to NADH is high, favouring reduction of NAD^+ to NADH[37]. NADPH is present at a higher concentration than $NADP^+$, favouring oxidation of NADPH to $NADP^+$. Although a few enzymes can use both NAD and NADP, most of the enzymes in living organisms have a strong preference for one over another. NADH is commonly involved in catabolic pathways, for example, glycolysis, where glucose is converted into pyruvate and ATP is produced. Then during the next step of glycolysis, the citric acid cycle also leads to abundant NADH production. NAD(H) is also involved in other catabolic pathways, such as fatty acid catabolism and amino acid degradation. Most importantly, NAD(H) is involved in oxidative phosphorylation when NADH is oxidised to NAD^+ and the reductive force is used to synthesise ATP in the respiration chain. This step generates most of the energy cells require, so it is crucial for living organisms to survive.

NADPH on the other hand, is involved in anabolism, most importantly photophosphorylation. In the light reaction of photophosphorylation, H_2O driven by light splits to O_2 and reduces $NADP^+$ to NADPH, while in the dark reaction NADPH is oxidised back to $NADP^+$ for carbon-assimilation where CO_2 converts to carbohydrates. NADP(H) is also involved synthesis of in lipids, amino acids, and other small molecules. Finally, NADP(H) is involved in some minor side patways of catabolism, for example, in glucose 6-phosphate metabolism and the pentose phosphate pathway of glucose oxidation, where NADPH is involved to convert glucose 6-phosphate to ribose 5-phosphate, used as building blocks for nucleotides, coenzymes, DNA and RNA.

NAD(H) and NADP(H) are crucial for industrial redox biocatalysis, as most of the oxidoreductases used in chemical industries are NAD(P)H-dependent enzymes that require $NAD(P)^+$ or NAD(P)H as their redox equivalent. For example, the reductions of ketones to alcohols catalysed by dehydrogenases requires either NADH or NADPH as redox equivalent. Co-factors are expensive chemicals, the prices for these cofactors are: NAD^+

£83/g, NADH £89/g, $NADP^+$ £263/g, and NADPH £1249/g (Sigma Aldrich, 10/10/2019), so stoichiometric addition of cofactors makes this type of biocatalysis economically impractical. In this context, a number of cofactor regeneration systems have been developed.

1.2.2 FMN and iron-sulfur clusters

Flavin mononucleotide (FMN) is another important cofactor involved in this thesis. It has three forms: oxidised form (FMN), semi-oxidised form (FMNH), and reduced form ($FMNH_2$) (**Figure 1-5**). It is bound non-covalently to a number of oxidoreductases as a prosthetic group, and such enzymes are called flavoproteins[39,40]. The majority of proteins involved in this study are flavoproteins. The NAD^+ reductases used in this work include the variants for $NADP^+$ reduction and the relevant subunits of complex I are flavoproteins which use FMN to accumulate the proton and two electrons needed to transfer a hydride to $NAD(P)^+$. The transhydrogenase, UdhA, is also a flavoprotein which uses FMN to mediate the transfer of a hydride from NADH to $NADP^+$ or NADPH to NAD^+. In these enzymes FMN works together with NAD(P)H to transfer electrons: free NADH binds with FMN in the enzyme and transfer electrons to FMN to form $FMNH_2$, while NADH is oxidised to NAD^+. The reduced FMN either passes electrons to downstream electron receptors or directly reduces a substrate. On the other hand, a reduced FMN can also pass its electrons to NAD^+ and reduces the latter to NADH.

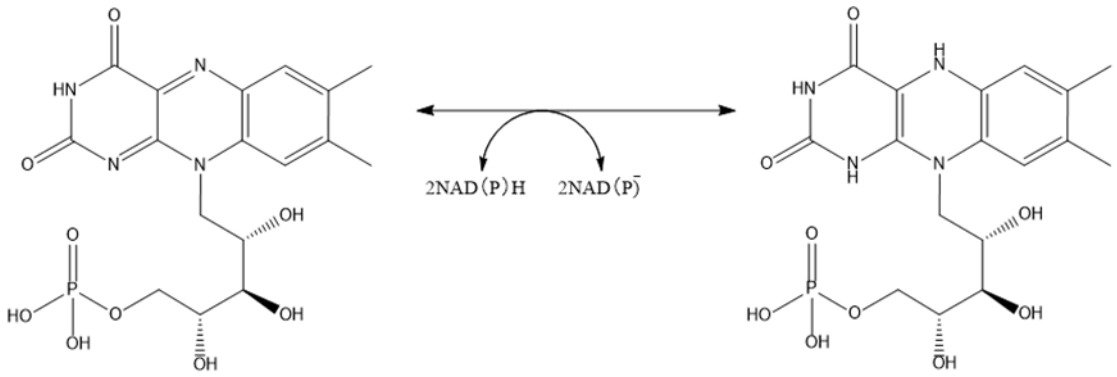


Figure 1-5: The structure of flavin mononucleotide (FMN), and its reduced form $FMNH_2$. The conversion of FMN to $FMNH_2$ is mediated by the electron transfer from the nicotinamide cofactors.

Iron-sulfur (FeS) clusters are another important cofactor in this thesis (**Figure 1-6**). A lot of enzymes involved in this study contain FeS clusters, including hydrogenase, and Complex I. FeS clusters are ensembles of iron and sulphide centres[41–46]. Proteins containing FeS clusters are called iron-sulfur proteins. FeS clusters have crucial biological roles in living organisms. They are used as electron transfer relays within proteins. Commonly, there are three major FeS clusters, the most simple [2Fe-2S] clusters that contain two iron and two sulfur centres, the cubic [4Fe-4S] clusters that contain four iron and four sulfur centres, and the [3Fe-4S] clusters which have one iron centre missing compared with the [4Fe-4S] clusters. There are also some unusual FeS clusters like [8Fe-8S] clusters and [7Fe-8S] clusters in nitrogenases, and the [4Fe-3S] cluster in *E. coli* hydrogenase Hyd-1. FeS clusters are normally co-ordinated within the proteins by the cysteine residues covalently bound with the iron atoms of the clusters.

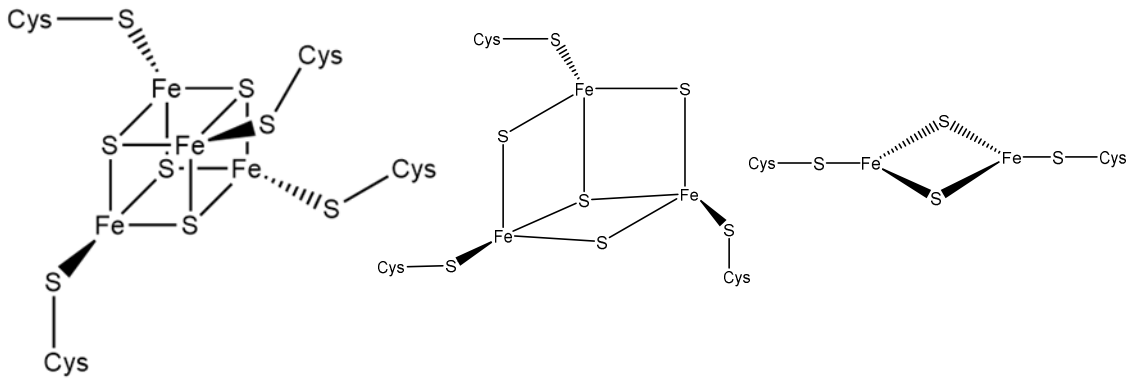


Figure 1-6: The structure of iron-sulfur clusters, the cubic [4Fe-4S] cluster, the [3Fe-4S] cluster, and the quadrangular [2Fe-2S] cluster. They are all incorporated into their host proteins by the cysteine residues from the protein sequence binding with iron atom of the clusters.

1.3 NAD(P)H-dependent enzymes

A great proportion of enzymes used in industrial chemical synthesis are NAD(P)H-dependent enzymes (**Figure 1-7**). For example, P450 monooxygenases use O_2 and NAD(P)H to insert an O atom to the C-H bond of an organic substrate to form an alcoholic group, and produce $NAD(P)^+$ and H_2O[47]. This reaction is very useful in organic synthesis as it selectively activates a non-activated C-H bond, which is very hard to achieve using conventional methods[48]. P450 monooxygenases are currently used in fine chemical industries to produce perfume compounds and a variety of other different chemical compounds[49,50]. They are also used in the pharmaceutical industry to produce drug metabolites, as the first step of the majority of drugs undergoing metabolism in human bodies is oxidation by P450 monooxygenase[51,52].

A lot of genetically engineered commercial alcohol dehydrogenases, like alcohol dehydrogenase 105 from Johnson Matthey catalyse the reverse reduction of pro-chiral ketones to chiral alcohols with high selectivity. These type of alcohol dehydrogenases require NAD(P)H as their redox equivalents to reduce the substrates[53–55]. Imine reductases (IREDs) are promising catalysts for the synthesis of optically pure secondary cyclic amines,

whose various physiological activities are explored and have huge potential for application in pharmaceutical industry[54,56–58]. Most IREDs require NADPH as redox equivalent[59,60]. Other examples of NAD(P)H-dependent enzymes include alkene-reductases that target reduction of pro-chiral C=C double bonds[61–65], glucose dehydrogenases which reversibly convert between glucose and glucono-1,5-lactone[66,67], and lactate dehydrogenases which reversibly convert between lactate and pyruvate[68,69]. All of these enzymes are very useful in variety of industries, and they all natively require a stoichiometric amount of NAD(P)H as redox equivalent. As discussed above, in many cases, the cofactors added are more expensive than the products, making the overall biotransformation process economically not viable.

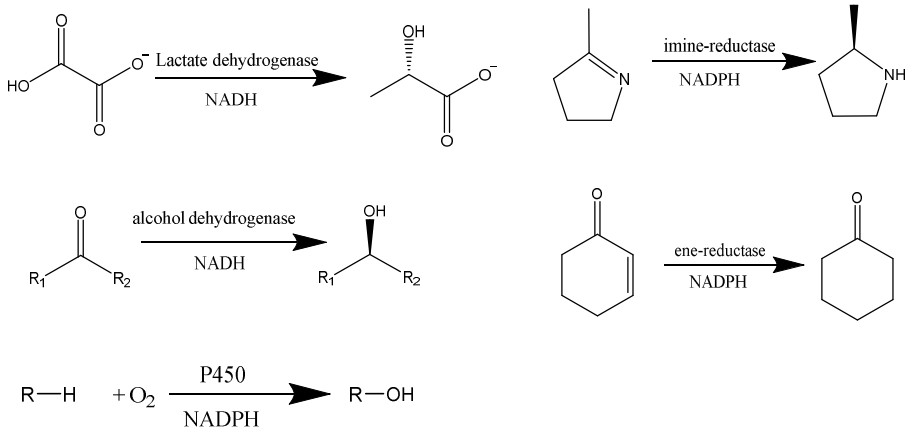


Figure 1-7: Examples of cofactor-dependent enzymes and the reactions they catalyse. Lactate dehydrogenases catalyse the reduction of lactate to pyruvate using NADH. Alcohol dehydrogenases catalyse the reduction of ketones to alcohols using NADH. Imine-reductases (IREDs) catalyse the reduction of imines to amines using NADPH. Alkene-reductases catalyse the reduction of alkene to alkane using NADPH. P450 monooxygenases catalyse the insertion of a hydroxyl group into a C-H bond by using O_2 and NADPH.

1.4 Cofactor regeneration system

To avoid using stoichiometric amounts of cofactors in enzymatic redox reactions, a cofactor regeneration system is coupled with these reactions[70–73]. A cofactor regeneration system utilises a sacrificial substrate to enzymatically recycle the consumed cofactor, and produce a byproduct. Thus, only a catalytic amount of cofactors is required, together with stoichiometric or an excess amount of sacrificial substrate. This produces enough reduced

cofactor for the reaction to proceed. There are a variety of cofactor regeneration systems that recycle different cofactors, such as NADH, NADPH, ATP, and sugar nucleotides[74–76]. This study focuses on recycling nicotinamide cofactors, namely NADH and NADPH. Sacrificial substrates are mostly carbon based simple molecules such as glucose[77], glucose-6-phosphate[66], glycerol[78], formate[79], isopropanol[2], which are much cheaper than cofactors, so the cost is greatly diminished, making the reactions economically viable. Traditionally, nicotinamide cofactor regeneration has used three approaches: a substrate-coupled system, an enzyme-coupled system, and a dual-enzyme hydrogen-borrowing cascade system[80] (**Figure 1-8**).

The substrate-coupled nicotinamide cofactor regeneration system is an elegant and simple approach that makes use of only one enzyme to couple both cofactor regeneration and product transformation. In this approach, alcohol dehydrogenases (ADHs) are commonly used, as a majority of commercially useful reactions are reductions of ketones, which can be achieved by ADHs. However, the sacrificial substrates need to be applied in large excess to drive the reaction in the desired direction. Thus, the sacrificial substrate, often a ketone, is regarded as a co-solvent. This leads to a number of disadvantages. First, some enzymes are not organic solvent tolerant, thus limiting the application of this method. Second, the large amount of remaining sacrificial substrate and co-product can make the downstream purification process more costly.

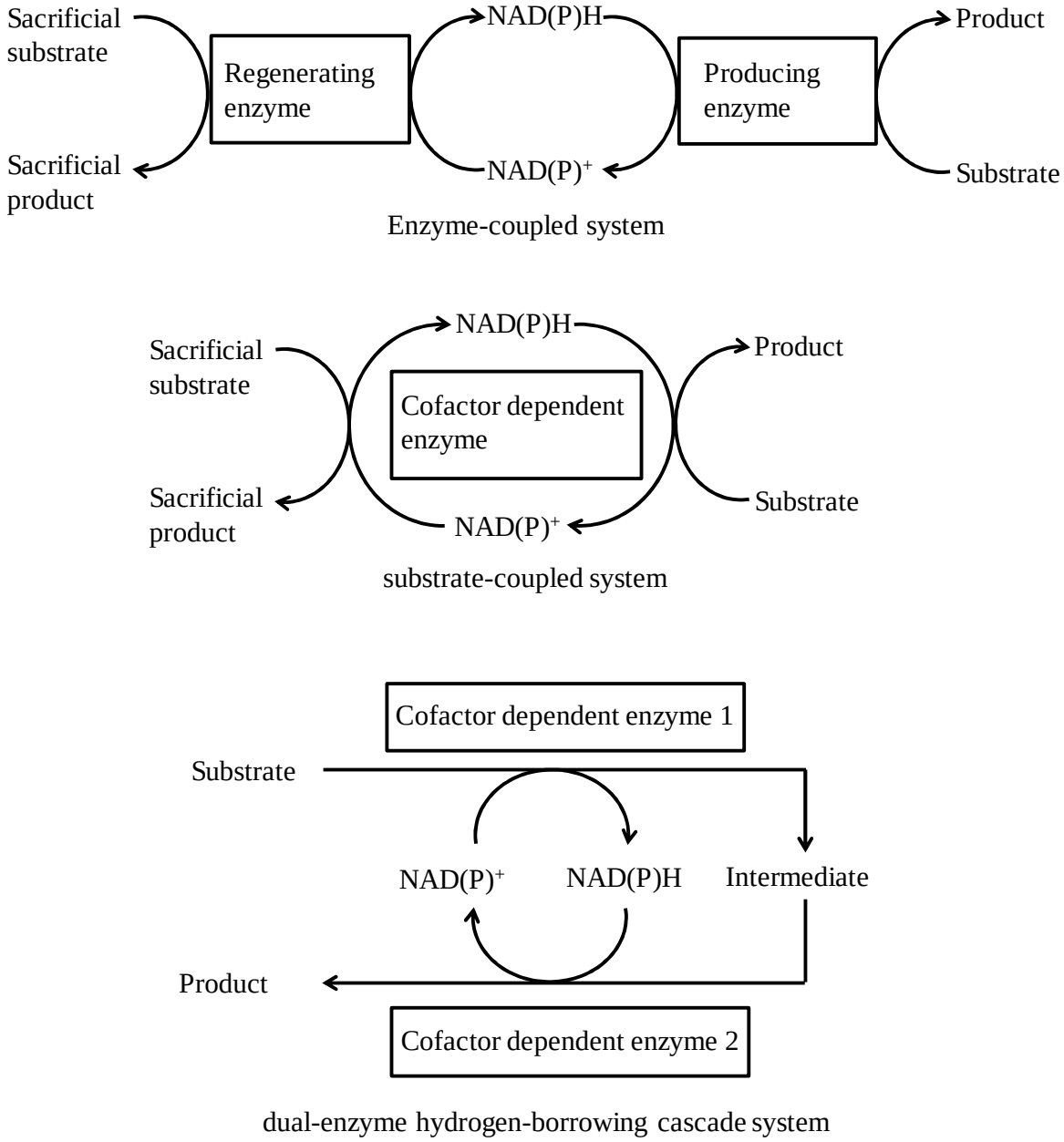


Figure 1-8: The enzyme-coupled cofactor regeneration system contains two enzymes, one is responsible for regenerating cofactors from a sacrificial substrate, while the other enzyme is responsible for using the regenerated cofactors to catalyse the desires reactions. The substrate-coupled system requires only one enzyme to regenerate cofactors and produce product simultaneously. The dual-enzyme hydrogen-borrowing cascade system uses two enzymes to catalyse the substrate to product via a two-step oxidation/reduction process.

The second approach is the enzyme-coupled system. This approach requires more than one enzyme to work together. Normally, one enzyme regenerates the cofactor by transforming the sacrificial substrate into co-product, while the other enzyme utilises the regenerated cofactor to catalyse the desired reaction.

The third approach is the dual-enzyme hydrogen-borrowing cascade system, which is a relatively new concept in the cofactor regeneration field[81]. In this system, one cofactor regeneration enzyme first catalyses the transformation of substrate into an intermediate, while the other enzyme catalyses the conversion of intermediate into the final product. This system requires one reaction consuming NAD(P)H and producing $NAD(P)^+$, and the other reaction consuming $NAD(P)^+$ and producing NAD(P), so that the two reactions couple together making the overall system self-sufficient in cofactor. However, this system applies to very few biosynthesis processes, such as the amination of alcohols.

There are a variety of enzymes that serve as cofactor regenerators. Formate dehydrogenase (FDH) has commonly been used in cofactor regeneration systems[79]. FDH essentially irreversibly catalyses the oxidation of formate ions to carbon dioxide, coupled to the reduction of NAD^+ to NADH. FDH is efficient in regenerating the cofactor NADH as the co-product carbon dioxide evaporates from the system and thus drives the reaction in the desired direction. FDH can couple with most NADH-dependent enzymes, so greatly broadens the scope of biocatalysis applications. However, FDH also has a number of disadvantages. The co-product carbon dioxide is a potential greenhouse gas, and in solution will acidify the system, and decrease the activity of the enzymes. Moreover, FDH has a lower specific activity compared with other cofactor regenerating enzymes.

Glucose dehydrogenase is the most commonly used cofactor regenerating enzyme. It has high activity and stability[36,82]. However, it produces carbon waste gluconic acid, which increases the acidity of the system and might lead to lowering of enzyme activity.

Glucose-6-phosphate dehydrogenase (G-6-PDH) is another candidate for a cofactor regeneration system[66]. G-6-PDH is used to recycle both NADH and NADPH. However, using G-6-PDH as a regeneration system also suffers from high cost of sacrificial substrate and low activity.

Phosphite dehydrogenase (PtxD) is an enzyme that catalyses the oxidation of phosphite to phosphate, while reducing NAD^+ to NADH[83,84]. PtxD also uses $NADP^+$/NADPH as its substrate, but with less activity[85]. Phosphite is a cheap substrate, and the system can use phosphite buffer, so during the reaction, it just simply converts it into phosphate buffer. But PtxD also suffers from low activity compared with other cofactor recycling enzymes.

The general disadvantage among all of these methods above is the production of co-product from sacrificial substrate. This is not atom efficient, and makes biocatalysis less environmentally-friendly. Moreover, the removal of undesired co-product is often costly and tedious, making it less likely to be commercialised.

In recent years, H_2 is emerging as a carbon-neutral, clean, and renewable alternative energy, as traditional energy sources, predominantly fossil based gasoline, are due to be exhausted in the foreseeable future, and produce greenhouse gas. As global warming becomes a more and more pressing issue, H_2 gains a lot of attention both in academia and industry. For example, Toyota Mirai launched the first hydrogen fuel cell vehicle to be sold commercially in 2015. On the other hand, to tackle the general problems of cofactor regeneration system which use carbon based sacrificial substrates, H_2 is also a promising alternative solution.

A typical H_2-driven cofactor regeneration system was proposed by Rita Mertens and co-workers, using hydrogenase I from *Pyrococcus furiosus*[86]. Hydrogenase I oxidases H_2 and reduces $NADP^+$ to NADPH[87,88]. In this way, the sacrificial substrate is H_2, and the whole process produces no co-product, making it 100% atom efficient. The remaining H_2 is easy to separate from the system. However, hydrogenase I is a hyperthermophilic enzyme which reaches its maximum activity at 80 °C. This is not a suitable condition for many other enzymes. Also, hydrogenase I is not very stable and is oxygen-sensitive, further limiting the application of this method[89]. Oliver Lenz and co-workers produced a whole cell H_2-driven NADH regeneration system by genetically engineering *Pseudomonas putida* KT2440[90]. The

necessary gene clusters for the soluble NAD^+-reducing hydrogenase (SH) from *Ralstonia eutropha*, together with cytochrome CYP153A and its accessory enzymes were transferred into the host cell *Pseudomonas putida* KT2440, and correspondingly induced expressed. Therefore the whole cell H_2 driven NADH regeneration system was able to produce 1-octanol from *n*-octane when bubbling with H_2. The whole cell approach addresses the problem of hydrogenase instability as proteins are generally much more stable in their native state within the cellular environment. However, the whole cell approach still suffers from a number of limitations such as by-products and substrate permeability.

1.5 Carbon particle based modular H_2-driven NAD(P)H recycling

Based on the previous success and limitations of H_2 driven cofactor regeneration systems, the Vincent research group has developed an alternative carbon particle based modular H_2-driven cofactor regeneration system (**Figure 1-9**).

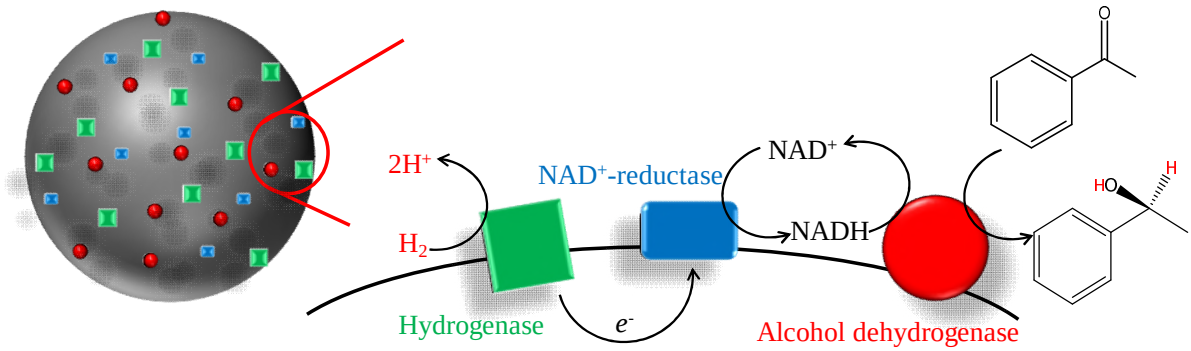


Figure 1-9: The schematic model on the left shows the modular H_2-driven NADH regeneration system developed by the Vincent group. Three enzymes are co-immobilised on a carbon particle (the grey sphere), including hydrogenase (green square), NAD^+-reductase (blue rectangle), and the third co-factor dependent enzyme, in this case alcohol dehydrogenase (red ball). The detailed illustration on the right shows how the system works. The hydrogenase splits H_2 to two protons and two electrons, and the electrons transfer to NAD^+-reductase via carbon particle. NAD^+-reductase utilises the electrons and the protons to reduce NAD^+ to NADH, and the latter supplies alcohol dehydrogenase to reduce the substrate to the product.

1.5.1 Structure of the modular H_2-driven NADH regeneration system

This modular H_2-driven NADH regeneration system contains a carbon particle, and three enzymes, Hydrogenase 2 (Hyd-2) from *Escherichia coli*, the NAD^+-reductase part of soluble

hydrogenase from *Ralstonia eutropha* H16, and a third catalytic enzyme co-immobilised on the particle[91]. The carbon particle currently used in recent published work is the commercially available Black Pearl® 2000 (BP2000) from Cabot. Moreover, a third catalytic enzyme that requires cofactor as its co-substrate is also immobilised on the carbon particle together with the other two enzymes. The modularity of this system also allows the three enzymes to be changed easily to work in different reactions and conditions. During the reaction, hydrogenase splits H_2 into two protons and two electrons. The electrons transduce via the carbon support from the hydrogenase to the NAD^+-reductase, and the latter takes up the electrons and the protons to reduce NAD^+ to NADH. The regenerated NADH supplies the third enzyme to carry out the desired NADH-dependent redox reaction. The three enzymes are co-immobilised on the carbon support non-covalently. The carbon particle BP2000 is essential in this system, as it not only acts as a support for enzyme immobilisation, but also as a conductor for electron transfer between the hydrogenase and the NAD^+-reductase. Other conventional materials for enzyme immobilisation such as polysaccharides, silicas, and zeolites are not suitable for this system as they are insulators, prohibiting the electron transduction between the hydrogenase and the NAD^+-reductase.

1.5.2 Advantages of the modular H_2-driven NADH regeneration system

This novel regeneration system features a number of advantages[92,93]. First, H_2 is a cheap sacrificial substrate and is easily separated from the reaction system, making the downstream purification process much easier than using a traditional carbon based sacrificial substrate. Second, the two protons from H_2 are both incorporated in the reduced product, so this novel system achieves 100% atom efficiency. Third, the modularity of this system means that each enzyme and even the carbon particle can be changed easily to fine tune for different requirements and conditions. For example, the third enzyme, the cofactor-dependent

enzyme, can be changed to a variety of enzymes ranging from alcohol dehydrogenase, imine-reductase, alkene-reductase to P450 monooxygenase to achieve different reactions. If the reaction needs to be carried out at high temperature, the NAD^+ reductase can be changed to the NAD^+ reductase from *Thermus thermophilus* which favours higher temperature. Last, the co-immobilised system has higher activity compared with free enzyme in the solution[94]. This system has been coupled with alcohol dehydrogenase (ADH) to reduce acetophenone to *(S)*-phenylethanol. The result showed that when ADH bind to the carbon support together with other enzymes, the conversion rate was higher than when ADH moved freely in the solution. This suggests that the enzymatic particle system creates a high local concentration of cofactors, leading to an increase in efficiency of the co-factor dependent enzyme. A possible explanation of high local concentration of co-factor is due to substrate channelling, a phenomenon existing in living organisms in which the intermediate product of one enzyme goes directly to another enzyme without going to the bulk solution. Substrate channelling is, in an enzymatic cascade reaction, the passing of one intermediate from one enzyme directly to another enzyme without release into the bulk solution. Substrate channelling is frequently seen in metabolism of living organisms, as it makes metabolic pathway more rapid and efficient.

1.6 Further development of current H_2-driven NADH regeneration system

The major part of this thesis will discuss the further development of this H_2-driven NADH regeneration system. There are two directions of focus for further development: towards a more robust NADH regeneration system, or towards a new NADPH regeneration system. Thanks to the modular nature of the system, the enzymes can easily be changed in the system to improve or alter its functions. Currently the NAD^+-reductase is a bottle neck for the

system due to its low activity and complexity to produce. A more robust and easy to produce alternative NAD^+-reductase is required to improve this system. On the other hand, a lot of enzymes require NADPH rather than NADH as redox equivalent, and NADPH is much more expensive than NADH. It is crucial to develop a new NADPH regeneration system based on the current NADH system.

1.6.1 Development of more robust NADH regeneration system

The current H_2-driven NADH regeneration has its limitations hindering its further and broader application. The NAD^+-reductase of the system we currently used is NAD^+-reductase moiety of *Ralstonia eutropha* soluble hydrogenase, HoxFU[95]. Although HoxFU has proven effective and robust on the NADH regeneration system, it has its own drawbacks. HoxFU is a relatively large enzyme that requires two different subunits HoxF and HoxU to bind together non-covalently. HoxFU contains four iron-sulfur clusters for transferring electrons. This makes the fermentation process complicated and energetically costly to the host cells. Moreover, HoxFU is currently produced from its native host *Ralstonia eutropha*, rather than the well-established *E. coli* expression system, further increasing the cost of enzyme preparation. The nuoF subunit of respiratory Complex I from *E. coli* is a promising candidate to replace the currently used HoxFU in the NADH regeneration system. NuoF located at the front of the L shaped Complex I, and is responsible for the oxidising of NADH to NAD^+ and passing the electrons to the rest of subunits. NuoF shares great similarity with HoxF, with over 50% amino acid sequence identity. NuoF catalyses the same reaction as HoxFU: the conversion between NAD^+ and NADH. NuoF is smaller and has fewer FeS clusters than HoxFU, making it easier to produce, and more likely to have higher activity. One of the goals of this project involves expression and isolation of NuoF, and incorporating it into the NADH regeneration system to make it more robust and economical to produce.

1.6.2 Transforming the current system to NADPH recycling

Another aspect of the project involves re-design of the current NADH recycling system to a new NADPH recycling system. As mentioned previously, a variety of enzymes use exclusively NADPH as their redox equivalent, especially some commercialised enzymes used broadly in the fine chemical industries. NADPH is also much more expensive than NADH, so it is urgent to develop a reliable NADPH regeneration system. The approach adopted to develop a NADPH system is using mutagenesis of the current NAD^+-reductase of the NADH system to allow it to accommodate NADP(H) as its substrate. This part of project is in collaboration with Dr Oliver Lenz from the Technical University Berlin.

1.7 Enzymes involved in development of an NAD(P)H regeneration system in this study

As mentioned above, there are a number of enzymes involved in the H_2-driven NADH regeneration system, as discussed in detail below. The hydrogenase used is Hyd-2 from *E. coli*, and the NAD^+-reductase used currently is a sub-complex of the soluble hydrogenase from *Ralstonia eutropha*. To further develop this system, some new enzyme moities are studied in this thesis, including NADH:ubiquinone oxidoreductase (complex I) from *E. coli*, and soluble transhydrogenase from *E. coli*. The NAD(P)H-dependent enzymes are usually well-developed commercial enzymes provided by our collaborators, so they will not be discussed in detail here.

1.7.1 Hydrogenase 2 from *E. coli*

The hydrogenase used in the NADH regeneration system for splitting H_2 is hydrogenase 2 from *E. coli*. Hydrogenases catalyse the reversible oxidation of hydrogen gas to two protons and two electrons. They play an important role in the energy metabolism of a broad range

of microorganisms. Hydrogenase can also be divided into three classes by their catalytic centre, Fe centre, FeFe centre, and NiFe centre (**Figure 1-10**)[96–98]. [FeFe]-hydrogenases are O_2-sensitive hydrogenase and inhibited by the presence of Oxygen. [FeFe]-hydrogenases have a di-iron catalytic centre, and are mainly involved in H_2 evolution. [Fe]-hydrogenases have only one iron in their catalytic centre for H_2 oxidation. [NiFe] hydrogenases are the most robust hydrogenases harbouring a heterodinuclear Ni-Fe-active site, and are usually engaged in H_2 uptake. [NiFe] hydrogenases are also the most interesting hydrogenases for applications, as the majority of them are O_2-tolerant hydrogenases that remain active in the presence of oxygen, making them potentially useful in industries.

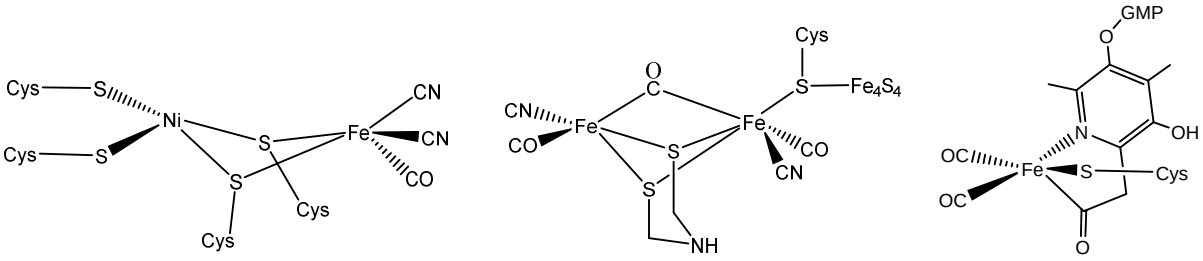


Figure 1-10 The structures of NiFe (left), FeFe (middle), and Fe (right) catalytic centre of hydrogenase

All the four hydrogenases from *E. coli* are NiFe hydrogenases, namely hydrogenase 1(Hyd-1), hydrogenase 2 (Hyd-2), hydrogenase 3 (Hyd-3), and hydrogenase 4 (Hyd-4). Hyd-3 is a cytoplasmic enzyme involved in the formate hydrogen lyase system, probably responsible for H_2 evolution under fermentative conditions. Hyd-1 and Hyd-2 are both membrane-bound periplasmic enzymes responsible for H_2-uptake. Hyd-1 is encoded by a six-gene operon *hya*ABCDEF located at 22' on the chromosome. *hya*A codes for the [FeS] cluster-containing *β*-subunit, *hya*B codes for the *α*-subunit, which binds the [NiFe] active site, and *hya*C codes for an integral membrane *b*-type cytochrome (**Figure 1-11**). The rest of the genes *hya*DEF are accessory genes for the assembly of the protein complex. Similarly, Hyd-2 is encoded by the *hyb*OABCDEFG operon, with *hyb*OABC genes coding for the structural components

and *hyb*DEFG are accessory genes for protein assembly. Hyd-1 is O_2-tolerant, while Hyd-2 is an O_2-sensitive enzyme that is reversibly inhibited by O_2. Electrochemical experiments revealed that Hyd-1 requires overpotential at around 0.05 V for H_2 oxidation, while Hyd-2 catalyses H_2 oxidation at the thermodynamic potential[99]. Therefore, Hyd-2 works more effectively when coupled with NAD^+-reductase than Hyd-1, but Hyd-1 works better in an aerobic environment. Hyd-1 and Hyd-2 are both used in this H_2-driven NADH regeneration system. In this project, Hyd-2 is used, and a similar structure and arrangement of redox centres to Hyd-1.

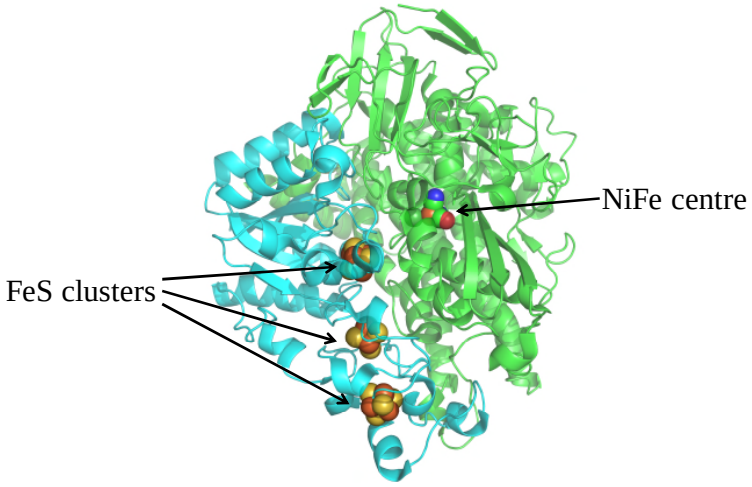


Figure 1-11 Crystal structure of *Hya*A (blue) and *Hya*B (green) subunits of hydrogenase 1 from *E.coli*. *Hya*A subunit contains the three FeS clusters in charge of electron transfer. *Hya*B subunit contains the NiFe centre for H_2 splitting.

1.7.2 Soluble Hydrogenase HoxHYFU from *Ralstonia eutropha*

Some bacteria in nature can utilise H_2 gas as their sole energy source, called Knallgas bacteria. They have developed mechanisms to sense, regulate, and oxidise H_2 gas to protons and extract and store energy, and *Ralstonia eutropha* is one of such. Hydrogenases play an important role throughout this process.

Soluble hydrogenase from *Ralstonia eutropha* H16 (*R.e* SH) is used as NAD^+-reductase in the NADH regeneration system. *R.e* SH contains two moieties, a hydrogenase part that splits H_2 and a NAD^+-reductase part that reduces NAD^+. The whole enzyme has attracted attention

for cofactor recycling because it is O_2 tolerant[98]. However, soluble hydrogenase is not very stable and robust, as the two moieties can dissociate or lose their FMN cofactor. The electron transfer from H_2 to NAD^+ relied on a series of iron-sulfur clusters buried in the enzyme. It is worth noting here that in this project, although *R.e* SH is a hydrogenase, it is not used as a hydrogenase in the NADH regeneration system. Instead *R.e* SH is just used as the NAD^+-reductase in the NADH regeneration system. A single mutation was introduced to block the NiFe active site of *Re* SH to inhibit its H_2 oxidation activity[100].

R.e SH consists of six different subunits, namely HoxHYFUI_2 (**Figure 1-12**). When isolated from the cell extract, the two HoxI subunits are often missing, and only HoxHYFU subunit are obtained, so *R.e* SH is also called HoxHYFU. HoxH and HoxY form the hydrogenase moiety, which splits hydrogenase gas to protons and electrons. A NiFe centre in the HoxH subunit is the catalytic centre responsible for H_2 splitting. HoxF and HoxU form the NAD^+ reduction moiety, which utilizes the electrons and protons to reduce NAD^+ to NADH. In this study, HoxFU is also called NAD^+-reductase. The catalytic centre of this moiety is an FMN in HoxF, which receives the electrons and passes them to NAD^+. Two HoxI subunits loosely bind with HoxF subunits and their function has not been fully understood. There are also a series of Iron-Sulfur (FeS) clusters buried in these Hox subunits, which function as electron transfer relays, so that the electrons from H_2 split in the HoxH subunit can transfer a relatively long distance to FMN in HoxF subunit. There is no FeS cluster in HoxH, but there is one [4Fe-4S] cluster in the neighbouring HoxY subunit, enabling the electrons acquired from H_2 oxidation to transfer from the NiFe centre to this FeS cluster. HoxU contains three FeS clusters, one [2Fe-2S] cluster and two [4Fe-4S] clusters, and this subunit mainly functions as an electronic wire to transport the electrons from the hydrogenase moiety to the NAD^+-reductase moiety. There is one [4Fe-4S] cluster adjacent to the FMN of subunit HoxF linking HoxF to, enable a direct transfer of electrons from HoxU to FMN for NAD^+

reduction to NADH. HoxY has an additional FMN, denoted as FMN-a, and the FMN in HoxF in charge of NAD^+ reduction is denoted FMN-b. It is interesting to note that although FMN-a is not responsible for NAD^+ and NADH conversion, loss of FMN-a also leads to the loss of NAD^+ reducing activity of the whole enzyme.

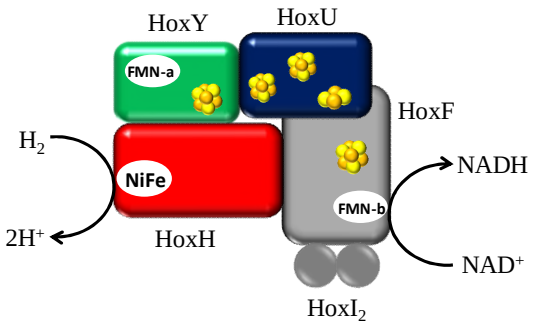


Figure 1-12: The schematic model of *R.e* SH structure. It contains six subunits $HoxHYFUI_2$. HoxH (red) contains a NiFe centre in charge of splitting H_2 to protons. HoxY (green) contains one [4Fe-4S] cluster and an FMN, denoted as FMN-a, whose function is still not fully understood. HoxU (dark blue) contains three FeS clusters, one [2Fe-2S] cluster and two [4Fe-4S] clusters. HoxF (grey) contains one [4Fe-4S] cluster and one FMN, denoted FMN-b in charge of converting between NAD^+ and NADH. The FeS clusters are electron relays to transfer electrons between NiFe centre in HoxH and the FMN-b centre in HoxF.

Oliver Lenz and co-workers have isolated the NAD^+-reductase part of soluble hydrogenase from *Ralstonia eutropha*. Both biochemical assays and electrochemical assays illustrated that isolated *R.e* SH retains NAD^+ reducing and NADH oxidising activity.

1.7.3 Soluble Hydrogenase variants

Site-direct mutagenesis has been applied to *R.e* SH to produce variants that can catalyse the conversion between $NADP^+$ and NADPH. The native .*Re* SH and four variants of *R.e* SH that showed activity towards NADPH in biochemical assays were provided by Dr Oliver Lenz. The homology modelling structure of HoxF (**Figure 1-13**) shows the catalytic pocket where conversion between $NAD(P)^+$ and NAD(P)H happens. The catalytic pocket contains FMN-b responsible for hydride or electron transfer from the cofactor, and a [4Fe-4S] cluster adjacent to FMN. The structure illustrates that three amino acid residues around the catalytic pocket, glutamic acid in position 341, serine in position 342, and aspartic acid in position

467, are likely to be crucial for binding NAD^+ and allowing NAD^+ to get into the pocket. Glutamic acid in position 341 was changed to alanine (E341A), and the serine in position 342 was changed to arginine (S342R), to try to enlarge the catalytic pocket to accommodate the additional phosphate group of $NADP^+$. Aspartic acid in position 467 was changed to Serine (D467S), to make it easier for $NADP^+$ to get into the catalytic pocket. Moreover, all these mutations make the catalytic pocket less negatively charged, to help accommodate the extra negative charge from the phosphate group in $NADP^+$. In this thesis, the native *Re* SH is denoted as wildtype, and the three variants are denoted as $HoxF^{E341A}$, $HoxF^{S342R}$, and $HoxF^{E341A+S342R}$.

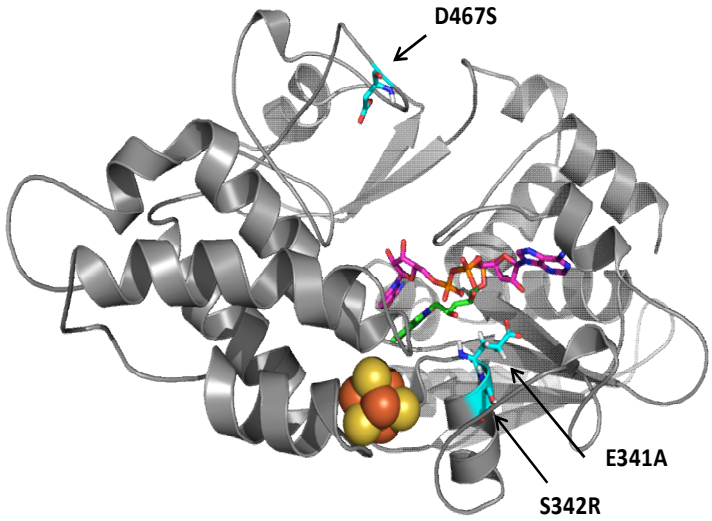


Figure 1-13: A homology modelling structure of HoxF based on the relevant part of the structure of respiratory Complex I from *Thermus thermophilus*. The residues altered are shown in blue, the FMN is in green, and the cofactor is in purple..

The aim is to identify the best enzyme variant that has sufficient activity and affinity towards NADPH, so that it can be coupled to the new NADPH regeneration system. By replacing the NAD^+-reductase from the current system with the variant that achieves best NADPH conversion activity, while keeping the hydrogenase of the system, a new NADPH regeneration system will be developed, and NADPH-dependent enzymes like P450

monooxygenases, imine-reductase and alkene-reductase, are ready to be incorporated into the new system to carry out enzymatic reactions (**Figure 1-14**).

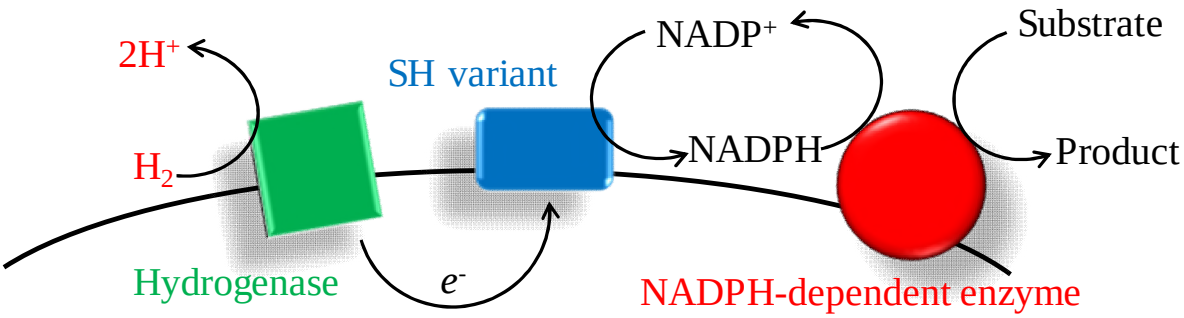


Figure 1-14: The schematic model of new NADPH regeneration system, which is very similar with the NADH regeneration system. The hydrogenase splits H_2 to protons and electrons, and the SH variant utilises them, but instead of regenerating NADH, it regenerates NADPH for the downstream NADPH-dependent enzyme to carry out reactions.

1.7.4 NuoF subunit of respiratory Complex I

To further develop the regeneration system, more robust and reliable enzymes that can be produced cheaply are required to incorporate into the system to replace existing enzymes. The NAD^+-reductase from *Ralstonia eutropha* H16 is very difficult to express in the well-established *Escherichia coli* expression systems, and is normally expressed in its original host, making the production process of this enzyme costly and time consuming.

Complex I (NADH:ubiquinone oxidoreductase) is the first protein complex in the respiration chain[101–103]. The whole respiration chain contains four complexes, namely complex I, II, III and IV, which are all bound to the membrane and adjacent to each other. Complex I oxidises NADH to NAD^+, Complex II oxidises succinate to fumarate, and they pass the electrons to ubiquinone (Q). Ubiquinone then passes the electrons to cytochrome c in Complex III, and then cytochrome c moves to Complex IV where O_2 is reduced by the electrons from cytochrome c to form H_2O. This process couples with proton pumping by Complex I, II, and IV, from the inner side of the membrane to the outer side of the membrane which is

thermodynamically unfavourable. At last, ATP is generated through ATP synthase pumping with reverse flow of protons[104].

Complex I oxidises NADH to NAD^+ and transports the two electrons to ubiquinone, coupled with pumping out four protons to the outer side of the membrane. Prokaryotic complex I consists of 14 subunits, and forms an L-shaped complex (**Figure 1-15**). The complex contains two arms, a hydrophilic arm and a hydrophobic arm[105–108]. The hydrophilic arm protrudes into the cytoplasm and is responsible for NADH oxidation, while the hydrophobic arm is bound in the cell membrane and in charge of passing through the electrons to ubiquinone coupled with proton pumping. The catalytic centre of hydrophilic arm in the first subunit contains a FMN molecule responsible for NADH oxidation. There are also a series of FeS clusters buried in complex I, which are used as electron transfer relays. As respiration is a key activity in living organisms, complex I widely exists in bacteria, and plants, as well as animals. Prokaryotic complex I has a minimum of 14 subunits, together with one FMN and at least six FeS clusters, but is sufficient to carry out its function. In eukaryotic cells, complex I has up to 32 additional subunits, which is one of the largest protein complexes among all cell components. The functions of the additional subunits are largely unknown. Prokaryotic complex I resides in the inner cell membrane, while eukaryotic complex I resides in the inner membrane of mitochondria. Despite these differences, prokaryotic and eukaryotic complex I share lots of similarities. They are both L shaped, with the hydrophobic arm buried in the membrane while the hydrophilic arm protrudes into the cytoplasm, or inner mitochondria plasma. And they have the same function in cell respiration. Prokaryotic complex I enzymes have been widely studied due to their simplicity. The structure of *Thermus thermophilus* HB-8 complex I has been reported by Sazanov and co-workers[107]. The fourteen subunits of *Thermus thermophilus* Complex I are denoted Nqo1-14. Nqo1, the first subunit of the hydrophilic arm, contains FMN, and one FeS cluster, and is in charge of

converting between NAD^+ and NADH. In *E. coli*, there are only 13 subunits in Complex I, denoted NuoA-N, where NuoC and NuoD are fused to form a NuoCD subunit.

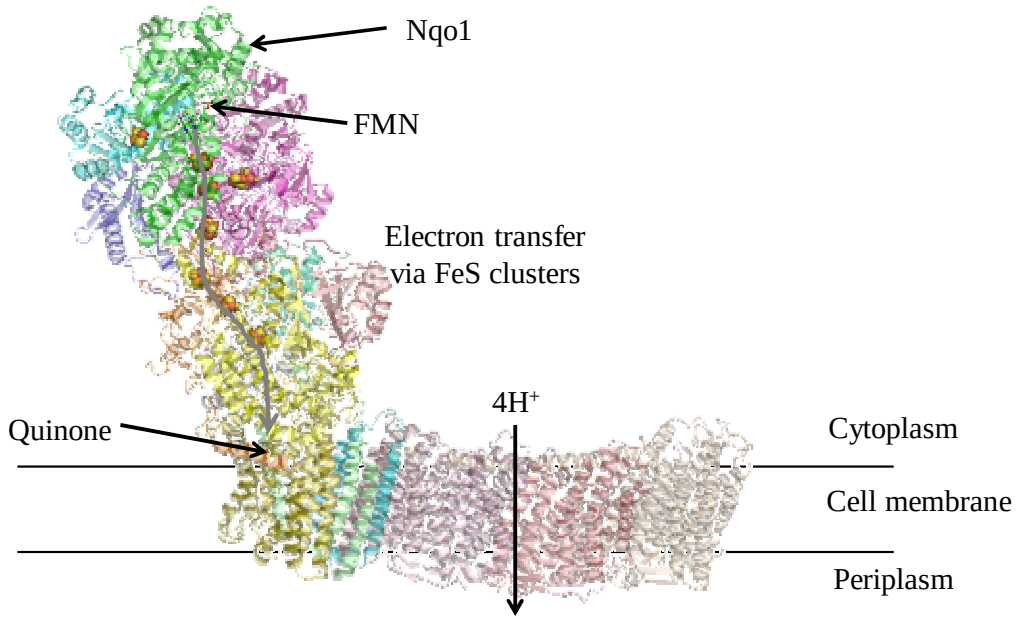


Figure 1-15: Crystal structure of respiratory Complex I from *Thermus thermophilus*. Complex I contains 14 subunits Nqo1-14, but in *E. coli* the equivalent of Nqo4 and Nqo5, namely NuoC and NuoD are fused to form NuoCD. Seven of the subunits form the hydrophilic arm that protrudes into the cytoplasm, while the rests form the hydrophobic arm buried in the membrane. Nqo1 subunit at the top of the hydrophilic arm contains a FMN and one FeS cluster which are in charge of converting between NAD^+ and NADH. The electrons from NADH go through a series of FeS clusters in the hydrophilic arm to the downstream Quinone and their transfer is coupled with four protons being pumped from the cytoplasmic side to the periplasmic side (PDB code: 4HEA).

Complex I enzymes are mostly conserved proteins in living organisms, so *Thermus thermophilus* Complex I and *E. coli* Complex I are highly related[107]. Studies also indicated that *Re* SH is also highly related to complex I with every subunit except for HoxI having orthologous counterparts within the peripheral arm of Complex I (**Table 1-2**). HoxY shares similarity with Nqo6, both contain a [4Fe-4S] cluster, and HoxY has an additional FMN. HoxH shares similarity with Nqo4, but the quinone-binding site in Nqo4 is replaced by the Ni-Fe active site in HoxH. HoxU is similar with truncated Nqo3, both of which have three FeS clusters in charge of electron transfer from FMN to the other receptors: either ubiquinone in Complex I or the NiFe centre in *Re* SH. Most importantly, HoxF shares great similarity with the combination of Nqo1 (**Figure 1-16**) and Nqo2. Both HoxF and the

combination of Nqo1 and Nqo2 have a FMN and a [4Fe-4S] cluster adjacent, in charge of converting between NAD^+ and NADH.

Table 1-2: Homology of *Thermus thermophilus* and *E. coli* hydrophilic arm of Complex I and *Ralstonia eutropha* soluble hydrogenase.

Thermus thermophilus Complex I	*Escherichia coli* Complex I	*Ralstonia eutropha* Soluble hydrogenase	Cofactors
Nqo1	NuoF	HoxF	FMN, one FeS cluster
Nqo2	NuoE		one FeS cluster
Nqo3	NuoG	HoxU	three FeS clusters
Nqo4	NuoCD	HoxH	
Nqo5		-	
Nqo6	NuoB	HoxY	one FeS cluster (one FMN in HoxY)
Nqo9	NuoI	-	two FeS clusters

The subunit we are interested in is the NuoF subunit of *E. coli* complex I. As discussed above, the NAD^+-reductase used in the current NADH regeneration system is from *Re* SH. In practice, the whole enzyme HoxHYFU is genetically engineered with one single mutation to inhibit the NiFe centre for H_2 oxidation, and then overexpressed in its native host and isolated. The enzyme is relatively large, containing for different subunits, two FMN, and five FeS clusters. It is therefore very taxing for the host cell to over express such a large enzyme with multiple cofactors. Also the multiple FeS clusters as electron transfer relays make the electron transfer process less efficient. Additionally, the relatively large volume of the enzyme makes the catalytic activity per volume ratio low. On the contrary, NuoF is a promising candidate as NAD^+-reductase in the NADH regeneration system. *In vitro* study has shown that NuoEF is a robust enzyme with high efficiency. NuoF only has one FeS

cluster adjacent to FMN, making its electron transfer chain more efficient, and it is only 50 kDa, much smaller than HoxFU, which has a total molecular weight of 110 kDa[95]. Most importantly, NuoF should be able to be over expressed in the well-established *E. coli* expression system as it is a native enzyme in *E. coli*, thus greatly decreasing the cost and the labour involved for expression. Previous work has shown some promising results for overexpression and activity of NuoF.

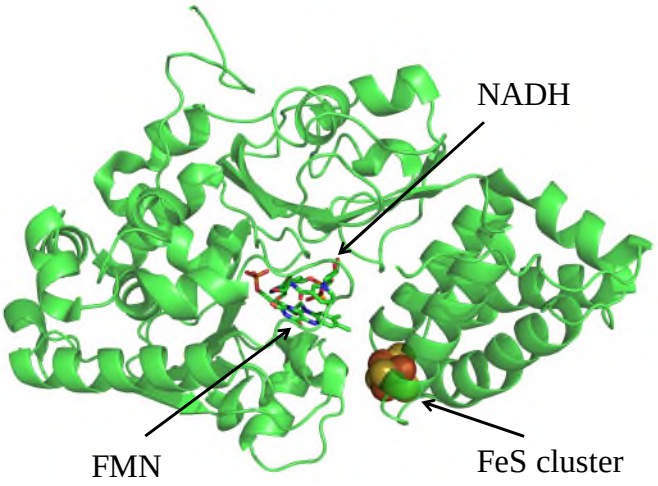


Figure 1-16 Crystal structure of Nqo1 subunit from *Thermus thermophilus* respiratory complex I binding with its substrate NADH. Nqo1 contains one FMN molecule and one [4Fe4S] cluster. FMN is closely positioned with the substrate NADH. NADH transfers its electrons to FMN, and FMN passes the electrons to the adjacent FeS cluster. The electrons are further passed to a series of FeS clusters of the other subunits of Complex I (PDB code: 4HEA).

Hirst and co-workers have successfully isolated the flavoprotein subcomplex of complex I from bovine heart mitochondria, the homologue of Nqo1 and Nqo2 in *Thermus thermophilus* HB-8. The flavoprotein subcomplex contains the 51 kDa and 24 kDa subunits of complex I and their associated cofactors, including the active site FMN, and two FeS clusters. Hirst and co-workers isolated the whole complex I from bovine heart mitochondria, and then the Fp subcomplex was separated from the rest of the complex. This Fp subcomplex had been tested using protein film electrochemistry and shown to retain the ability to catalyse NADH. Friedrich and co-workers have expressed and purified a soluble fragment of complex I from *Aquifex aeolicus*. *Aquifex aeolicus* complex I is very similar to that of *Escherichia coli* both

structurally and functionally. Friedrich and co-workers cloned the soluble fragment, namely NuoE, F, and G subunits of complex I from *Aquifex aeolicus* into pETBlue-1 vector, and transferred this vector into *Escherichia coli* Rosetta (DE3) pLacI strain. The soluble fragment was heterologously overexpressed in *Escherichia coli* and isolated affinity via chromatography. The results showed that NuoE (25 kDa) and NuoF (52 kDa) were successfully expressed and associated together due to strong protein-protein interaction. NuoG however was not expressed. NuoEF subcomplex also showed NADH oxidoreductase activity at high temperature.

In this work, our aim is to express either NuoEF or just the NuoF subunit of complex I, the soluble part of the respiration complex I from *Escherichia coli* catalysing the conversion between NAD^+ and NADH. As NuoF is only 50kDa, much smaller than *Re* SH, it renders a high catalytic site versus volume ratio, and thus would enable more efficient catalysis. In this way, NuoF could replace the current NAD^+-reductase from *Ralstonia eutropha* to be incorporated into a new, more robust NADH regeneration system (**Figure 1-17**).

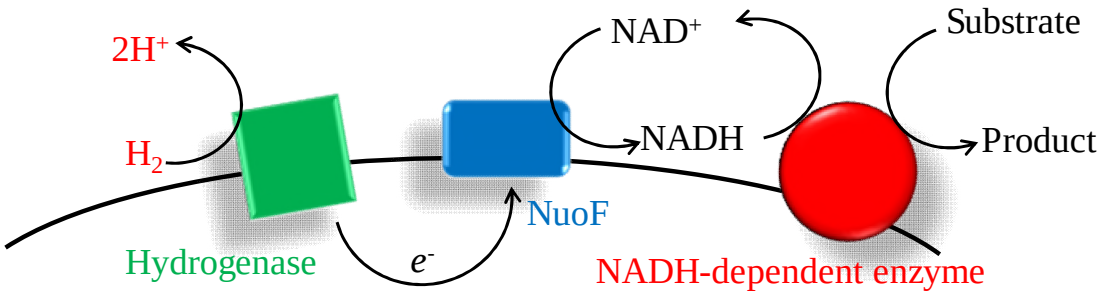


Figure 1-17: The schematic model of a new H_2-driven NADH regeneration system. The NAD^+-reductase is replaced by NuoF for a more robust and lower cost system.

1.7.5 NuoF variants

Mutagenesis on the HoxF subunit of *Re* SH has shown promising results for $NADP^+$ reduction. NuoF shares great sequence similarity with HoxF, and has the same function of converting between NADH and NAD^+, so we hypothesise that mutagenesis of NuoF may

also allow it to use $NADP^+$ and NADPH. Autiol and co-workers reconstructed the central metabolic pathway of *E. coli* to create a higher inner ratio of NADPH to NADH, and the adaptive evolution produced two *E. coli* strains that can utilise both NADH and NADPH[109]. Whole genomic mapping showed that both strains have mutations of NuoF ($NuoF^{E183A}$ and $NuoF^{E183G}$). Biochemical assay showed that both mutations of NuoF had increased activity towards NADPH, with the k_{cat}/K_M for $NuoF^{E183A}$ being $3.6 \pm 1.0\ s^{-1}\ \mu M^{-1}$, and the k_{cat}/K_M for $NuoF^{E183G}$ being $3.5 \pm 1.0\ s^{-1}\ \mu M^{-1}$, compared with that of wildtype NuoF of $0.011 \pm 0.001\ s^{-1}\ \mu M^{-1}$. Friedrich and co-workers identified that the carboxylate group of Glu183 in NuoF interacts with hydroxyl groups of NADH by hydrogen bonds based on the crystal structure of the hydrophilic domain of respiratory complex I from *Thermus thermophilus* with bound NADH (**Figure 1-18**)[110]. This structural insight partly explained why complex I had hardly any activity at all towards NADPH: the additional phosphate group of NADPH suffered from the steric hindrance and electrostatic repulsion with Glu183. Mutations of NuoF at residue Glu183 showed increased activity towards NADPH, with the k_{cat}/K_M for $NuoF^{E183H}$ is $0.40 \pm 0.003\ s^{-1}\ \mu M^{-1}$, 200 times higher than the wildtype NuoF.

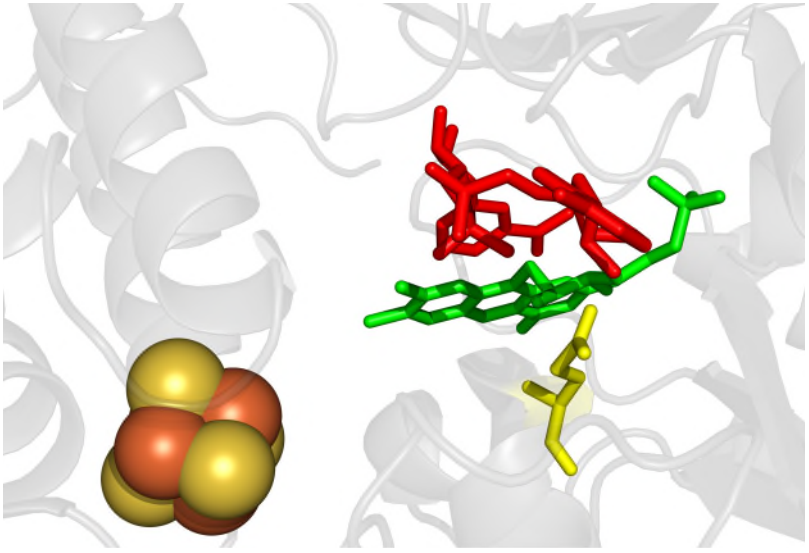


Figure 1-18 Structure of the nucleotide-binding site of Nqo1 subunit of Complex I with bound NADH. The protein is shown in grey. The [4Fe4S] cluster is shown in yellow and orange spheres, the FMN in green, and the bound NADH in red. The glutamic acid residue in position 183 is shown in yellow (PDB code: 3IAM).

In this work, the original plan was to also do mutations on Glu183 in NuoF, and produce a series of NuoF variants. Then the variants would be characterised electrochemically and biochemically to determine the best variant that has highest activity towards NADPH. The best variant would be incorporated into the new NADPH regeneration system. However, due to the instability of NuoF, this part of work is yet to be done, and can be explored in the future.

1.7.6 Soluble transhydrogenase

Pyridine nucleotide transhydrogenase (UdhA) is an energy-independent soluble enzyme that directly catalyses the reversible hydride transfer between NADH and NADPH[111]. The physiological function of UdhA is to maintain homeostasis of these two cofactors in a living organism. The gene encoding UdhA in *E. coli* is *sthA*. There is another transhydrogenase in *E. coli*, membrane-bound transhydrogenase (PntAB) which has similar function with UdhA[112]. However, PntAB is an energy-dependent enzyme that favours the hydride transfer from NADH to $NADP^+$, while UdhA is an energy-independent enzyme that favours the other way around (**Scheme 1-1**). Transhydrogenase is expected to be used in a new NADPH regeneration system. Since PntAB is a membrane bound protein, which is difficult to isolate and handle outside the cell, and PntAB requires addition of extra ATP as its energy source, it is not suitable for the cofactor regeneration system. Therefore, this study focused on the soluble transhydrogenase UdhA. UdhA belongs to a well-known family of flavoprotein disulfide oxidoreductases with three clearly delineated domains: one for FAD binding, one for NAD(P)H binding and one for dimerization.

$$NAD^+ + NADPH \xrightleftharpoons{UdhA} NADP^+ + NADH$$

Scheme 1-1: UdhA catalyses the energy independent reversible reaction of transferring a hydride from NADPH to NAD^+ forming NADH and $NADP^+$.

Previous work by Zhu and co-workers has demonstrated over expression and isolation of UdhA from *E. coli* [113]. The results showed that UdhA has an apparent molecular weight of 52 kDa, and catalyses the hydride transfer from NADPH to NAD^+ *in vitro*. Their study also indicated that the isolated enzyme had highest activity at 35 °C, pH 7.5. Coupling UdhA to the current NADH regeneration system is an alternative approach to extend it to NADPH regeneration. UdhA can utilise the regenerated NADH and a catalytic amount of $NADP^+$ to form NADPH and NAD^+, and NADPH can thus be supplied to an NADPH dependent enzyme. Although UdhA favours hydride transfer from NADPH to NAD^+, NADH is constantly produced by the regeneration system and NADPH is constantly consumed by NADPH-dependent enzyme, thus driving the whole reaction towards the desired direction of NADPH production. Shimizu and co-worker took advantage of soluble transhydrogenase from *Pseudomonas fluorescens* to design a two-step *in vitro* NADPH regeneration system to supply Cytochrome P450 BM3 monooxygenase to oxidise *p*-nitrophenoxydecanoic acid (**Figure 1-19A**)[114]. They co-expressed glycerol dehydrogenase (GDH), UdhA, and P450 BM3 and isolated them separately. The three enzymes were put into buffer with catalytic amount of NAD^+, $NADP^+$, and large amount of substrate. Upon adding glycerol, GDH and UdhA acted as a two-step NADPH regeneration system, and P450 BM3 could use the regenerated NADPH to transform substrate to product. Boonstra and co-workers also used isolated UdhA for *in vitro* production of hydromorphone (**Figure 1-19B**)[115]. They co-expressed morphine dehydrogenase and morphinone reductase. The former enzyme oxidases the reactant, morphine to morphinone, and the latter enzyme reduces the intermediate morphinone to the product, hydromorphone. However, the two enzymes have different cofactor specificity. UhdA was used to negotiate this difference of cofactor specificity. This system achieved up to 84% yield within 9 hrs.

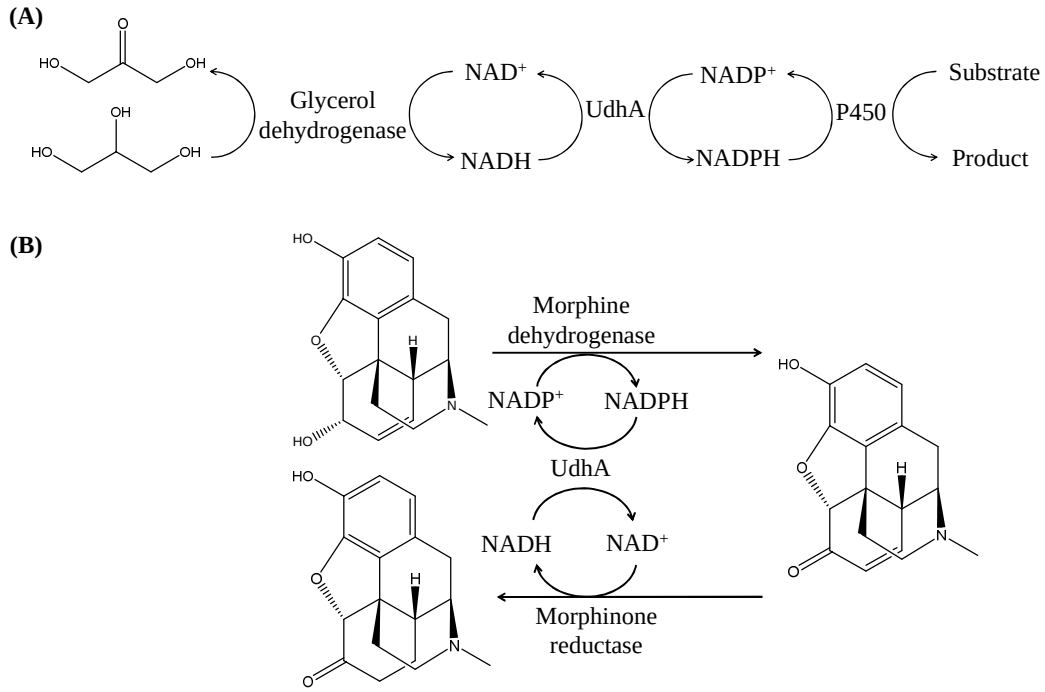


Figure 1-19 (A) The schematic illustration of a UdhA coupled NADPH regeneration system. Glycerol dehydrogenase was used to regenerate NADH, and UhdA was used to regenerating NADPH from NADH. The NADPH was used for P450 monooxygenase. (B) The schematic illustration of UdhA coupled with morphine dehydrogenase and morphinone reductase to produce hydromorphone from morphine.

Transhydrogenase has been proven feasible, so the goal in this project is to insert an additional transhydrogenase into our current NADH system to transform it into a new NADPH regeneration system using transhydrogenase as a mediator from NADH to NADPH (**Figure 1-20**). In this new system, a catalytic amount of both NAD^+ and $NADP^+$ are required.

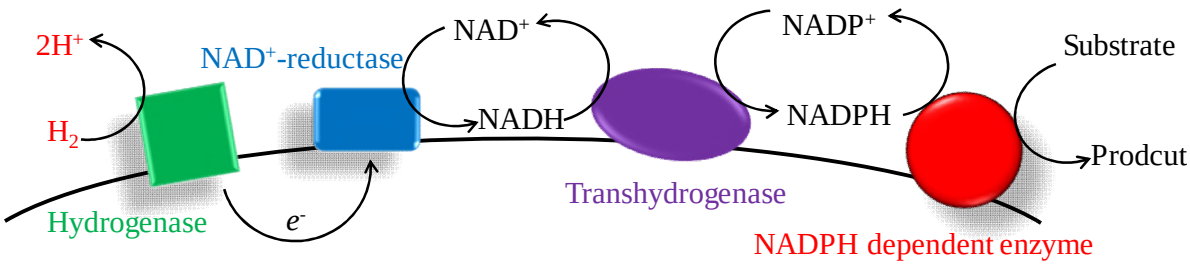


Figure 1-20: The new NADPH regeneration system. The new system consists of four enzymes, in addition to the hydrogenase, NAD^+-reductase, and the NADPH-dependent enzyme; there is an additional transhydrogenase in charge of converting NADH to NADPH by transfer of the hydride from the NADH to $NADP^+$.

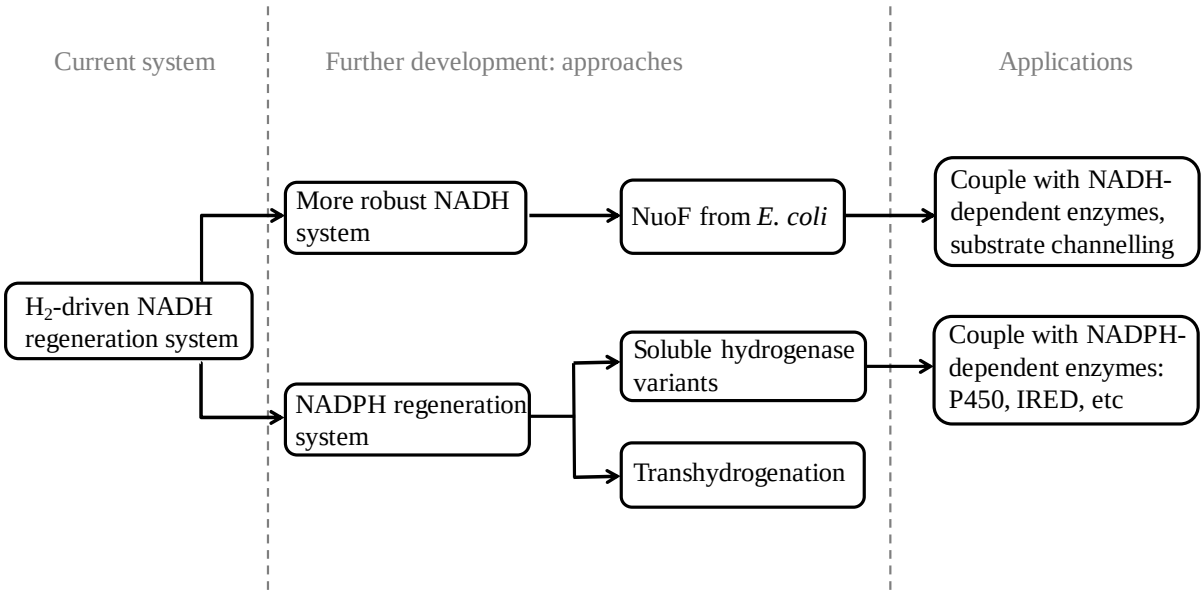
1.8 Applications of a H_2-driven regeneration system

The H_2-driven NADH regeneration system developed by the Vincent group has been demonstrated as robust in a number of applications. Reeve and co-workers coupled the system with ADH 105 provided by Johnson Matthey to reduce acetophenone to (*S*)-phenylethanol with over 90% conversion and over 99% *ee*, using only catalytic amount of NAD^{+}[116]. The current system works as a platform to supply cofactors for a variety of enzymes. The goal is to extend the scope of the third enzymes working together with the platform system. Also, the successful development of the new NADPH regeneration system provide with an opportunity to couple the system with a lot of new enzymes that require NADPH rather than NADH as redox equivalent, including alkene-reductase, imine-reductase, as well as P450 monooxygenase.

1.9 Structure of this thesis

This thesis includes two parts: further development of the current H_2-driven NADH regeneration system in Vincent group, and the application of the current and further developed systems. To further develop the system, there are two directions: towards a more robust NADH regeneration system, and development of a new NADPH regeneration system based on the current NADH system. To develop a more robust NADH system, a new enzyme NuoF is expressed and isolated to substitute NAD^{+}-reductase in the current system. To develop a novel NADPH regeneration system, three approaches are investigated in this thesis. The content of this thesis follows the logic of the structure of my projects. Chapter one will discuss about the introductory and background knowledge of this thesis, including the basic idea of biocatalysis and its importance in industries, cofactors, enzymes involved in this study, and the general strategies of how our targets are approached. Chapter two will discuss about the basic theory applied in this study including enzyme kinetics and

electrochemistry, as well as molecular biology approaches to produce native and genetically modified enzymes. Chapter three, four, five and six would focus on discuss the results achieved in this project. Chapter three focuses on the electrochemical characterization of *Re* SH variant to determine the best variant for the new NADPH regeneration system. Continuously, chapter four discussed about the application of the new NADPH regeneration system: couple the system with NADPH dependent enzyme P450 and imine reductase. Chapter five discusses about an alternative approach to NADPH regeneration system based on the soluble transhydrogenase. Chapter six mainly discusses the efforts to develop a more robust NADH by replacing the NAD^+ reductase from *Re* SH to *E. coli* Complex I. At last, chapter seven would give a summary and outlook for this whole project.



Chapter Two: Methods and Theory

A broad range of technical methods and scientific theories are applied in this thesis, and they will be discussed in detail in this chapter. These methods include molecular biology techniques and electrochemistry. This chapter covers theoretical and background information including recombinant DNA manipulation, mutagenesis, and protein expression and purification. For electrochemical methods, protein film electrochemistry was regularly used for testing the electrochemical activity of enzymes. Other techniques used in this study include Gas Chromatography (GC), High Performance Liquid Chromatography (HPLC), Nuclear magnetic resonance (NMR), Ultra Performance Liquid Chromatography (UPLC), and biochemical characterization of enzymes via enzymatic assays. All these methods and theory will be discussed in detail below.

2.1 Gene cloning and protein expression

Throughout this thesis, a number of enzymes are used. Some of which are provided by collaborators, or from commercial sources, while some are produced in our laboratory. The enzymes produced in our laboratory include the soluble *E. coli* transhydrogenase (UdhA), and the NuoF subunit of *E. coli* Complex I[108]. The gene sequences of these proteins were obtained from the *E. coli* genome, amplified using the Polymerase Chain Reaction (PCR)[117] and cloned into appropriate expression vectors. Protein overexpression was carried out in a suitable strain of *E. coli*. This section will discuss in detail how these enzymes are cloned, expressed, mutated and isolated.

2.1.1 Protein expression and purification of *nuo* genes

To express the *nuo* genes, a seed culture of 15 mL of *E. coli* BL21(DE3) cells bearing the corresponding plasmid in LB media with 50 µg/ml kanamycin was grown in a shaking incubator to OD_{600} at or above 0.8. Then the seed culture was transferred to 1.5 L of LB

media with a dilution rate of 1:100, and grown for three to four hours until OD_{600} reaches 0.8. Protein expression was induced with 0.1 mM IPTG and grown at 16 °C overnight.

The cells were harvested by centrifugation at 10000 x *g* for 30 min, and the cell pellet resuspended in 40 mL Tris Buffer (50 mM Tris, pH 8.0). The cells were disrupted by sonication: sonicating 3 s and pausing for 9 s, 2.5 min of total sonication time, and 40% intensity (Fisherbrand™ Model 505 Sonic Dismembrator from Fisher Scientific). Then the cell lysate was cleared by centrifugation at 10000 x *g* for 30 min, and the cell debris discarded. The soluble extract was filtered and kept at -20 °C for further usage. The *nuo* proteins were extremely difficult to express, solubilise, and stabilise. Different conditions, including growing temperature, buffer pH, ionic intensity, and other additives were tested to determine the best condition for growing, and keeping the functionality of the enzymes. The detailed experiments and procedures will be discussed in chapter six.

To purify the *Nuo* proteins, an AKTA protein purification system and HisTrap^{TM} HP 1 mL column (GE healthcare) was used. Then, the column was washed with elution buffer, a gradient of imidazole concentration was generated during the washing. The elusion fractions were collected at 1 mL scale. The fractions with peak absorption were collected and analysed by SDS-PAGE.

2.1.2 Protein expression and purification of *udhA* gene

To express UdhA, a similar protocol to that used for expression of NuoF was used. A seed culture (15 mL) of *E. coli* BL21 cell bearing the pET28a-UdhA plasmid in LB media with 50 µg/mL kanamycin was grown in an incubator for 8-12 hours at 30 °C until OD_{600} reached or above 0.8. Then the seed culture was transferred to 1.5 L of LB media with a dilution rate of 1:100, and grows for another 4-5 hours until OD_{600} reaches 0.8. The cell culture was put

on ice to cool down to 30 °C, and 0.5 mM IPTG was added, cells were grown at 30 °C overnight for induced expression.

The cells were harvested by centrifugation at 10000 x *g* for 30 min, and the cell pellet was resuspended in 40 mL Tris Buffer (50 mM, NaCl 100 mM, pH 7.5). Sonication was used to break the cell membrane by the following programme: sonicating 3 s and pausing for 9 s, 2.5 min of total sonication time, and 40% intensity. Then the cell lysate was once again centrifuged 10000 x *g* for 30 min, and the cell debris was discarded. The soluble extract is then filtered and kept at -20 °C for further usage. The purification process of UdhA was the same as that of *Nuo* proteins.

2.2 Protein film electrochemistry

Electrochemistry is widely used to study redox reactions, where electrons transfer between reactants and products[90]. This kind of reaction occurs through the application of an external voltage or through the release of chemical energy. The terms oxidation and reduction are used to describe the change of oxidation state that takes place in the chemical species involved in an electrochemical reaction. Oxidation state is defined as the hypothetical charge that an atom would have if all bonds to atoms of different elements were 100% ionic. An atom or ion that gives away an electron to another atom or ion has its oxidation state increased, while the recipient of the negatively charged electron has its oxidation state decreased. In electrochemical experiments, a redox reaction is separated into two half reactions: the reduction reaction, and the oxidation reactions. In electrochemistry, the Nernst equation describes the behaviour of a redox reaction under standard condition[118].

$$E = E^0 + \frac{RT}{nF} ln \frac{[ox]_{eq}}{[red]_{eq}}$$

In this equation, E is the thermodynamic potential, E^0 is the standard reduction potential, R is the universal gas constant, T is the absolute temperature, F is the Faraday constant, and n is the number of number of moles of electrons transferred in the reaction. The standard reduction potential of a given redox couple is reported against a reference electrode, usually a Standard Hydrogen Electrode (SHE). SHE is defined to be 0 V at any temperature, at 1 bar H_2 when protons are at unit activity[119]. In practice, as SHE requires H_2 gas, it is not very convenient for use in experiments, so other reference electrodes are used. In this particular project, a saturated calomel electrode (SCE) is used[120], but all the final data are presented vs SHE after correction.

In this thesis, protein film electrochemistry (PFE) is extensively used to characterise kinetic and thermodynamic properties of redox enzymes (**Figure 2-1**)[121]. The target enzyme is adsorbed on the surface of an electrode to form a sub- or monolayer film, and the enzyme retains its biological function and activity, allowing direct electron exchange between the enzyme and the electrode[122]. The electrode is controlled by a potentiostat that can alter the applied potential. Usually, a redox enzyme couples an oxidation half reaction and a reduction half reaction by oxidising a substrate and passing the electrons to reduce another substrate. For example, *R.e* SH couples the oxidation H_2 to protons and electrons and the reduction of NAD^+ to NADH[98]. The half reactions cannot proceed independently.In solution, *R.e* SH cannot only oxidise H_2 without reducing NAD^+, nor can it only reduce NAD^+ without oxidising H_2. For a reduction reaction, by applying a potential more negative than the redox potential of the substrate, the enzyme can extract electrons from the electrode and reduce its substrate. If the enzyme is reversible, by applying a potential more positive than the redox potential of the substrate, the enzyme can oxidise its substrate and pass the electrons to the electrode.

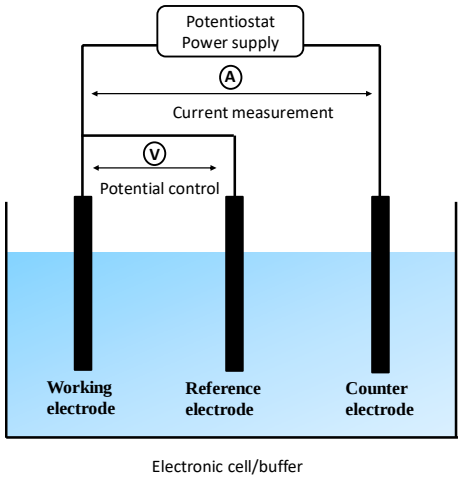


Figure 2-1 The illustrative diagram shows the protein film electrochemistry system used in this thesis. The system consists of three electrodes, the working electrode, the reference electrode and the counter electrode. All are attached to the central potentiostat control system, and they also intrude into the electrochemical cell containing buffer and substrate. A potential is applied between the working electrode and the reference electrode to allow the redox reaction to happen. In the meantime, the current between the working electrode and the counter electrode is recorded.

2.2.1 Equipment and set-ups

In this study, to set up protein film electrochemistry, three electrodes are required: a working electrode, reference electrode, and counter electrode. They all contact with the buffer in the electrochemical cell, and form a closed circuit with a power supply. There is a water bath surrounding the outside of the electrochemical cell, connected to a water circulation system to control the experiment temperature. The system is controlled by a potentiostat. The potentiostat applies a specific potential between the working electrode and the reference electrode. If a current is generated, most of the current is flowing through working electrode to the counter electrode rather than the reference electrode. This design helps keep a precise and stable potential between the working electrode and the counter electrode, as high current flowing through the reference electrode makes the potential between the reference electrode and the working electrode hard to maintain (**Figure 2-2**).

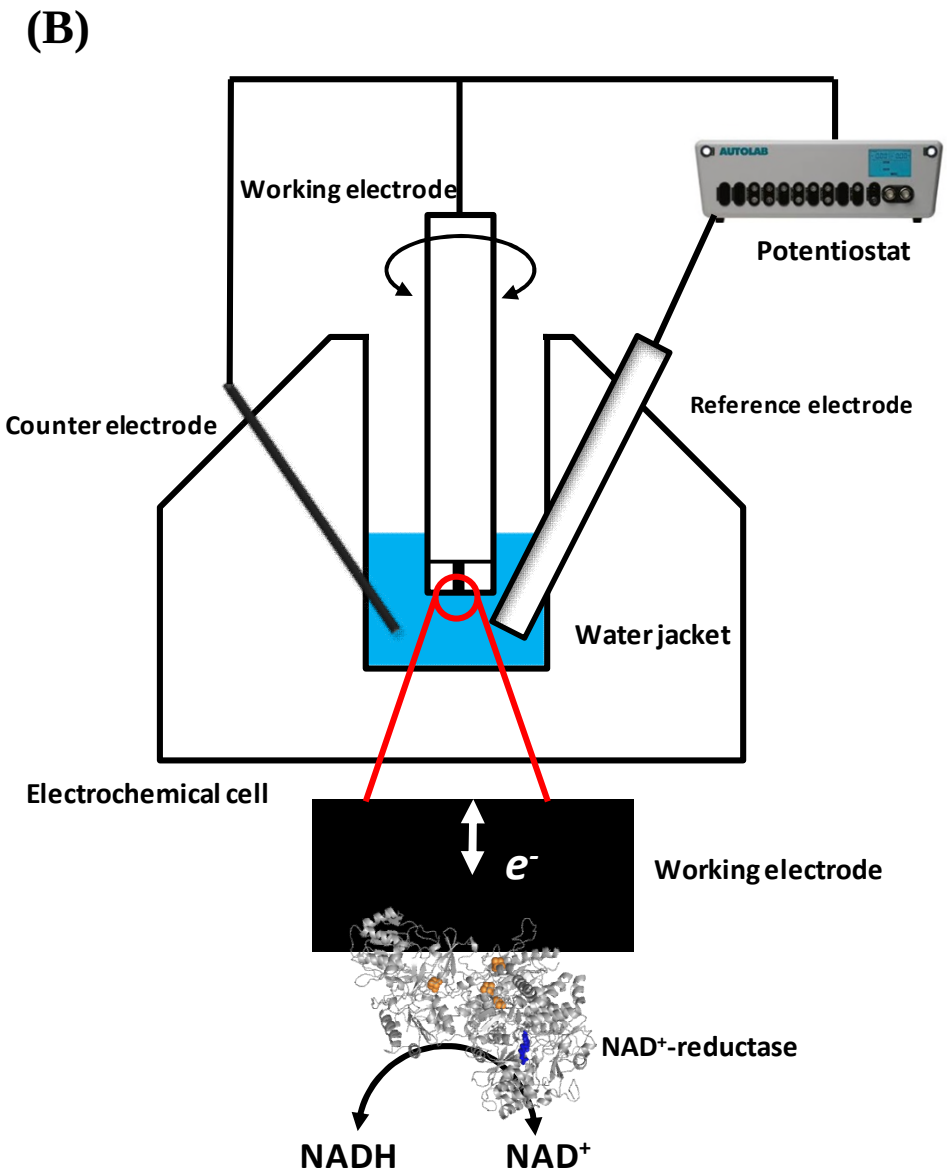


Figure 2-2 This picture shows the set-up of a protein film electrochemistry experiment. When the system is set up, the target enzyme (in this case NAD^+-reductase) is adsorbed on the surface of working electrode. The substrate is dissolved in the buffer of the electrochemical cell. When a proper potential is applied, the redox reaction happens on the surface of the working electrode, leading to the electron exchange between the enzyme and the electrode. Meanwhile, the working electrode is rotating rapidly to avoid any accumulation of the product, so that the product does not inhibit the enzyme, and the concentration of the substrate is regarded as being constant throughout the experiment.

The working electrode used in this thesis is a homemade pyrolytic graphite edge (PGE) electrode consisting of a screw-threaded steel insert, a PTFE casing, a graphite tip with surface area of 0.03 cm^2, a Delrin rotating disk electrode case and an insulating epoxy resin[123]. To make the working electrode, the graphite tip, roughly 1 cm length of graphite is stuck on the stainless-steel insert in the Delrin rotating disk electrode case using silver loaded

epoxy glue (RS). The graphite tip is then coated with insulating epoxy resin (Aradur hardener and Araldite resin, Robnor Resins), so only the surface of the graphite tip is exposed. The surface is then sanded until it is flat by sand paper. A PGE electrode is desirable for enzyme immobilisation.

In the experiments, the working electrode protrudes into the buffer with substrate in the electrochemical cell, and rotates rapidly. Enzyme samples are stored in a -80 °C freezer due to their instability at higher temperatures over long time. The sample was put on ice and transferred into glovebox for defrosting. The enzyme is immobilised non-covalently onto the working electrode by directly spotting roughly 0.5 µL enzyme solution (1 mg/mL) onto the electrode and waiting for 1 or 2 minutes to allow it to adsorb on the electrode. The enzymes then stick on the electrode surface by non-covalent interaction, probably hydrophobic interactions and π stacking and electrostatic interactions. This allowed a direct electron transfer through the substrate, the enzyme and the electrode, so when a potential was applied, a correlated catalytic current resulting from the redox reaction of the substrate can be observed through the monitoring potentiostat. The rapid rotation of the working electrode prevents enzyme catalytic product accumulating around the working electrode which could inhibit the reaction, and provides a constant supply of substrate. In the timescale of this experiment, the products produced at the electrode are much less than the substrate, so its concentration is negligible in the bulk solution. In this way, the buffer in the cell remained homogenous, and the concentration of substrate was regarded as constant throughout the experiment.

A saturated calomel electrode (SCE, from ALS) was used as reference electrode, and the potential was corrected to SHE. Most of the electrochemical experiments in this thesis were carried out at 30 ° C, so the correction was based on the following equation:

$$E_{SHE} = E_{SCE} + 0.243\ V\ at\ 30\ °C$$

The counter electrode is a platinum wire (Surepure Chemetals, 99.95 %, 0.4 mm diameter) which takes the current from the working electrode to complete the circuit.

In this study, two types of electrochemical technique were used: chronoamperometry and cyclic voltammetry.

2.2.2 Cyclic Voltammetry

In a cyclic voltammetry experiment, the working electrode is swept over a defined range of potentials at a given scan rate, and the current at each potential point is recorded, and thus forms a cyclic voltammogram[124]. The current response in cyclic voltammetry consists of two different types of current, non-Faradaic current and Faradaic current[125]. When the working electrode is subjected to a range of potentials, the electrode surface becomes charged, so the ions in the buffer solution rearrange in order to neutralise the charge at the electrode surface. Thus, an electrical bi-layer is formed, and acts as a capacitor leading to the non-Faradaic current contribution to the cyclic voltammetry. The magnitude of this non-faradaic current depends on the electrode surface, scan rate, temperature and a range of other factors. This kind of non-Faradaic current explains why a 'blank' cyclic voltammogram with no redox reaction happening on the electrode will still produce current. Also, when the potential is sweeping from negative to positive or positive to negative, the rearranged charge on the electrode is different, so even when the same potential is applied, the resulting non-Faradaic current is different according to the direction of potential sweep. The result is a typical 'blank' cyclic voltammogram which forms a spindle shape (**Figure 2-3**), the thickness of which depends on the magnitude of the non-Faradaic current. Therefore it is important to have a background scan for cyclic voltammetry for the comparison with a voltammogram in which a redox reaction happens. Faradaic current caused by an enzyme

catalysed redox reaction on electrode is meaningful to observe in cyclic voltammetry, as it demonstrates the activity of enzymes.

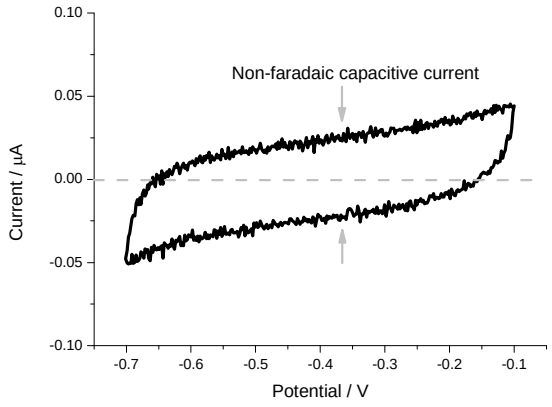


Figure 2-3 Cyclic voltammetry of a blank electrode with no redox reaction happening. The potential is swept between -0.1 V to -0.7 V, and the current is recorded. The current observed during the cyclic voltammetry is due to the non-Faradaic capacitive current.

2.2.3 Chronoamperometry

In a Chronoamperometry experiment, the electrode is held at a specific potential, and the catalytic current is continuously recorded during a given period of time, mostly a few seconds to a few minutes, and conditions can be varied during this time. In this thesis, chronoamperometry is used to study the affinity constant of the $NAD(P)^+$ reductase towards its substrate. The electrode is held at a potential that either favours $NAD(P)^+$ reduction or NAD(P)H oxidation. In practice, there are a number of considerations limiting the potential window available for redox reactions. For cofactor reduction, the more negative the redox potential, the higher the catalytic current, so for a higher signal-noise ratio, a low potential should be chosen. However, the enzyme exhibits poor stability at potentials more negative than -0.46 V vs SHE. Therefore as a compromise between activity and stability, -0.31 V vs SHE is chosen as the $NAD(P)^+$ reduction potential. For cofactor oxidation, although the enzyme tolerates high potential, other electrochemical reactions happen on the carbon

electrode above 0.24 V Vs SHE, and interfere with the cofactor oxidation. In this way, 0.1 V vs SHE is chosen as the most suitable NAD(P)H oxidation potential.

To determine the affinity constant of enzymes, when the electrode is held at a specific potential, first there is no substrate in the buffer, so no Faradaic current is observed. Then a series of injections of substrate are made into the buffer in the cell, and between each injection, a few seconds pause is given for the current to stabilise. After each injection, a jump of catalytic current is observed from the chronoamperometry. Therefore, the chronoamperometry forms a staircase-like shape (**Figure 2-4**). In theory, the current curve of a chronoamperometry should be flat during the pause between each injection. However, sometimes the enzyme film on the electrode suffers from enzyme loss due to the rapid rotation, and some of the enzyme may also denature during the electrochemical experiment. Therefore both of these effects result in the current curve during pause time decaying slightly.

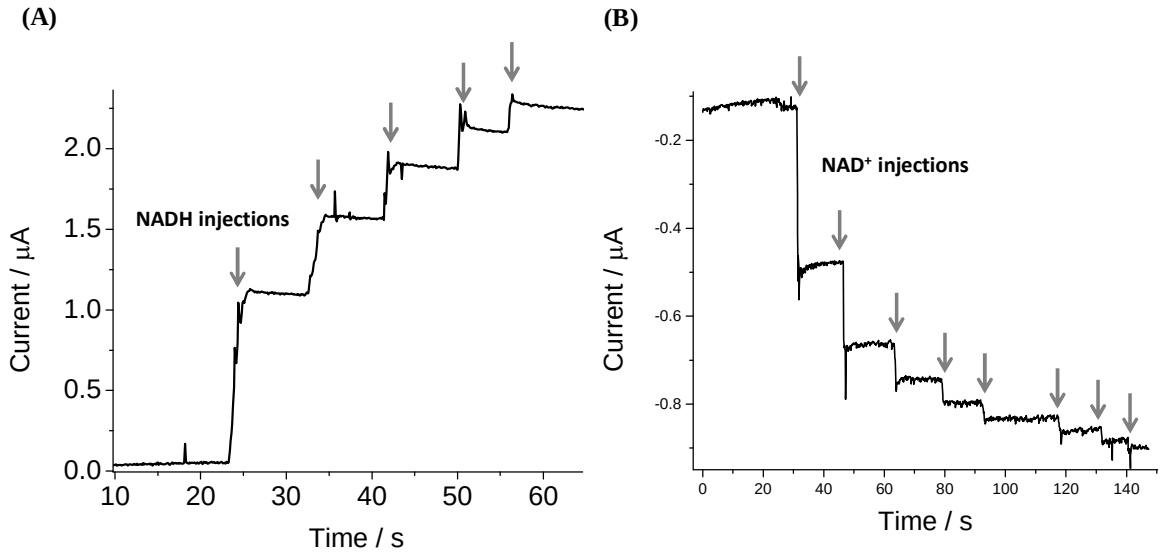


Figure 2-4 Chronoamperometry of NADH oxidation and NAD^+ reduction. (A) Chronoamperometry of NADH oxidation. The working electrode modified with wildtype *R.e* SH is poised at -0.1 V favouring NADH oxidation, and rotating at 2000 rpm. A series of NADH injections are made into Tris buffer (50 mM, pH 8.0), and the corresponding catalytic current jumps are observed from chronoamperometry. (B) Chronoamperometry of NAD^+ reduction. The working electrode modified with wildtype *R.e* SH is poised at -0.65 V favouring NAD^+ reduction, and rotating at 2000 rpm. A series of NAD^+ injections are made into Tris buffer (50 mM, pH 8.0), and the corresponding catalytic current jumps are observed from chronoamperometry.

2.2.4 Experiment considerations

In practice, there are a number of experimental considerations for the electrochemistry operations. First, O_2 is reduced on a PGE electrode at -0.2 V vs SHE, so any O_2 in the buffer solution would potentially interfere with the redox current of nicotinamide cofactors, especially the reduction of $NAD(P)^+$. For this reason, all the buffers were degassed and bubbled with N_2 overnight before usage, and all the electrochemistry experiments were carried out in a glovebox filled with N_2 to avoid any possible O_2 contamination of the experiment system. The working electrode requires processing before and after every experiment. As discussed before, the non-Faradaic current of the electrode partially depends on the surface of the electrode, and the enzyme is immobilised on the surface of working electrode by non-covalent interaction to form an enzyme film. Therefore before each experiment, the working electrode needs to be polished to ensure that the surface area produces low non-Faradaic current. During the experiment, as the working electrode rotates rapidly, some of the enzymes are lost from the electrode surface, and some of the enzymes still stick on the electrode surface but lose their activity. Therefore after every scan, the electrode is taken out and polished with sandpaper again to remove inactive enzymes and form a new surface to allow a new layer of enzymes to adsorb.

It is worth noting that although the electrochemistry experiments are carried out anaerobically, the enzyme particle cofactor regeneration system can carry out the catalytic reactions in a normal environment, as the enzymes are all O_2 tolerant.

2.3 Other equipment

In addition to the molecular cloning facilities and the protein film electrochemistry set-ups, there are a number of other types of equipment used in this study. Gas chromatography and high-performance liquid chromatography are used to analyse, separate and quantify small

molecules including nicotinamide cofactors, substrates and products of enzymatic reactions. Ultraviolet-visible spectrometry is used specifically analysing nicotinamide cofactors, as NAD^+ and $NADP^+$ have a clear absorption peak at 260 nm, while NADH and NADPH have absorption peaks at both 260 nm and 340 nm (**Figure 2-5**). In the following section, these techniques will be discussed in detail.

2.3.1 Ultraviolet-visible spectrometry

A Cary® 50 ultraviolet-visible spectrophotometer from Agilent Technologies is used for cofactor scanning, and kinetics. According to the Beer-Lambert Law, the absorption (A) is equal to the concentration of the substrate (c) multiplied by the extinction coefficient (ε), and the path length (l). The concentration of nicotinamide cofactors is thus directly proportional to the absorbance[126].

$$A = \varepsilon c l$$

Therefore, in the experiments, to determine the concentration of nicotinamide cofactors, a standard curve is made by plotting the concentration of cofactor against the absorbance (260 nm for NAD^+ and $NADP^+$, 340 nm for NADH and NADPH). Then, the slope is used to calculate the cofactor concentration of unknown solutions.

A NanoVue™ from GE healthcare is also used for other non-quantitative detection of nicotinamide cofactors.

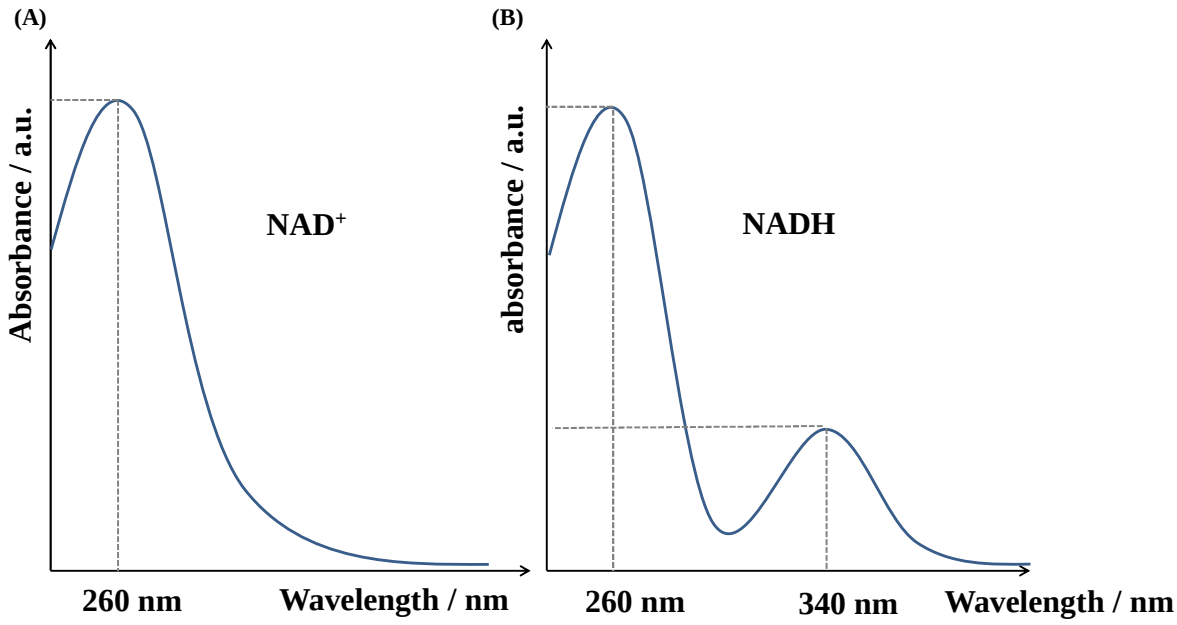


Figure 2-5 The UV-visible absorption spectrum of cofactors. (A)UV-visible spectrum of NAD(P)$^+$, a distinctive absorption peak at 260nm. (B) UV-visible spectrum of NAD(P)H, two distinctive absorption peaks at both 260 nm and 340 nm.

2.3.2 Gas chromatography

Gas chromatography (GC) is used in this study to detect the presence and the quantity of the reactant, intermediate and the product[127]. TRACE 1300 Gas Chromatograph from Thermo Scientific was used for these this experiments. This GC consists of a sample injector, a flame ionisation detector for sensing the signals of the samples, an auxiliary oven for heating up the samples, and the mobile phase carrier gas is helium. The GC column is TG-1MS (60 m×0.32 mm×1.0 µm, max temperature: 330/350 °C). The software we used was Chromeleon 7. In this study, GC is mainly used to separate, quantify, and analyse the substrates and products reactions with cofactor dependent enzymes coupled with the H_2 driven cofactor regeneration system. In order to detect and separate these chemicals in this experiment, the samples were first extracted from the aqueous phase to diethyl ether, and injected into the GC, then the following GC program was used: maintain at 45 °C for 5 minutes, increase the temperature to 220 °C with a rate of 60 °C/min, and maintain the temperature for another 3

minutes. The internal standard was 1-undecanol, which was added into the aqueous phase mixed with the samples and extracted to diethyl ether.

GC was also used to quantitatively determine the concentration of molecules and hence the conversion rate of reactions, as the peak area is directly proportional to the concentration of the corresponding chemical species when refered to a standard.

2.3.3 High-Performance Liquid Chromatography

High-Performance Liquid Chromatography (HPLC) is used in this study to detect, separate, and analyse different small molecules including nicotinamide cofactors, and other small organic substrates, intermediates, and products. High Performance Liquid Chromatography (HPLC) is a kind of column chromatographic instrument with pumps[128]. The HPLC pumps a sample mixture in a solvent (mobile phase) at high pressure through a column with chromatographic packing material (stationary phase). Different compounds of the sample mixture are separated through the column ready to be detected by the downstream sensors. Sample retention time, which is the time lapse for one chemical species to come out through the column and be detected by the sensor, is dependent on the column, and the solvent used. In this study, Prominence modular HPLC from Shimadzu was used.

A SeQuant® ZIC-HILIC column from Merck was used to separate nicotinamide cofactors. The base particle is silica, and the functional group is Sulfobetaine. The particle size of the column is 3.5-5 μm, and the pore size is 100-200 Å. The mobile phase used was Buffer A: 20 mM ammonium acetate in pure acetonitrile (pH 7.5), and Buffer B: 20 mM ammonium acetate in deionised water (pH 7.5). The method used to separate nicotinamide cofactors is: the cofactor mixture or individual cofactors are filtered prior to injecting to the system in order to get rid of any enzymes or particle debris that have the potential risk to block the column, then the HPLC starts with 80% Buffer A and 20% Buffer B, and this is gradually

changed to 20% Buffer A and 80% Buffer B over 8 min, and changed back to 80% Buffer A and 20% Buffer B over 1 min, and held for another 1 min. The flow rate is controlled at 1 $mL \cdot min^{-1}$ during this process. To detect the nicotinamide cofactors, ultraviolet–visible detection at wavelength of 260 nm and 340 nm was used. All the four nicotinamide cofactors are separated in the retention time range between 4 min and 8 min. Ideally each cofactor has the same unique retention time in different runs under the same conditions, so different cofactors can be distinguished from each other. In practice, the retention times for each cofactor shift a little bit between each run, due to slightly different conditions for the column, or the small concentration difference for the buffer made each time. In extreme conditions, the retention time changes dramatically, or the pressure of the column increases considerably, which indicates the column needs regeneration. To regenerate the column, the column is attached in reverse to the system, and washed with at least 30 column volumes of deionised water, then with at least 30 column volumes of 0.5 M NaCl buffer, and with at least 30 column volumes of deionised water, and at last the column is equilibrated with Buffer A and Buffer B. The regeneration step is expected to restore the functionality and give the right retention time for each cofactor.

2.4 Enzyme kinetics

Enzymes play important roles in living organisms, as almost every reaction that happens in living organisms is an enzymatic catalytic reaction. Most biological molecules are stable and slow to react with other molecules in the biological environments with neutral pH, mild temperature and aqueous phase. An enzyme can circumvent these problems by catalysing reactions within the cell. An enzymatic reaction takes place at the active site of the enzyme, which is usually a cave or a pocket on the surface of the enzyme consisting of a line of amino acids. The molecule bound within the active site is called substrate, and upon the action of

the enzyme, the substrate will be converted to product. The enzyme bound with its substrate is called an enzyme-substrate complex, which plays an important role in the theory of enzyme kinetics. A simplified enzyme reaction can be written as follow[37]:

$$E + S \rightleftharpoons ES \rightleftharpoons E + P \qquad [1]$$

Where E stands for enzyme, S stands for substrate, ES stands for enzyme-substrate complex, and P stands for product (**Figure 2-**).

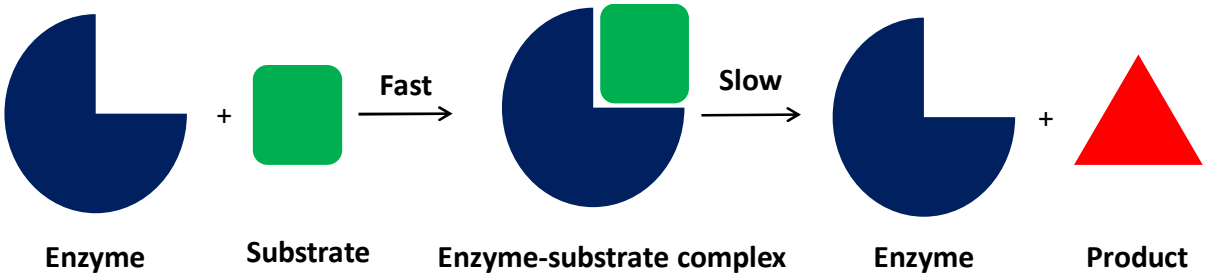


Figure 2-6 The schematic figure illustrates how a generalised enzymatic reaction works. The enzyme (blue) first binds with substrate (green) to form an enzyme-substrate complex, and this is a fast step. Then, the enzyme-substrate complex transforms into enzyme and product (red), and this is a slow step.

Another important parameter, free energy (G), describes the energy in the biological components. In a typical reaction, the substrate and the product have relative lower free energy, while in between them, there is a transition state when the substrate undergoes bond rearrangement, unstable charges, or other temporary transformation required for the reaction to proceed. The transition state has a much higher free energy compared with the product and the substrate, as they are highly unstable. The free energy difference between the transition state and the substrate (ΔG) is defined as the activation energy, which is the energy barrier to be overcome. The rate of a reaction is largely dependent on its activation energy: the higher the activation energy is, the slower the reaction is. Generally, by increasing temperature or pressure, more molecules will accumulate enough energy to overcome the activation energy so that the reaction will proceed. Alternatively, a catalyst can lower the activation energy of a reaction; therefore, it can accelerate the reaction (**Figure 2-**).

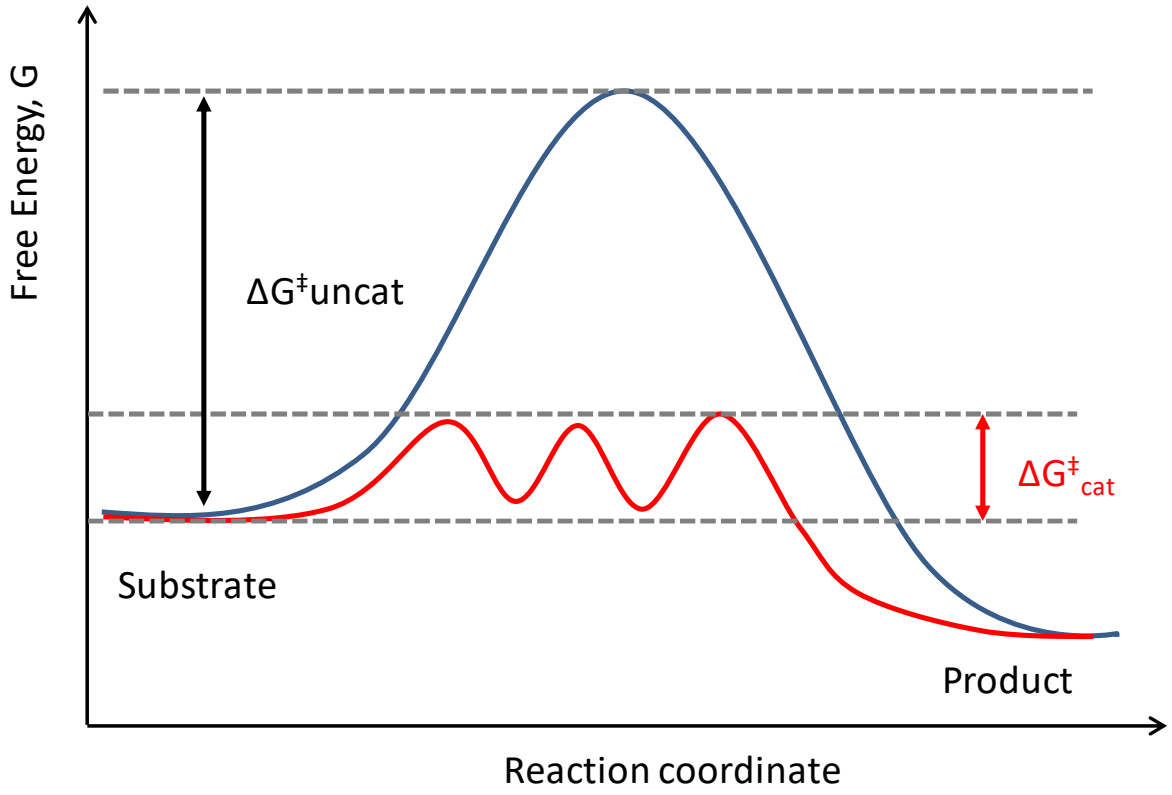


Figure 2-7 The diagram of free energy change in an enzymatic reaction. The blue line shows the energy change of a reaction without catalyst, the activation energy of which is $\Delta G^{\ddagger}_{uncat}$. The red line shows the energy change of a reaction with catalyst, the activation energy of which is $\Delta G^{\ddagger}_{cat}$. The catalyst lower the activation energy thus makes more molecules have enough free energy to overcome the barrier.

2.4.1 Affinity constant

An important parameter for enzyme kinetics is the initial rate V_0, when reaction commences. Initial rate is proportional to the substrate concentration [S], and as the reaction proceeds, substrate is consumed, so the rate will correspondingly drop. Michaelis and Menten proposed an enzymatic mechanism theory in 1913 that the enzyme first combines reversibly with its substrate to form enzyme-substrate complex[129]. The enzyme-substrate complex then breaks into free enzyme and product in a much slower step. As the second step is much slower than the first step, the overall rate of the reaction is determined by the second step, meaning that the overall rate is proportional to the concentration of enzyme-substrate complex. In an ideal reaction, the enzyme is present exclusively in two forms, the free

enzyme [E], and the enzyme-substrate complex [ES]. If the enzymes are saturated with substrate, meaning all the enzymes are in the [ES] form, then the reaction achieves its maximum rate, V_{max}. At the start of a reaction, there is hardly any product formed, so it is assumed that the enzyme-substrate complex to free enzyme and product step is irreversible, and described as k_2, while the reversible step of enzyme and substrate to enzyme-substrate complex are described as k_1 and k_{-1}.

$$E + S \underset{k_{-1}}{\overset{k_1}{\rightleftharpoons}} ES \xrightarrow{k_2} E + P \quad [2]$$

V_0 is determined by [ES].

$$V_0 = k_2[ES] \quad [3]$$

Then, the total concentration of enzyme is designated as $[E_t]$, which equals the free enzyme [E], and the enzyme-substrate complex [ES].

$$[E_t] = [E] + [ES] \quad [4]$$

The rate of [ES] formation is proportional to k_1, [E] and [S].

$$v_{[ES]formation} = k_1([E_t] - [ES])[S] \quad [5]$$

The rate of [ES] breakdown is the rate of [ES] return to [E] and [S], together with the rate [ES] turn to [E] and [S]:

$$v_{[ES]breakdown} = k_{-1}[ES] + k_2[ES] \quad [6]$$

According to the steady-state assumption, the initial rate of the reaction reflects a constant concentration of [ES], which means the breakdown of [ES], is the same as the rate of formation of [ES].

$$v_{[ES]breakdown} = v_{[ES]formation} \quad [7]$$

The expressions above can give:

$$k_1([E_t] - [ES])[S] = k_{-1}[ES] + k_2[ES] \quad [8]$$

The expression can be rewritten as an equation for [ES]:

$$[ES] = \frac{[E_t][S]}{[S] + \frac{k_{-1} + k_2}{k_1}} \quad [9]$$

The term $(k_{-1}+k_2)/k_1$ is defined as the Michaelis-Menten constant, K_M. So the equation can be simplified as:

$$[ES] = \frac{[E_t][S]}{[S] + K_M} \quad [10]$$

Coupled with [3]:

$$V_0 = \frac{k_2[E_t][S]}{K_M + [S]} \quad [11]$$

According to the definition of V_{max}, it is the velocity when all the enzymes are saturated with substrate ([ES] = [E_t]):

$$V_{max} = k_2[E_t] \quad [12]$$

Therefore, [11] can be further simplified as follow:

$$V_0 = \frac{V_{max}[S]}{K_M + [S]} \quad [13]$$

This is the Michaelis-Menten equation, which describes the relationship between the initial velocity, the maximum velocity, and the initial substrate concentration (**Figure 2-**). Given $K_M = [S]$, then $V_0 = \frac{1}{2}V_{max}$, which means K_M equals to the concentration of substrate when the enzyme reaches half of its maximum velocity. At low substrate concentration, K_M >>[S], the Michaelis-Menten equation can be rewritten as:

$$V_0 = \frac{V_{max}}{K_M}[S] \quad [14]$$

So the initial velocity is linearly dependent solely on the concentration of substrate. On the other hand, at very high substrate concentration, K_M <<[S], the Michaelis-Menten equation can be rewritten as:

$$V_0 = V_{max} \quad [15]$$

In practice, V_{max} cannot be reached, but when [S] is higher than ten times K_M, $V_0 > 0.9\ V_{max}$, it is regarded that V_0 is close to V_{max}.

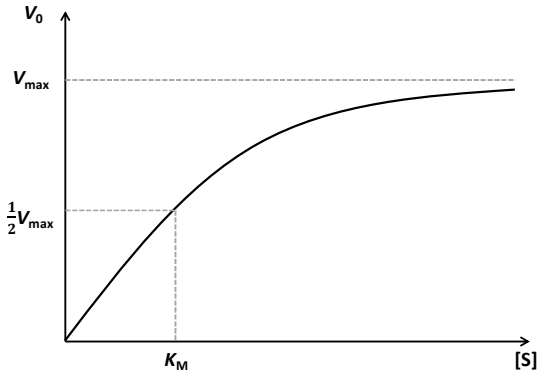


Figure 2-8 The Michaelis-Menten plot shows that when the concentration of the substrate reaches K_M, the speed of the reaction reaches half of its maximum. When the concentration of substrate increases the speed of the reaction also increases until ever close to the theoretic maximum speed V_{max}.

In this study, K_M is a crucial parameter to describe the affinity of enzymes to their substrate. If K_M is low, the enzyme can work efficiently at low concentration of substrate. As a desirable $NADP^+$-reductase is explored in this study, an ideal candidate of $NADP^+$-reductase should have a low K_M^{NADP} so that it can work as a NADPH regenerator with only a catalytic amount of $NADP^+$ present in the system. A major task of this project is to characterise the K_M for different cofactors for different $NADP^+$-reductases electrochemically. In order to determine K_M a series of substrate concentrations was added, and the initial velocity was obtained electrochemically. As the Michaelis-Menten equation does not plot a straight line, it is hard to calculate the K_M value directly. In this way, a number of rewritten Michaelis-Menten equations are proposed to simplify the calculation process. By taking reciprocals of both sides of the Michaelis-Menten equation, a Lineweaver Burk equation is obtained[130]:

$$\frac{1}{V_0} = \frac{1}{V_{max}} + \frac{K_M}{V_{max}} \cdot \frac{1}{[S]} \qquad [16]$$

A plot of $1/V_0$ against $1/[S]$ will generate a straight line, and the slope equals to K_M/V_{max} and the y-interception equals $1/V_{max}$.

By multiplying both sides of Lineweaver and Burk equation with [S], an equation for a plot called the Hanes-Woolf plot is obtained[131]:

$$\frac{[S]}{V_0} = \frac{K_M}{V_{max}} + \frac{1}{V_{max}}[S] \quad [17]$$

A plot of $[S]/V_0$ [S] will give a straight line as well, and the x-intercept is -K_M. In this study, K_M calculated with all three methods (Michaelis-Menten, Lineweaver Burk, and Hanes-Woolf) will be presented and discussed.

Another important parameter to characterise enzyme kinetics is the rate constant k_{cat}, which describes the limiting rate of enzyme-catalysed reaction when enzymes are saturated with substrate. k_{cat} is also called turnover number, which represents the number of substrate molecules converted to product in a unit time by a single enzyme molecule. In this way, k_{cat} can be written as follows:

$$k_{cat} = {V_{max}}/{[E_t]} \quad [18]$$

So the Michaelis-Menten equation can be rewritten:

$$V_0 = \frac{k_{cat}[E_t][S]}{K_M + [S]} \quad [19]$$

The affinity constant K_M and the turnover number k_{cat} are both important parameters to evaluate enzyme efficiency, but either of the parameters alone is not enough to characterise the overall performance of an enzyme. Therefore the best way to compare the behaviour of two enzymes is to compare the ratio of k_{cat}/ K_M, called a specificity constant. A high specificity constant indicates the enzyme is robust and efficient for catalysing reactions.

2.4.2 Inhibition constant

Enzymes can be inhibited by some molecules called inhibitors[132]. For example, hydrogenases can be inhibited by carbon monoxide[133]. There are generally three different

types of inhibition: competitive, uncompetitive, and mixed inhibition. In the case of competitive inhibition, the inhibitor competitively binds to the enzyme catalytic site and prohibits the substrate from binding. This process is usually reversible. When the inhibitor is removed, the enzyme will recover its activity. The CO inhibition of hydrogenase is a typical example of competitive inhibition. In the case of uncompetitive inhibition, the inhibitor binds to the enzyme-substrate complex and prevents the further transformation. In the case of mixed inhibition, the inhibitor binds to both the enzyme catalytic site and the enzyme-substrate complex. In all these three cases, the inhibition decreases the apparent maximal activity V_{max}^{app}, and the apparent Michaelis-Menten constant K_M^{app}. V_{max}^{app} and K_M^{app} for different types of inhibition are summarised in the table below, where [i] represents the concentration of inhibitor, K_{IC} represents the inhibition constant for competitive inhibition, and K_{IU} represents the inhibition constant for uncompetitive inhibition (**Table 2-1**).

Table 2-1 Kinetic constants for different types of inhibition.

Type of inhibition	V_{max}^{app}	K_M^{app}
Competitive	V_{max}	$K_M(1+\frac{[i]}{K_{IC}})$
uncompetitive	$\frac{V_{max}}{1+\frac{[i]}{K_{IU}}}$	$\frac{K_M}{1+\frac{[i]}{K_{IU}}}$
mixed	$\frac{V_{max}}{1+\frac{[i]}{K_{IU}}}$	$\frac{K_M(1+\frac{[i]}{K_{IC}})}{1+\frac{[i]}{K_{IU}}}$

A modified Michaelis-Menten equation was proposed by Dixon to describe competitive inhibition[134].

$$V_0 = \frac{V_{max}[S]}{K_M\left(1+\frac{[i]}{K_{IC}}\right)+[S]} \quad [20]$$

Taking reciprocals of both sides of the modified Michaelis-Menten equation gives:

$$\frac{1}{V_0} = \frac{K_M[i]}{V_{max}[S]K_{IC}} + \frac{1}{V_{max}}(1 + \frac{K_M}{[S]}) \quad [21]$$

A plot of $1/V_0$ against the concentration of inhibitor [i] generates a straight line, while the concentration of substrate [S] is constant. At several different substrate concentrations, the corresponding plots intersect when [i] and $1/V_0$ are the same, and the point of intersection of Dixon plots equals to $-K_{IC}$. The Dixon equation can be further changed to a Cornish-Bowden equation by multiplying both sides by [S][135]:

$$\frac{[S]}{V_0} = \frac{K_M}{V_{max}.K_{IC}}[i] + \frac{[S] + K_M}{V_{max}} \quad [22]$$

If $[S]/V_0$ is plotted against [i], a straight line is generated, namely Cornish Bowden plot. In the case of competitive inhibition, Dixon plots of different substrate concentration intersect at $-K_{IC}$, while Cornish-Bowden plots of different substrate concentration give a set of parallel lines. In the case of uncompetitive inhibition, Dixon plots of different substrate concentration give a set of parallel lines, while Cornish-Bowden plots intersect at $-K_{IU}$. In the case of mixed inhibition, both Dixon plots and Cornish-Bowden plots of different substrate concentration intersect at $-K_I$. In this way, both the type of inhibition and the inhibition constant can be determined by a combination of both plots (**Figure 2-6**).

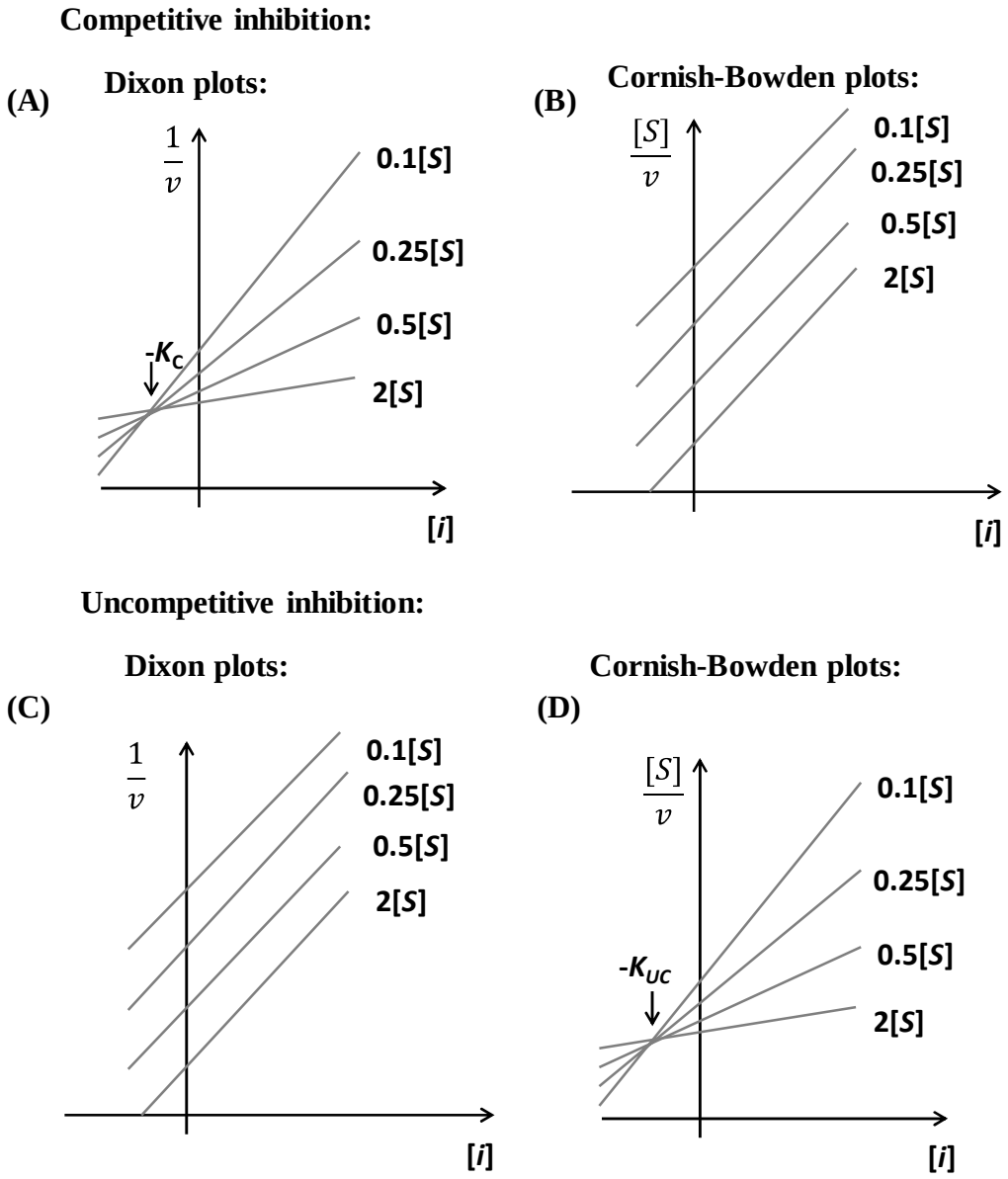


Figure 2-6 (A) The Dixon plots for competitive inhibition intersect at $-K_C$ (B) The Cornish-Bowden plots for competitive inhibition are parallel. (C) The Dixon plots for uncompetitive inhibition are in parallel. (D) The Cornish-Bowden plots for uncompetitive inhibition intersect at $-K_{UC}$.

Inhibition is also very important in this study, especially for NAD^+ reductase and its variants, $NADP^+$-reductases, as previous work illustrated that these enzymes are inhibited by their own products. For example, NAD^+ reduction catalysed by NAD^+-reductase is inhibited by NADH. Therefore, as the reaction proceeds, the products are accumulated, the activity of the enzymes decreases. In this way, it is crucial to determine the inhibition type and constant for these enzymes. In the cofactor regeneration systems, both the reduced and oxidised

cofactors are present, so a desirable NAD(P)$^+$-reductase for a cofactor regeneration system is expected to have a high inhibition constant, which means it will not be inhibited at low concentration of either form of the cofactor.

2.4.3 The relationship between enzyme kinetics and electrochemistry

In this thesis, the affinity constants of NAD(P)$^+$-reductases are characterised using protein film electrochemistry described earlier in this chapter. Conventionally, biochemical approaches are applied to determine the kinetic and thermodynamic parameters for oxidoreductases, using a chemical reductant such as benzyl viologen or methyl viologen in solution activity assays. Benzyl viologen or methyl viologen can be reduced by NAD(P)H catalysed by NAD(P)$^+$-reductase. The reduced benzyl viologen and methyl viologen are purple, while the oxidised forms are colourless. In this way, the reaction can be monitored by UV visible spectroscopy, and the conversion of cofactors can be calculated indirectly. In this way, K_M and k_{cat} can be determined. However, biochemical approaches are limited by the requirement for benzyl viologen or methyl viologen as artificial redox co-substrate, which might hinder or confuse the determination of enzyme parameters.

On the contrary, an electrochemical approach only requires cofactors as the sole substrate for enzyme catalysed reactions. Instead of passing the electrons to viologen, the destination of the electrons of the electro-driven reaction is through the electrode to the potentiostat. So in protein film electrochemistry, to calculate the converted cofactor in a unit time, the catalytic current is measured. According to the half reaction of cofactors, each NAD(P)$^+$ requires two electrons to be converted to NAD(P)H, and each NAD(P)H loses two electrons as it is oxidised to NAD(P)$^+$. The number of electrons passing through the electrode in a unit time is the catalytic current. In this way, the magnitude of the catalytic current is directly proportional to the catalytic rate of the enzyme film.

In a chronoamperometry experiment, a series of substrate injections are applied causing the catalytic current to jump. As the magnitude of the current is directly proportional to the enzyme catalytic rate, a plot of the catalytic rate against substrate concentration can be drawn. By fitting the plot to the Michaelis-Menten equation, the affinity constant K_M is thus determined. In this thesis, as it is less reliable to fit a sigmoidal function, substrate concentration divided by catalytic rate is plotted against substrate concentration to obtain a Hanes-Woolf plot which in the ideal case is a straight line. By fitting the Hanes-Woolf plot, the affinity constant K_M can also be determined.

In theory, calculating the catalytic current can also determine the turnover number of the enzyme. The catalytic current indicates the number of electrons going through the electrode at a unit time, which is directly proportional to the number of substrate molecules converted by the enzymes on the electrode. So the turnover number at a specific potential can be determined by the current divided by the number of enzyme molecules adsorbed on the electrode. However, as the actual number of enzymes adsorbed on the surface of electrode is unknown, it is usually impossible to obtain the turnover number by protein film electrochemistry. It is not necessary to know the enzyme coverage in order to determine a K_M value however.

Chapter Three: Electrochemical characterisation of *Ralstonia eutropha* soluble hydrogenase and its variants

As discussed in Chapter one, the Vincent group has developed a modular H_2-driven NADH regeneration system, and has coupled it with a number of NADH-dependent enzymes to demonstrate its efficiency. However, a number of redox enzymes are NADPH-dependent; either exclusively using NADPH, or favouring NADPH over NADH. For instance, $P450_{BM3}$ monooxygenase which catalyses the hydroxylation of C-H bonds requires exclusively NADPH as its redox equivalent. Imine reductase and alkene reductase favour NADPH over NADH. Therefore, the established NADH regeneration system is either not feasible, or gives low efficiency. Thus, a novel NADPH regeneration system is required for recycling NADPH for these enzymes.

There are a number of strategies for NADPH recycling such as glucose and glucose dehydrogenase, and there have been a few reports of successful H_2-driven NADPH regeneration system. For instance, Liese and co-workers has isolated the soluble hydrogenase I from the marine hyperthermophilic strain of the archaeon *Pyrococcus furiosus*, and coupled it with thermophilic NADPH-dependent alcohol dehydrogenase from *Thermoanaerobium* sp. to catalyse the reduction of acetophenone and (*2S*)-hydroxy-1-phenyl-propanone to the corresponding (*S*)-alcohol and (*1R,2S*)-diol. The soluble hydrogenase I was used as NADPH regenerating enzyme by supplying H_2. However, this hydrogenase is very sensitive to O_2, therefore greatly limiting its applications. The work in this chapter seeks to develop an O_2 insensitive modular H_2 driven cofactor regeneration system. The NAD^+-reductase enzyme is targeted to convert the system from NADH recycling to NADPH recycling by either replacing the enzyme with a new $NADP^+$ reductase or modifying the NAD^+-reductase to form a $NADP^+$-reductase. This chapter focuses on the screening of variants generated by site directed mutagenesis of NAD^+-reductase *Re*SH (HoxHYFU). As discussed in chapter one, the H_2-driven NADH regeneration system consists of three enzymes. The hydrogenase (hyd-2 from *E. coli*) is in charge of splitting H_2 molecules and transferring the electrons and protons. The soluble hydrogenase HoxHYFU from *Ralstonia eutropha* (*R.e* SH) reduces NAD^+ to NADH utilising the electrons from H_2 splitting. The third enzyme, a NADH-dependent enzyme, takes the recycled NADH to perform the desired reactions. In this system, *R.e* SH plays a central role. In order to recycle NADPH, it is essential to allow *R.e* SH to bind $NADP^+$ and to reduce it to NADPH. A number

of *R.e* SH variants were produced by site directed mutagenesis based on the homologue structure of *R.e* SH catalytic pocket for binding cofactors. Three residues around the catalytic site are identified as crucial for cofactor binding and four variants are produced. To screen the best candidate for a NADPH recycling system from the four variants, electrochemistry methods were applied. As discussed in chapter two, protein film electrochemistry methods are applied to determine the activity and affinity constant of each enzyme towards different cofactors. This project is in collaboration with Dr Oliver Lenz from Technical University Berlin. The enzymes used in this chapter are wildtype *R.e* SH, variant HoxF^{E341A}, variant HoxF^{D467S}, variant HoxF$^{E341A, D467S}$ and variant HoxF$^{E341A, S342R}$, supplied by Lenz Group.

3.1 Electro-catalytic behaviour assays

First, electro-catalytic behaviour for each enzyme was investigated. According to enzymology theory, enzyme activity measures the number of substrate molecules one single enzyme catalyses within one-unit time. The activity is sometimes referred as turnover number. Turnover number is a crucial parameter to characterise the capability of an enzyme. The activity of an enzyme depends on a number of factors including pH, temperature, and it is also affected by inhibitors or activators. In traditional biochemical approaches, the substrate or product change is measured directly or indirectly at the beginning of an enzyme-catalysed reaction to calculate the activity of the enzyme. Colorimetric assays are often applied to simplify the process.

On the other hand, in protein film electrochemistry approaches, the current response is used to characterise the electro-catalytic behaviour of enzymes. As discussed in chapter two, a target enzyme is immobilised on the working electrode and the electrode is immersed into an electrochemical cell containing buffer and substrate. In a cyclic voltammetry experiment, the potential applied on the electrode is swept between given values. At the potential where the catalysed reaction occurs, a catalytic current is observed. The magnitude of the current varies dependent of the electrochemical driving force. The magnitude of catalytic current also depends on pH, temperature, substrate concentration, and the number of active enzyme molecules immobilised on the electrode surface.

The magnitude of catalytic current reflects the number of electrons passing through the electrode due to the catalytic reaction within a unit time. Thus, the magnitude of the current is directly proportional to the activity of the enzyme, or the turnover number. It is worth noting that the exact activity or the turnover number usually cannot be calculated based on protein film electrochemistry, as there is no easy way to calculate the exact number of enzyme molecules adsorb on the electrode and contribute to the current. In this way, the magnitude of current from PFE only provides a relative activity.

Usually a couple rounds of cyclic voltammetry are carried out on an enzyme film, to examine the behaviour of the enzyme in response to one particular set of conditions. In most cases, at each round of the cyclic voltammetry, the catalytic current decreases. This is partly due to the enzyme film loss caused by the high-speed rotation of the electrode, but may also be due to the loss of activity of the enzyme during the electro-driven redox reaction. The cyclic voltammetry also showed that on the first round, the non-Faradaic current was often much higher than the rest of the rounds. In this way, the second round of cyclic voltammetry is used in this thesis for any figures, analysis, comparisons and discussions.

3.1.1 Cyclic voltammetry of NAD^+ reduction

First, the cyclic voltammetry of wildtype *R.e* SH for NAD^+ reduction was tested for comparison with published data[95]. The protein film electrochemistry facility was set up follow the protocol described as follow. Five mL Tris buffer (50 mM, pH 8.0) with 5 mM NAD^+ dissolved in it was put into the electrochemical cell, and the water jacket surrounding the cell was set to be 30 °C. This temperature was chosen because previous work done by Idris demonstrated *R.e* SH reached its highest activity at 30 °C and pH 8.0[95]. Then 0.5 µL enzyme solution containing *R.e* SH (1-3 mg/mL) was spotted on the working electrode, left for 1-2 min to allow the enzyme to adsorb on the electrode. The working electrode was screwed to the rotator and rotated at 2000 rpm, and a potential range between +0.2 V to -0.45 V (vs SHE) was applied to the system at the rate of 0.1 V/s. The result showed that *R.e* SH had high activity towards NAD^+ reduction as expected. At high potential, no current is observed.

When the potential reached -0.3 V, negative catalytic current was observed, and as the potential was swept more negative, the current magnitude increased significantly. When the potential reached - 0.46 V, the catalytic current was around -5 μA. The theoretical potential for the NAD^+/NADH couple is -0.34 V at pH 7, defined for 1:1 NAD^+ : NADH. As expected, the onset for catalysis is more positive than this when only NAD^+ is added to the solution. For comparison, according to the thesis of Zul Idris[136], the same experiment was carried out on a blank electrode under the same conditions. The working electrode was not modified with enzyme this time and the potential was swept between 0.2 V to -1.0 V. At bare electrode, the reduction of NAD^+ occurred at -0.75 V, and when the potential reached -0.1 V, the current was around -20 μA. This indicated that without enzyme catalyst, the NAD^+ reduction still happens but required a large overpotential. The enzyme *R.e* SH thus significantly lowers the overpotential so that the reaction happens near the theoretical redox potential of NAD^+ reduction. The overpotential is crucial as it determines whether the overall H_2-driven cofactor recycling process is feasible or not. The overpotential for NAD^+ and $NADP^+$ reduction is a critical parameter for determination of whether a new enzyme is feasible for the cofactor regeneration system or not. As discussed before, the H_2 splitting catalysed by hydrogenase *hyd2* and the reduction of NAD^+ is coupled, so it is necessary that the potential of NAD^+ reduction is higher than H_2 splitting thus allowing the electrons to flow from H_2 to NAD^+ spontaneously. Otherwise, if the enzyme catalysing NAD^+ reduction has a large overpotential such that the potential for NAD^+ is lower than the H_2 splitting, the overall process would no longer occur at a reasonable rate.

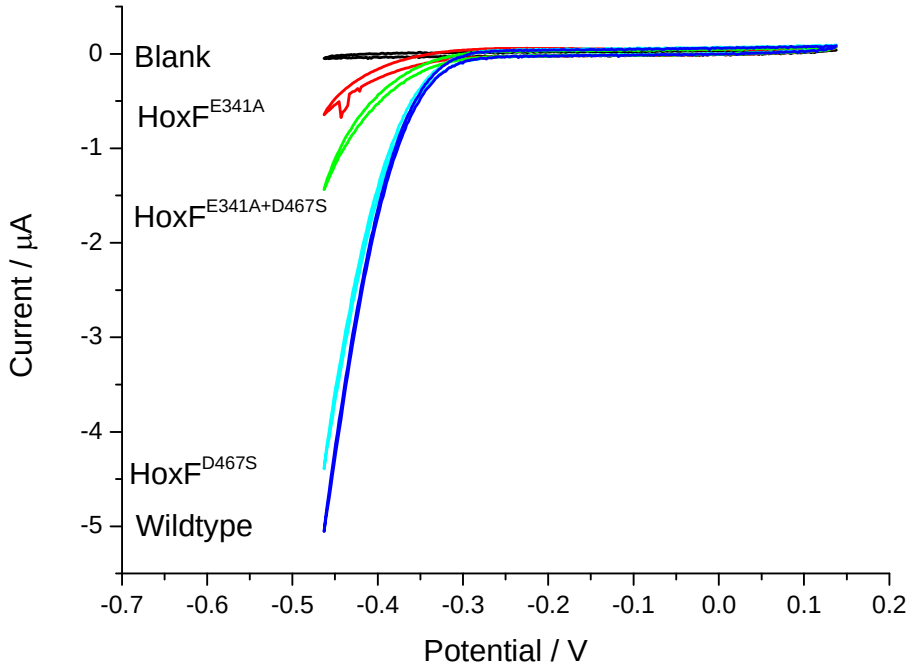


Figure 3-1: Cyclic voltammetry of the variants (5 mL Tris buffer, pH 8.0, 5 mM NAD^+, 30 °C): bare electrode with no cofactor presence blank (black), variant $HoxF^{E341A}$ (red), variant $HoxF^{E341/D467S}$ (green), $HoxF^{D467S}$ (cyan), and wildtype (blue).

Cyclic voltammetry for NAD^+ reduction catalysed by other variants was also carried out, under the same conditions as that of wildtype *R.e* SH, so that it was easier to compare the performance of different variants (**Figure 3-1**). The results showed that different variants behaved differently. The variant *R.e* SH $HoxF^{D467S}$ had high NAD^+ reduction activity, and the catalytic current reached -4.5 µA at -0.45 V (vs SHE), which was comparable to that of native *R.e* SH. This indicated that the single mutation which altered the residue of HoxF subunit from aspartic acid to serine did not significantly change the activity of the NAD^+ reduction of the enzyme. In contract, the other single variant *R.e* SH $HoxF^{E341A}$ showed greatly decreased activity towards NAD^+ reduction, and the catalytic current only reached around -0.5 µA at -0.45 V (vs SHE). This was ten times lower than that of the native *R.e* SH and nine times lower than that of variant *R.e* SH $HoxF^{D467S}$. This indicated that the single mutation which altered the residue of HoxF subunit from aspartic acid to serine great lowered the activity of the NAD^+ reduction of the enzyme. The double variant combining the two mutations of the single variants *R.e* SH $HoxF^{E341A,\ D467S}$ also showed significantly lower activity

towards NAD^+ reduction. The catalytic current of *R.e* SH $HoxF^{E341A, D467S}$ for NAD^+ reduction at -0.45 V (vs SHE) was about -1.5 μA, which was significantly lower than that of native *R.e* SH and the single variant *R.e* SH $HoxF^{D467S}$, but higher than that of variant *R.e* SH $HoxF^{E341A}$. The other double variant *R.e* SH $HoxF^{E341A, S342R}$ has similar NAD^+ reduction activity, and the catalytic current at -0.45 V (vs SHE) was -0.6 μA, very close to that of variant *R.e* SH $HoxF^{E341A}$.

It is worth noting that although different variants had different NAD^+ reduction activity, the onset potential for NAD^+ reduction remained the same for all variant and the native *R.e* SH, all at -0.30 V (vs SHE).

3.2 Cyclic voltammetry of $NADP^+$ reduction

As the purpose of this project is to find the best candidate for NADPH recycling, the more important data were the behaviours of the variants for $NADP^+$ reduction. The cyclic voltammetry of $NADP^+$ reduction for native *R.e* SH and all the variants were carried out.

HPLC testing showed that the $NADP^+$ sample contained trace amounts of NAD^+, which could convolute the results of $NADP^+$ reduction. The previous experiments had demonstrated that although variant *R.e* SH $HoxF^{E341A}$ and double variant *R.e* SH $HoxF^{E341A, S342R}$ were inert to NAD^+, both the native *R.e* SH and the single variant *R.e* SH $HoxF^{D467S}$ were highly activity towards NAD^+. Thus, only a trace amount of NAD^+ contamination in $NADP^+$ would potentially significantly change the cyclic voltammetry results. Moreover, NADH samples also contained trace amount of NAD^+, while NADPH samples contained trace amounts of NAD^+, NADH, and $NADP^+$. For this reason, unless otherwise stated, all NADH, $NADP^+$, and NADPH samples were purified according to the procedure stated in Chapter two prior to using in any electrochemistry assays.

In the electrochemistry of NAD^+-reductase enzymes such as *R.e* SH and its variants, substrate is essential for the stability of the protein at the potential where the redox reaction happens. Cyclic voltammetry of the NAD^+-reductase in the absence of the cofactors showed a peak at around -0.25 V vs SHE, which correlates with the reduction potential of FMN at a carbon electrode. As the protein

contains FMN at the catalytic site, this suggested that the FMN in the protein might fall out and interact with the electrode. In the presence of the cofactors, it will enter the catalytic site of the enzymes, and act as a bottle stopper to prevent the FMN from falling out. However, at the absence of the cofactors, FMN has a high tendency to disassociate from the protein catalytic site and either release to the buffer or stick on the electrode when the enzyme is posed at a potential that the redox reaction happens. To exclude the possibility that free FMN on the electrode catalyses the redox reaction of NAD^+ and NADH, a set of control experiments were carried out. First, the electronic cell was filled with Tris Buffer (50 mM, pH 8.0) and 1 mM FMN. The bare electrode remained unmodified by enzyme. Then a cyclic voltammetry was carried out between 0.234 and -0.667 V vs SHE (**Figure 3-2A**). The electrode was kept with no rotation. The result clearly showed that FMN reduction commenced at -0.22 V vs SHE and the catalytic current increased as the potential went lower until reaches its maximum of around 6 μA at -0.34 V vs SHE, and then the catalytic current began to decrease. At the reverse scan, the oxidation of FMN was observable, as the electrode was not rotating, so the reduced FMN accumulated around the electrode. In this way, at the reverse scan, FMN would be oxidised back to its oxidation state. The result showed that FMN oxidation started at around -0.41 V vs SHE and the catalytic current increased as the potential went higher until reaches its maximum of around 3 μA at -0.28 V vs SHE, and then the catalytic current began to decrease. Next, the electrode was modified by FMN. High concentration FMN solution was spotted on the electrode and waited for 1 min to allow it to adsorb on the electrode. The electronic cell was filled with Tris Buffer (50 mM, pH 8.0) and no FMN was added into the buffer. Then a cyclic voltammetry was carried out, and the electrode was rotating at the speed of 2000 rpm. For better comparison, a black cyclic voltammetry was also carried out that no FMN was added to the buffer, and the electrode was not modified by FMN (**Figure 3-2B**). Although the result was less obvious than the previous result when FMN was dissolved in the buffer, by compare with the blank cyclic voltammetry, the FMN redox peaks could still be identified. Particularly, the oxidation peak was more obvious than the reduction peak. At last, the electronic cell was filled with Tris buffer (50 mM, pH 8.0), 1 mM NAD^+ and 1 mM NADH. The electrode was modified by FMN. Another cyclic voltammetry was

carried out, and the electrode was rotating at 2000 rpm. This time, the redox peaks of FMN was also observed. Nevertheless, no NAD^+ reduction or NADH oxidation was observed. These results showed that although FMN has redox activity on the electrode, and catalytic current is observable, it cannot catalyse the redox reaction of cofactors. Only FMN-bound NAD^+ reductase and its variants have the potential of catalyse the cofactors reactions.

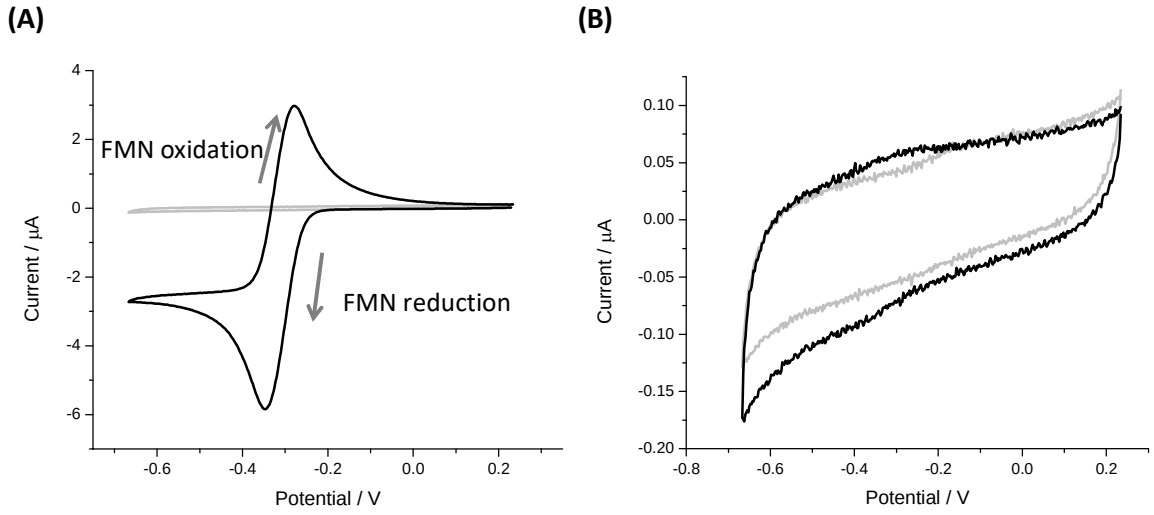


Figure 3-2: (A) Cyclic voltammetry of 1 mM FMN in the solution (black), and a blank cyclic voltammetry with only buffer (grey). (B) Cyclic voltammetry of the FMN adsorb on electrode (black), and bare electrode (grey).

Cyclic voltammetry of $NADP^+$ reduction catalysed by *R.e* SH and its variants were carried out. The procedure was similar with that of NAD^+ reduction cyclic voltammetry. The electronic cell was filled with Tris buffer (50 mM, pH8.0), and 5 mM $NADP^+$. The electrode was modified with relevant enzymes. When the cyclic voltammetry was carrying out, the electrode rotated at 2000 rpm, and the potential range applied was between 0.2 V to -0.45 V (vs SHE), at a scan rate of 0.1 V/s. The results were different from NAD^+ reduction. Generally, all the cyclic voltammetry showed reduced activity towards the reduction of $NADP^+$ compared with the reduction of NAD^+. Therefore, the noise-to-signal ratio was significantly lower for the $NADP^+$ reduction cyclic voltammetry than that of NAD^+ reduction. The vibration of current was clearly seen. This was partly due to the reason that the electrode was rapidly rotating causing the whole electrochemical system vibrating.

The results for the *R.e* SH wildtype enzyme and its variants were also different for $NADP^+$ reduction. Compared with the blank cyclic voltammetry, the wildtype enzyme showed hardly any activity at all towards $NADP^+$ reduction. This indicated that the wildtype enzyme only accepts NAD^+ and NADH as its substrate. As discussed in chapter two, the crystal structure of *R.e* SH wildtype enzyme and its catalytic site is a key factor for substrate binding. In this way, the hypothesis is that two reasons lead to the fact that $NADP^+$ cannot bind with the wildtype enzyme. First, the size of catalytic site is not big enough to accommodate the extra phosphate group in $NADP^+$. Second, the negatively charged catalytic site expels the also negatively charged $NADP^+$, as the additional phosphate group of $NADP^+$ introduce additional negative charges on the whole molecule. The variants showed increased activity towards $NADP^+$ reduction, as the mutations introduced to the enzyme was designed to either enlarge the catalytic site or make the catalytic site less negatively charged in order to fit in $NADP^+$. Nevertheless, the activity of $NADP^+$ reduction varied for different variants. The variant $HoxF^{D467S}$ is designed to make the catalytic site less negative, as aspartic acid is negatively charged while serine is an electro-neutral amino acid. This mutation contributes little to alter the size of the catalytic pocket, as this residue is distal away from the substrate binding centre. Although the cyclic voltammetry showed catalytic current for $NADP^+$ reduction compared with the wildtype enzyme, the activity of $NADP^+$ reduction for $HoxF^{D467S}$ is low, with the catalytic current only reached -0.15 µA at -0.45 V (vs SHE). This is more than ten times lower than the catalytic current for wildtype enzyme catalysed NAD^+ reduction. The variant $HoxF^{E341A}$ on the other hand, was dedicated to both enlarge the catalytic site and decrease the negative charge altogether. Glutamic acid is a long chain negatively charged amino acid, while alanine is a short chain electro-neutral amino acid. Moreover, unlike residue 467 which is at the edge of the catalytic pocket, far from the substrate binding site, residue 341 the glutamic acid interacts closely with the hydroxyl group of NAD^+ or NADH. In this way, by replacing this residue from glutamic acid to alanine, the catalytic pocket became less negatively charged, and the shorter chain alanine also made more space for the additional phosphate group in $NADP^+$ and NADPH. The result for variant $HoxF^{E341A}$ cyclic voltammetry showed higher

activity for $NADP^+$ reduction than that of variant $HoxF^{D467S}$. Lastly, the double mutant $HoxF^{E341A, D467S}$ which combined both tow mutations was tested for cyclic voltammetry. The result for $HoxFE341A^{, D467S}$ showed that this variant had higher activity for $NADP^+$ reduction than the previous two variants. The cyclic voltammetry of $NADP^+$ reduction for $HoxF^{E341A, D467S}$ showed a clear onset at the potential where the redox reaction happens, and the catalytic current reached 0.38 μA at -0.45 V vs SHE.

The cyclic voltammetry result for $NADP^+$ reduction also indicates the behaviours of substrate interact with the enzymes. *R.e* SH wildtype and its variants have shown a tendency of FMN molecule in their catalytic pocket falling out from the enzyme at low potential with absence of substrate. Sometimes, the falling FMN molecules stick on the electrode and can be detected and observed from cyclic voltammetry. The cyclic voltammetry of wildtype enzyme and variant $HoxF^{D467S}$ both showed a peak related to FMN reduction. There are two possible reasons for low activity of $NADP^+$ reduction for the *R.e* SH wildtype and variant $HoxF^{D467S}$: the substrate binds with the enzyme but the enzyme cannot catalyse the reaction, or the substrate does not bind with the enzyme. The cyclic voltammetry had clearly showed the falling out of FMN indicating that the substrate $NADP^+$ did not bind with the enzyme at all (**Figure 3-3**). This is within our expectation as the size of the catalytic pocket is crucial for accommodating the substrate, particularly Glu341 at the bottom of the catalytic pocket.

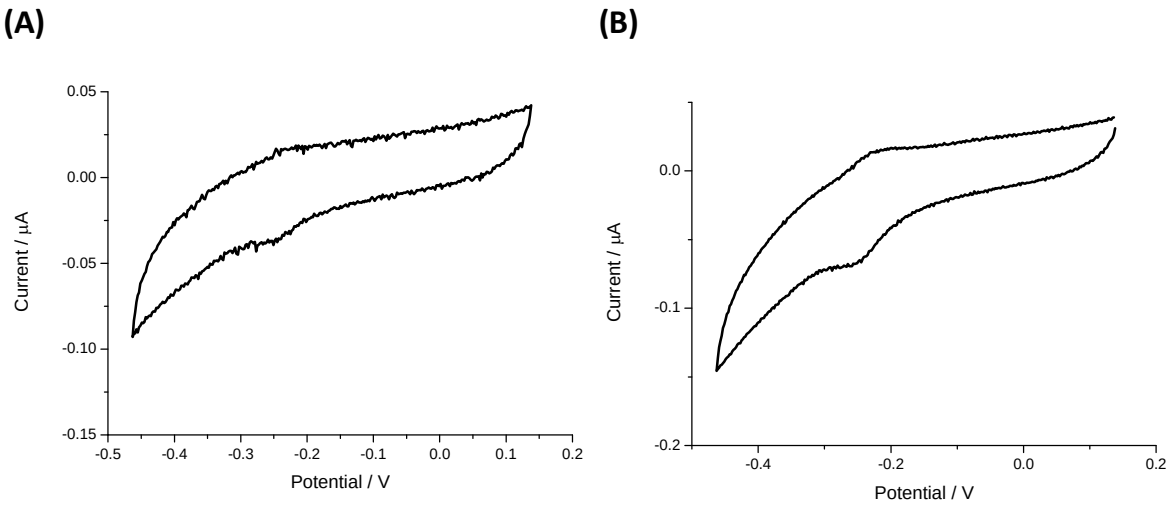


Figure 3-3: The cyclic voltammetry of R.e SH wildtype (A) and variant HoxFD467S (B), in the presence of 5 mM $NADP^+$ in 5 mL Tris buffer (50 mM, pH 8.0).

The cyclic voltammetry of NAD^+ and $NADP^+$ reduction for *R.e* SH and its three variants have exhibited different behaviours towards different substrate, and provided with information to select candidate for the new NADPH regeneration system (**Figure 3-4**). *R.e* SH wildtype enzyme showed highest activity towards its native substrate NAD^+, but had no observable activity for $NADP^+$ reduction. This was within expectation as the enzyme natively catalyse the reduction of NAD^+. And by a structural analysis of its cofactor binding pocket, there was not enough space to accommodate the extra phosphate group of $NADP^+$. The variant $HoxF^{D467S}$ had similar behaviours with the wildtype enzyme. It retained 90% activity for NAD^+ reduction and only above detectable activity for $NADP^+$, which indicated that the alteration of this residue did not significantly change its catalytic behaviours. The cyclic voltammetry for $NADP^+$ reduction catalysed by both enzymes showed an FMN reduction peak indicating that FMN from the enzyme catalytic site falling out due to lack of substrate binding. The mutation Asp467Ser decreased the negative charge of the catalytic pocket; it hardly changed the behaviours of the enzyme. The variant still showed high activity towards its native substrate NAD^+, and cannot bind $NADP^+$. In this way, sorely changing the charge of the catalytic pocket contributes little to the substrate specificity. The variant $HoxF^{E341A}$ had increased activity towards $NADP^+$ comparing with variant $HoxF^{D467S}$, while the activity for NAD^+ reduction

of variant HoxF^{E341A} was significantly lower. The Glu341Ala mutation had a more obvious effect on the enzyme by enlarging the catalytic pocket. As the catalytic pocket was much larger than the substrate molecule NAD^+ in variant HoxF^{E341A}, the binding strength between the substrate and the enzyme active site was significantly lower, leading to a low activity for NAD^+ reduction. At the same time, $NADP^+$ could get access to the activity site and bind with it due to the larger pocket size, so the activity for $NADP^+$ reduction increased. At last, the double variant HoxF$^{E341A,\ D467S}$ combined both the mutations for the other two variants had the highest activity for $NADP^+$ reduction due to the combined effects of enlarging the pocket size as well as creating a less negative micro environment to attract $NADP^+$ binding.

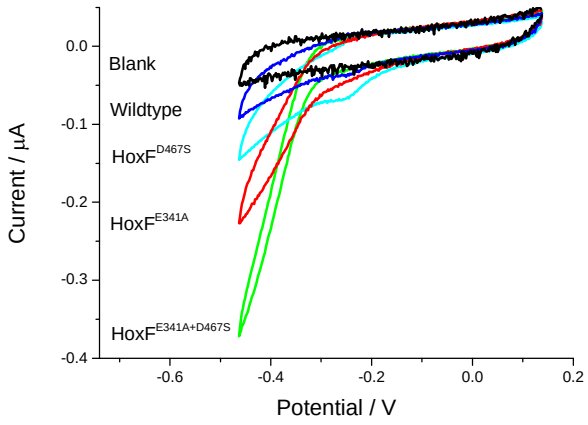


Figure 3-4: Cyclic voltammetry of the variants (5 mL Tris buffer, pH8.0, 5 mM $NADP^+$, 30 °C): blank (black), variant HoxF^{E341A} (red), variant HoxF$^{E341/D467S}$ (green), HoxF^{D467S} (cyan), and wildtype (blue).

3.3 Determination of affinity constants for the variants

The electro-catalytic behaviours of the enzymes cannot give quantitative results, and the electro-catalytic behaviours of the enzymes describe only part of the enzyme performance. Other than the electro-catalytic behaviours of the enzymes, the affinity constant for the enzyme to bind with its substrate is another important parameter to characterise the performance of the enzyme. As discussed in chapter two, the affinity constant K_M is the substrate concentration when the enzyme reaches half of its maximum speed, so a low K_M for $NADP^+$ indicates that the enzyme can function at low substrate concentration. This is what to be expected as a desirable candidate for NADPH regeneration system. An ideal NADPH regeneration system requires high substrate/cofactor rate in

order to minimise the cost for cofactor. Thus a low K_M for $NADP^+$ is crucial and an ideal candidate $NADP^+$ reductase enzyme is expected to have K_M around or lower than 1 mM. To determine the affinity constants for the enzymes, chronoamperometry was used. The detailed methods were described at chapter two.

3.3.1 Affinity constants for NAD^+ reduction

As the wildtype enzyme showed highest activity for NAD^+ reduction from cyclic voltammetry data, it was first carried out for affinity constant determination. The electrochemical setup for chronoamperometry was the same as cyclic voltammetry. The electrode was modified with target enzyme, as held at the constant potential. This potential was chosen in the wake of a compromise between signal for catalytic current and stability of the enzyme. Although the cyclic voltammetry showed that a lower potential led to a higher catalytic current for $NADP^+$ reduction, the stability of the enzyme was also dependent on the potential of the electrode. At low potential, the enzyme had a higher tendency to collapse and cease to catalyse reactions, and the catalytic current would thus decrease. As a chronoamperometry requires at least one minute, it is crucial to choose a potential that not damages the enzyme within this time scale. In this time the potential was -0.42 V vs SHE. At the beginning of the chronoamperometry, ten to twenty seconds was given to make the current signal stable, as sometimes at the beginning, considerable non-Faradaic current was observed, and this kind of current would dismiss after waiting for a few second. After the current was stable, a series of NAD^+ injection was made. In the case, the substrate injection made the concentration of NAD^+ in the electronic cell reached 49.9 μM, 99.5 μM, 198.0 μM, 392.1 μM, 676.3 μM, 952.4 μM, 1395.3 μM, and 1818.2 μM. A few seconds pause was given between each injection to make the signal current equilibrium and stable (**Figure 3-5A**). In the case of wildtype enzymes, eight injections were made. At the beginning of the chronoamperometry when no substrate was injected, and at each plateau phase after the injection, the catalytic current data was recorded. After the injections, the catalytic current reached -1.13 μA. In theory, the current should be zero when no injection was made. However, due to capacitive effect, non-faradaic current was observed when no substrate was injected

into the cell. Moreover, the non-faradaic current was proportional to the potential applied on the electrode. In this way, there was always a current reading when the chronoamperometry was stable when no substrate was in the cell. In this experiment, the current before injections was -0.091 μA. Each current data point subtracted the non-faradaic current reading at first, and got the actual current at each substrate concentration. Then a Michaelis-Menten plot was made by plotting the catalytic current against the substrate concentration. The fitting was accomplished by Origin 8.0 software with R^2 equalled 0.9997, and K_M was 0.109 mM (**Figure 3-5B**). After the first K_M was obtained, it was crucial to adjust the injection of substrate. In order to obtain an accurate K_M data from fitting a Michaelis-Menten plot, enough data points of substrate concentration below K_M value, and above K_M value ideally up to 10 times of K_M value were required. As the first K_M was around 0.1 mM, of all the eight injections, three of them were below K_M, while six of them were exceeding K_M, and the highest injection concentration was around 1.4 mM, much more than ten times of K_M. So these substrate injections were desirable for fitting an accurate Michaelis-Menten plot. A Lineweaver and Burk plot was then obtained from the deduction of Michaelis-Menten plot, and the affinity constant was then calculated (**Figure 3-5C**). Seven other same repeat experiments were made, and the data was dealt as described before. In the end, eight K_M figures were obtained, and the average K_M was 0.118±0.013 mM. All the fitted Michaelis-Menten equations had R^2 over 0.99.

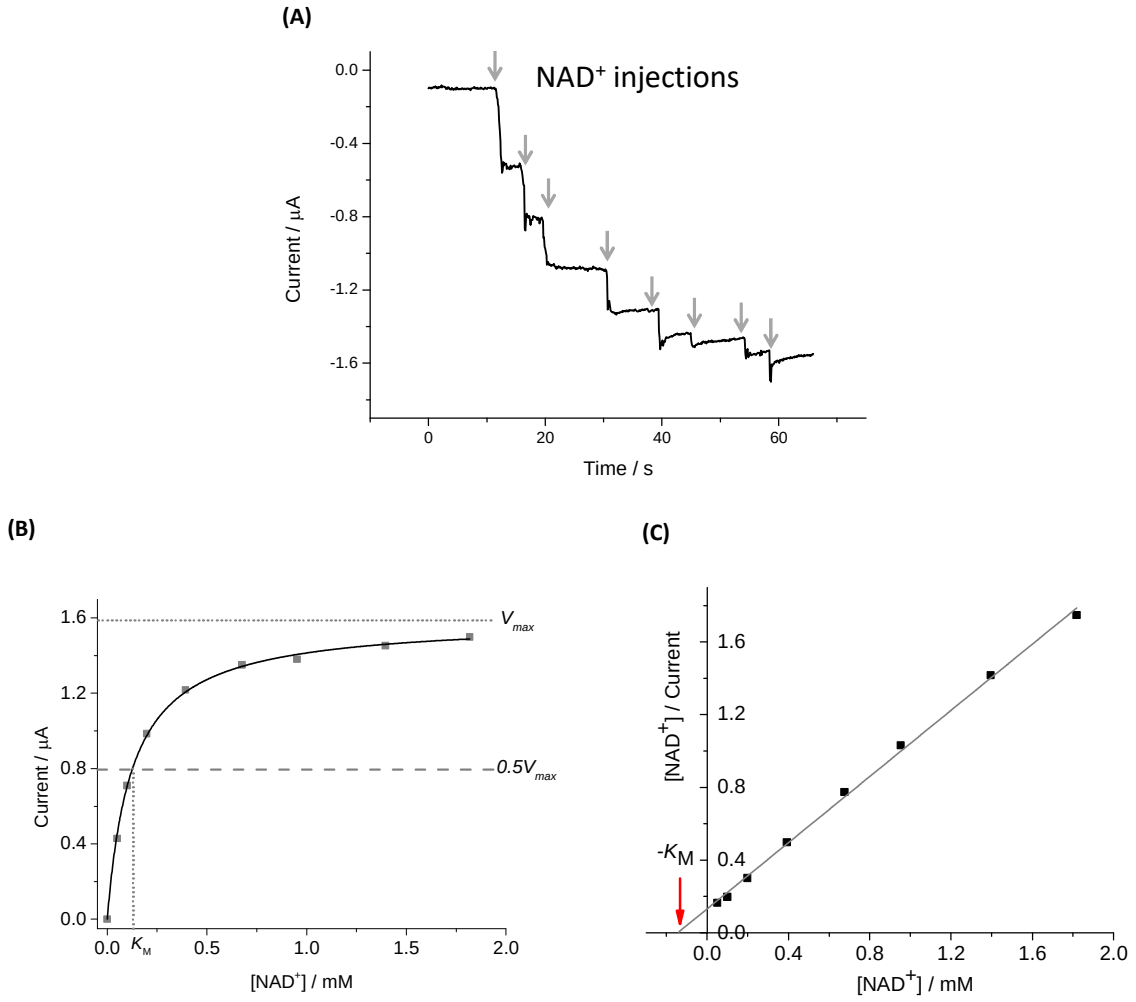


Figure 3-5: The determination of affinity constant K_M of *R.e* SH wildtype for NAD^+. (A) Chronoamperometry of wildtype *R.e* SH enzyme reduction of NAD^+, the grey arrows indicated the injection of NAD^+ solution time points to the electrochemical cell. (B) The Michaelis-Menten plot of wildtype *R.e* SH enzyme reduction of NAD^+. (C) Lineweaver and Burk plot of wildtype *R.e* SH enzyme reduction of NAD^+ deducted from the Michaelis-Menten plot.

Then, the affinity constant for NAD^+ reduction catalysed by variant $HoxF^{D467S}$ was determined by following the same procedure (**Figure 3-6**). Before the injections, the non-Faradaic current was -0.099 μA. After eight same injections of NAD^+ as did for the wildtype enzyme, the catalytic current reached -1.639 μA. Then a Michaelis-Menten plot with the same approach as that of wildtype was obtained. This time the R^2 equalled 0.9996, and K_M was 0.101 mM. Seven other same repeat experiments were made, and the data was dealt as described before. In the end, eight K_M figures were obtained, and the average K_M was 0.106±0.012 mM. The chronoamperometry of variant $HoxF^{D467S}$

was similar to that of wildtype enzyme. And the affinity constant was also very close to that of wildtype enzyme. This result was in accordance with the electro-catalytic behaviours of the both enzymes. That further showed that the mutation did not contribute significantly to the binding and catalysing of the enzyme with NAD^+.

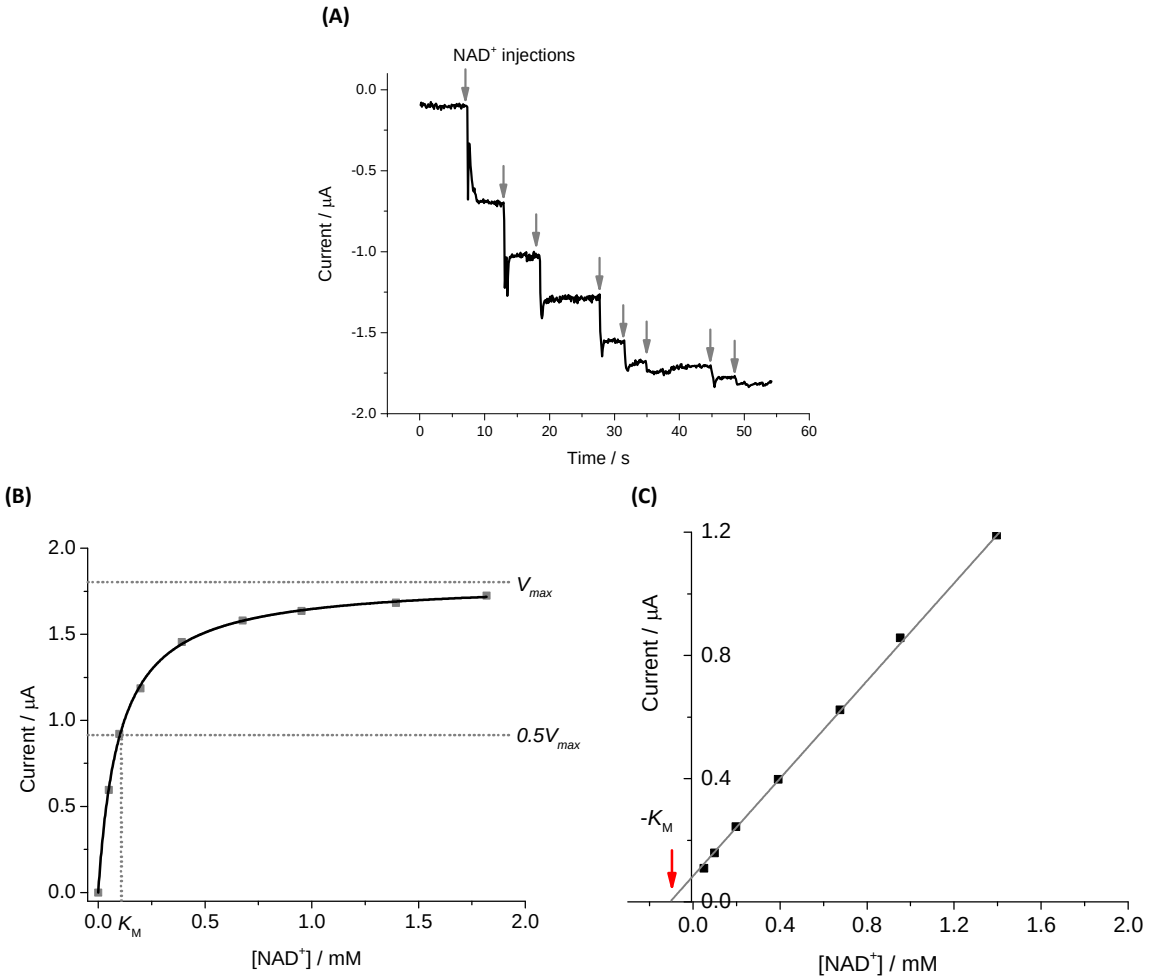


Figure 3-6: The determination of affinity constant K_M of variant $HoxF^{D467S}$ for NAD^+. (A) Chronoamperometry of variant $HoxF^{D467S}$ enzyme reduction of NAD^+, the grey arrows indicated the injection of NAD^+ solution time points to the electrochemical cell. (B) The Michaelis-Menten plot of variant $HoxF^{D467S}$ enzyme reduction of NAD^+. (C) Lineweaver and Burk plot of variant $HoxF^{D467S}$ enzyme reduction of NAD^+ deducted from the Michaelis-Menten plot.

The affinity constant for variant $HoxF^{E341A}$ was significantly different from the previous two enzymes, as $HoxF^{E341A}$ showed much lower activity for NAD^+ reduction. The chronoamperometry of NAD^+ reduction for $HoxF^{E341A}$ at -0.42 V vs SHE showed very low catalytic current response upon injection of NAD^+, making it almost impossible to determine each time point. However, this

enzyme had showed significant high stability and high catalytic current under lower potential at -0.57 V vs SHE. In this way, the chronoamperometry of NAD^+ reduction for $HoxF^{E341A}$ was carried out at -0.57 V vs SHE. In this case, the catalytic current was significantly higher than under potential -0.42 V vs SHE. To determine the affinity constant, a total of 15 injections of NAD^+ were made into the electronic cell and making the final NAD^+ concentration at 9.1 mM. However, although the data points could fit Michaelis-Menten equation perfectly with R^2 over 0.99, the data points at high substrate concentration was significantly deviated from the curve. The fitting results gave the affinity constant at 0.773±0.197 μM. If only take into consideration the data points under the substrate concentration of 2 mM, the affinity constant would be 0.379±0.104 μM, significantly lower than the previous value.

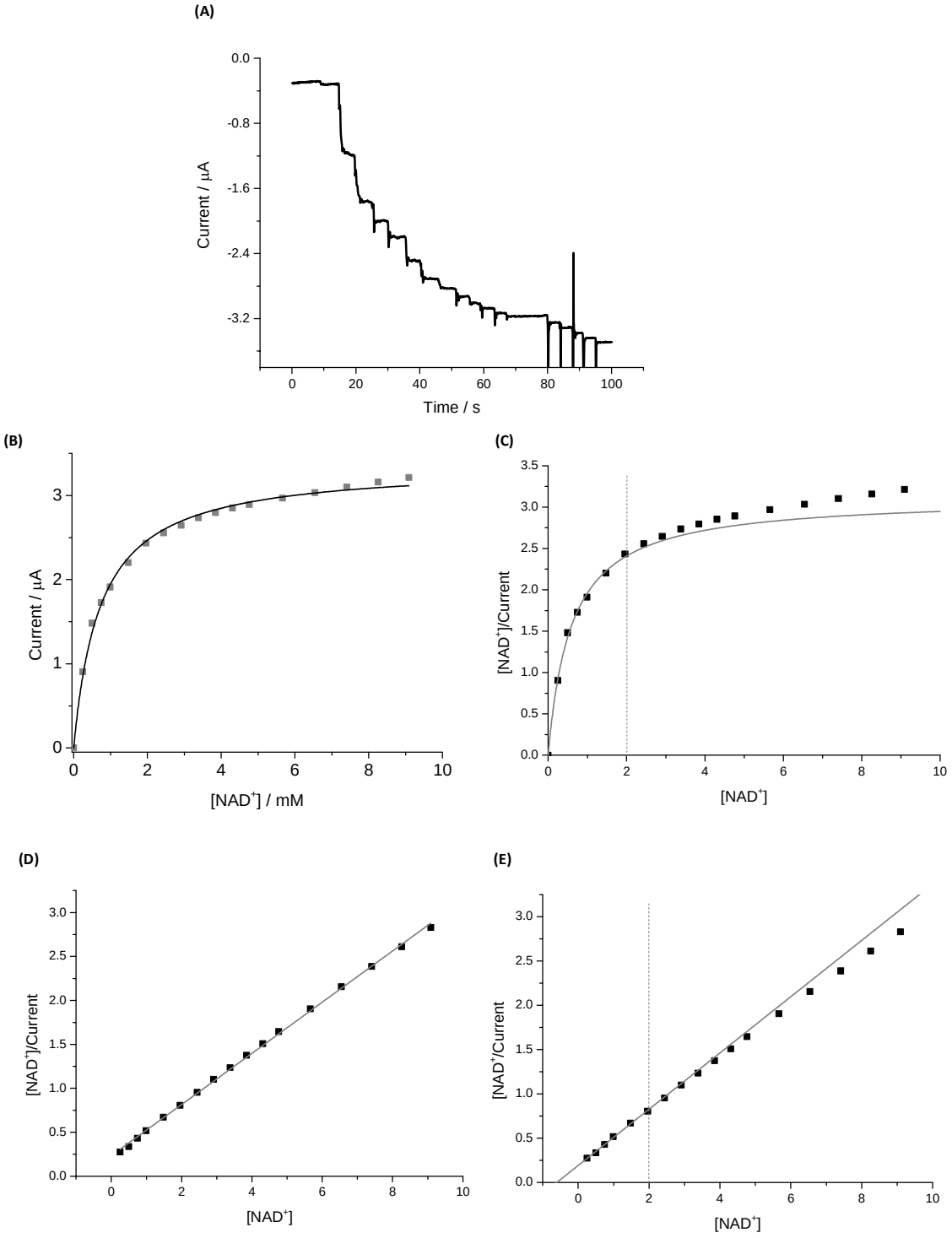


Figure 3-7: The determination of affinity constant K_M of variant variant HoxF^{E341A} for NAD$^+$. (A) Chronoamperometry of variant HoxF^{E341A} enzyme reduction of NAD$^+$. (B) The Michaelis-Menten plot of variant HoxF^{E341A} enzyme reduction of NAD$^+$ when all data points were taken into consideration. (C) The Michaelis-Menten plot of variant HoxF^{E341A} enzyme reduction of NAD$^+$ when only data points below 2 mM NAD$^+$ concentration were taken into consideration. (D) Lineweaver and Burk plot of variant HoxF^{E341A} enzyme reduction of NAD$^+$ deducted from the Michaelis-Menten plot when all the data points were taken into consideration. (E) Lineweaver and Burk plot of variant HoxF^{E341A} enzyme reduction of NAD$^+$ deducted from the Michaelis-Menten plot when only data points below 2 mM NAD$^+$ concentration were taken into consideration.

At last, the affinity constant of NAD^+ reduction for $HoxF^{E341A, D467S}$ was determined. As this variant was unstable at -0.57 V vs SHE, the potential was held at -0.42 V vs SHE during the chronoamperometry. Then, the same procedure was applied to this variant. A series of NAD^+ injections up to 14.2 mM were injected into the electronic cell. At high substrate concentration, the catalytic current was much higher than expected, and deviated from the fitted Michaelis-Menten plot. This was similar with that of $HoxF^{E341A}$. Thus, it was highly possible due to the same reason that at high substrate concentration, the bare electrode could reduce NAD^+ and contributed to the overall catalytic current. However, as $HoxF^{E341A, D467S}$ was not active enough when small amount of NAD^+ was injected, only seven data points were collected when the substrate injection reached 14.2 mM. There were not enough data points at low substrate concentration level to determine the affinity constant value. In this way, all the seven data points were used to determine the affinity constant value. At last, eleven affinity constant values were determined, and the average value was 1.774±0.320 mM.

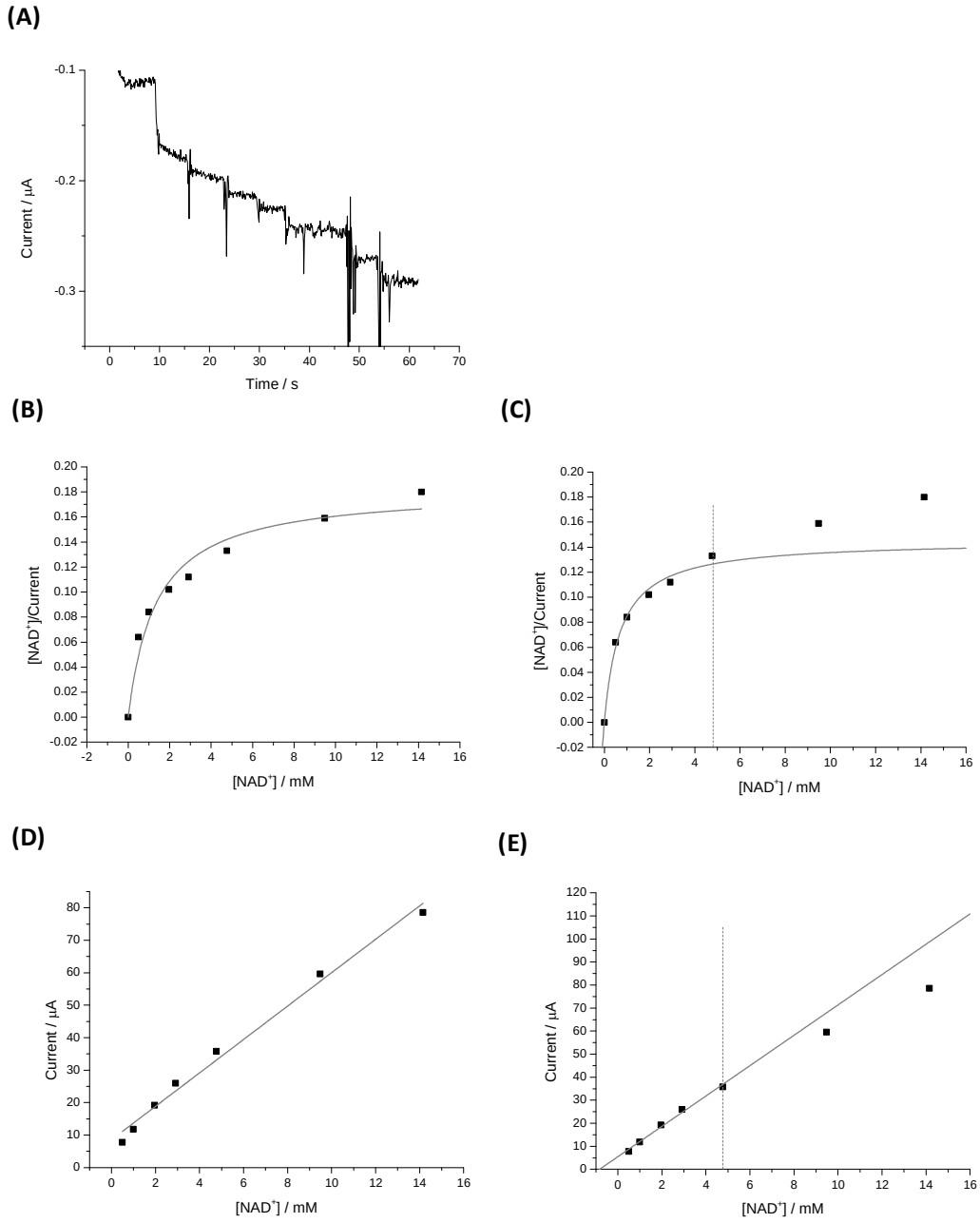


Figure 3-8: The determination of affinity constant K_M of variant variant HoxF$^{E341A,\ D467S}$ for NAD^+. (A) Chronoamperometry of variant HoxF$^{E341A,\ D467S}$ enzyme reduction of NAD^+. (B) The Michaelis-Menten plot of variant HoxF$^{E341A,\ D467S}$ enzyme reduction of NAD^+ when all data points were taken into consideration. (C) The Michaelis-Menten plot of variant HoxF$^{E341A,\ D467S}$ enzyme reduction of NAD^+ when only data points below 2 mM NAD^+ concentration were taken into consideration. (D) Lineweaver and Burk plot of variant HoxF$^{E341A,\ D467S}$ enzyme reduction of NAD^+ deducted from the Michaelis-Menten plot when all the data points were taken into consideration. (E) Lineweaver and Burk plot of variant HoxF$^{E341A,\ D467S}$ enzyme reduction of NAD^+ deducted from the Michaelis-Menten plot when only data points below 2 mM NAD^+ concentration were taken into consideration.

The possible reason to explain the behaviour not following Michaelis-Menten kinetics is that at high substrate concentration, the substrate NAD^+ would be reduced by the blank electrode, which incurs additional current besides the catalytic current by the enzyme (**Figure 3-9**). For those very active enzymes, the enzymatic catalytic current is high enough that the current produced by the bare electrode is negligible. However, for the enzymes not that active such as the variant $HoxF^{E341A}$ and the variant $^{HoxFE341A, D467S}$, the current generated by the bare electrode is comparable to the current by the enzyme. In this way, this effect would lead to big error, especially at high substrate concentration level. So in this way, only the data points below substrate concentration of 2 mM was taken into consideration to determine the affinity constant. Thus it was concluded that the affinity constant for NAD^+ reduction of $HoxF^{E341A}$ was 379±104 μM. This was three times higher than that of wildtype enzyme and $HoxF^{D467S}$, indicating that the larger catalytic pocket for $HoxF^{E341A}$ decrease the affinity between the enzyme and the substrate NAD^+.

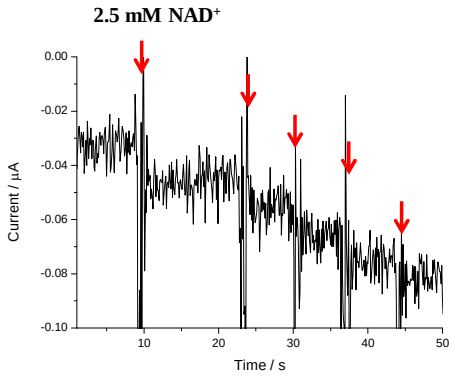


Figure 3-9: Chronoamperometry of bare electrode with no enzyme modification reduction of NAD^+, red arrows indicated the time points when NAD^+ solution was injected into the electronic cell beffur.

3.3.2 Affinity constants for NADH oxidation

To determine the affinity constants for NADH oxidation, the working electrode was held at 0.13V vs SHE, which favours NADH oxidation. At high potential, proton reduction would occur at the bare electrode intervening the catalytic current of NADH oxidation. Thus 0.13 V vs SHE was chosen as

the potential with highest possible NADH oxidation catalytic current while no proton reduction occurring (**Figure 3-10**). To determine the affinity constant for the wildtype enzyme, ten NADH injections were made into the electronic cell up to 0.6 mM. Nine repeat experiments were carried out and the average affinity constant was 192±28 μM. To determine the affinity constant for the rest variants, the same procedure was applied. The affinity constant for $HoxF^{E341A}$ was 86±25 μM, $HoxF^{D467S}$ 229±51 μM, and $HoxF^{E341A, D467S}$ 85± 31 μM.

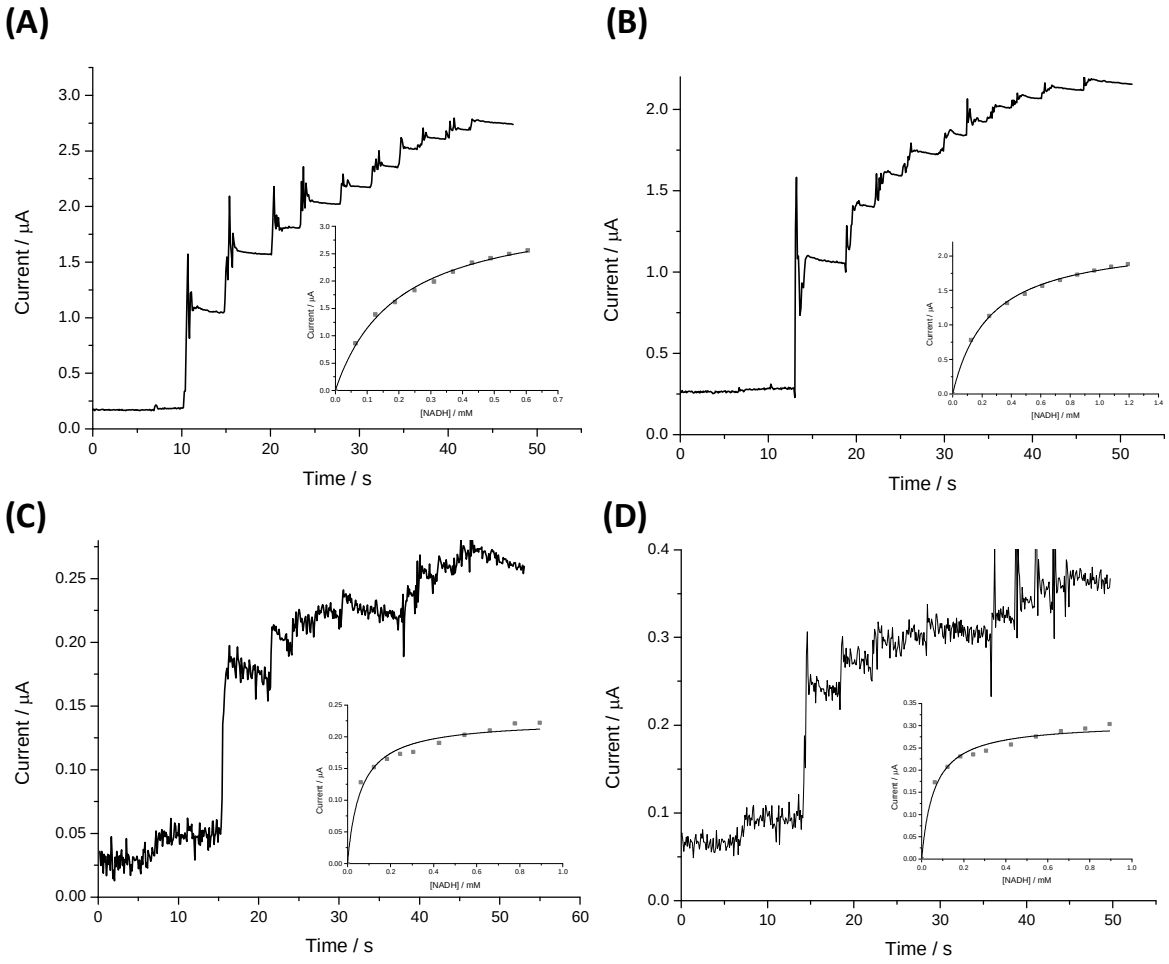


Figure 3-10: The determination of affinity constant for NADH oxidation of all the four enzymes. Chronoamperometry of NADH oxidation, and the corresponding Michaelis-Menten plot for wildtype *R.e* SH (A), variant $HoxF^{E341A, D467S}$ (B), variant $HoxF^{D467S}$ (C), and variant $HoxF^{E341A, D467S}$ (D).

3.3.3 Affinity constants for $NADP^+$ reduction

As the aim of this project was to develop a NADPH regeneration system, the most important parameter was the affinity constant for $NADP^+$ reduction. To determine the affinity constants for $NADP^+$ the same procedure as determination of the affinity constant for NAD^+ reduction was followed. The cofactor $NADP^+$ was purified prior to the electrochemical experiment to eliminate any affect by the trace amount of other cofactors in the sample. The wildtype enzyme was inert to $NADP^+$. For chronoamperometry of the wildtype enzyme, upon injection of 5 mM $NADP^+$, no observable catalytic current was produced. Thus, it was not possible to determine the affinity constant. Therefore, it was concluded that the affinity constant for wildtype enzyme reducing $NADP^+$ was over 5 mM.

$HoxF^{E341A}$ and $HoxF^{D467S}$ both showed activity for $NADP^+$ reduction. Their affinity constants were determined by chronoamperometry (**Figure 3-11**). The affinity constant for $HoxF^{E341A}$ was 1322±361 μM, and that for $HoxF^{D467S}$ was 3695±326 μM. This was in accordance with the results of the cyclic voltametric experiments. Both mutations showed increased affinity for $NADP^+$ compared with the wildtype enzyme. Glu341 had a greater effect and contribute more for increasing the affinity for $NADP^+$, while Asp467 contribute less. Although both variants showed increased affinity for $NADP^+$, they were still not ideal to incorporate into the new NADPH regeneration system.

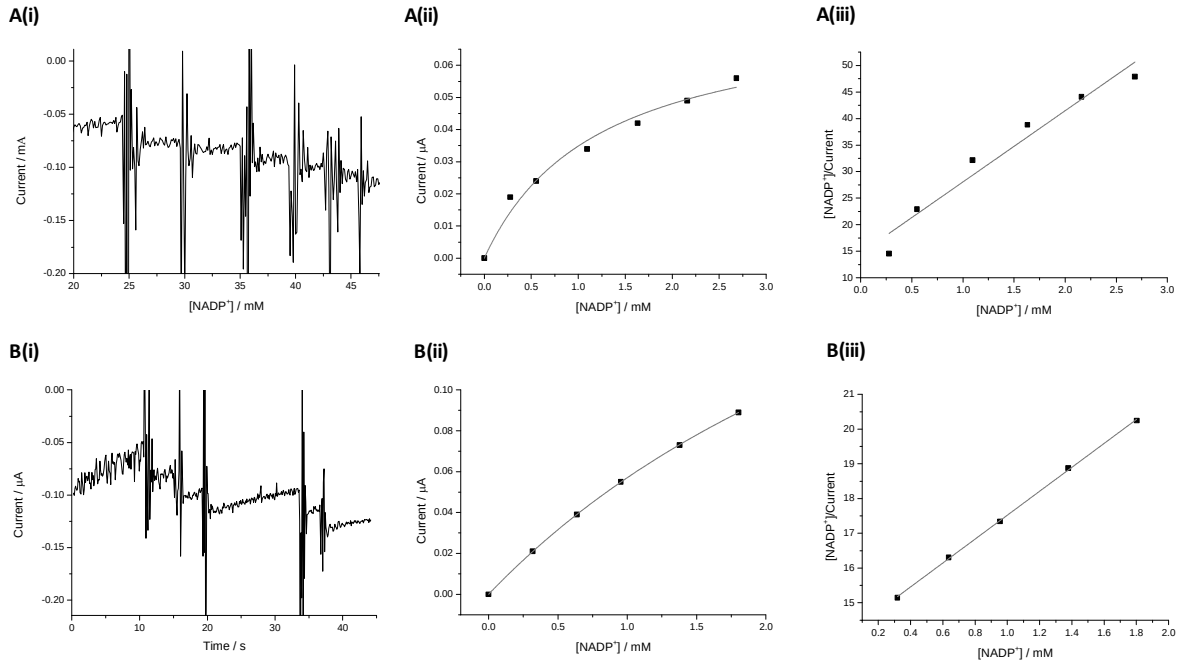


Figure 3-11: The determination of affinity constant for $NADP^+$ reduction by variant $HoxF^{E341A}$ and $HoxF^{D467S}$. Chronoamperometry (Ai) of $NADP^+$ reduction by variant $HoxF^{E341A}$, and the corresponding Michaelis-Menten plot (Aii), and Lineweaver and Burk plot (Aiii). Chronoamperometry (Bi) of $NADP^+$ reduction by variant $HoxF^{D467S}$, and the corresponding Michaelis-Menten plot (Bii), and Lineweaver and Burk plot (Biii).

The chronoamperometry of $HoxF^{E341A, D467S}$ showed that the catalytic current decreased upon each injection of $NADP^+$ (**Figure 3-12**). This was not seen from other enzymes, so it was not due to the enzyme film loss effect. Therefore it was hypothesised that the two mutations lead to destabilization of the enzyme particularly under low potential and at the presence of $NADP^+$. A total of nine affinity constant values were determined, and the average value was 1116±287 µM. Since the affinity constant for $NADP^+$ reduction was around 1 mM for $NADP^+$ reduction, this was ideal for NADPH regeneration system, meaning that at 1 mM $NADP^+$ concentration, the system would function robustly. Provided that the substrate concentration was 100 mM, the system could potentially reach 1:100 cofactor/substrate ratio, and making it economically ideal for a cofactor regeneration system.

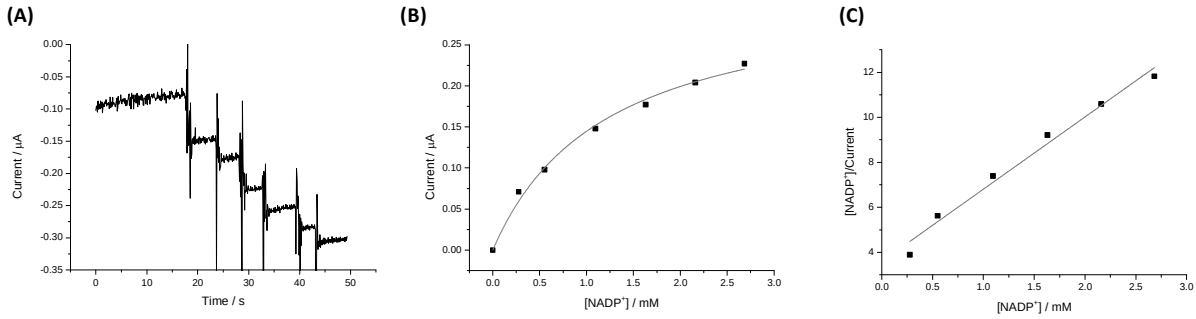


Figure 3-12: The determination of affinity constant for $NADP^+$ reduction by variant $HoxF^{E341A/D467S}$. Chronoamperometry (A) of $NADP^+$ reduction by variant $HoxF^{E341A}$, and the corresponding Michaelis-Menten plot (B), and Lineweaver and Burk plot (C).

The best candidate enzyme for NADPH regeneration system had been identified as the $HoxF^{E341A,D467S}$ double variant, which was robust enough, and had low enough affinity constant for $NADP^+$.

3.3.4 Affinity constants for NADPH oxidation

At last, affinity constants for NADPH oxidation of the enzymes were tried to determine. However, none of the four enzymes showed observable NADPH oxidation activity both in cyclic voltammetry and chronoamperometry (**Figure 3-13**). As discussed before, the wildtype enzyme and variant $HoxF^{D467S}$ were not able to accommodate $NADP^+$ so they showed hardly any activity for $NADP^+$ reduction. In this way, as NADPH also has an additional phosphate group, it might also not be able to bind with the wildtype enzyme and the variant $HoxF^{D467S}$, thus no redox activity. Nevertheless, the variant $HoxF^{E341A}$ and $HoxF^{D467S}$ showed activity for $NADP^+$ reduction, and particularly $HoxF^{E341A,\ D467S}$ which had a relatively high activity and affinity. The possible reason might be that these two enzyme variants had an extreme catalytic bias towards $NADP^+$ reduction. In this way, the affinity constant for NADPH oxidation cannot be determined.

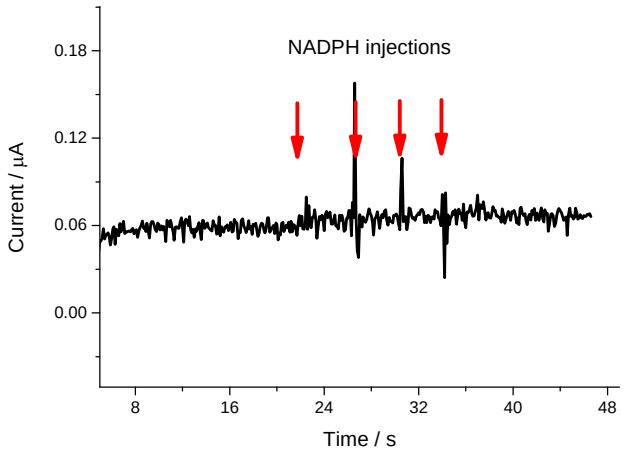


Figure 3-13: Chronoamperometry of NADPH oxidation by variant HoxF$^{E341A, D467S}$

3.4 Determination of inhibition constants

Besides affinity constant, the inhibition constant is also a crucial parameter for cofactor regeneration system, as *R.e* SH and its variants are reported to be inhibited by its own product. In the NADH regeneration system, NAD^+ was reduced to NADH, and the regenerating NADH was used by the third enzyme. Thus, the system formed a dynamic equilibrium, and both NAD^+ and NADH were present in the system.

The method to determine the inhibition constant has been described in chapter two. Here, *R.e* SH was used to illustrate the process of determination of NADH inhibition of *R.e* SH NAD^+ reduction. First, *R.e* SH was immobilised on the electrode. And the electrode was posed at -0.57 V vs SHE favouring NAD^+ reduction. Then, a control step of 50 µM NAD^+ was injected into the electronic cell, and a corresponding catalytic current was observed. For the first test, after the control step, a series of seven equal injection of final concentration 0.05 mM NADH were made into the electronic cell. As the enzyme is reversibly inhibited by its product, upon each injection, the catalytic current decreased. Then, a series of additional four tests were carried out with similar procedure. First, a control step of 50 µM NAD^+ was injected. Then an additional 50 µM, 100 µM, 150 µM, or 200 µM NAD^+ was further injected into the system, thus making the final NAD^+ concentration of the five

tests 50 µM, 100 µM, 150 µM, 200 µM, and 250 µM. After NAD^+ injections, a series of seven equal injection of final concentration 0.05 mM NADH were made into the electronic cell (**Figure 3-14A**). In order to compare between different tests, the current plots were further corrected and normalised. At the beginning of the chronoamperometry when no substrate was added, in theory the current should be zero. However, as discussed in chapter two, the chronoamperometry is affected by the non-Faradaic capacitate current. Therefore in practical, the current at the beginning was around -0.1 to -0.2 µA. These non-faradaic current was taken away for each test making the current at the beginning zero. The current also need to be normalised. Provided the number of enzyme molecules adsorbed on the surface of working electrode was the same, the catalytic current should be the same when injecting same amount of substrate. However, the number of enzyme molecules adsorbed on the electrode was not the same, making the magnitude of the catalytic current varied for each test when injecting same amount of substrate. In this way, at the beginning of each test, a control step of 50 µM NAD^+ was injected, and the corresponding catalytic current was normalised as one (**Figure 3-14B**).

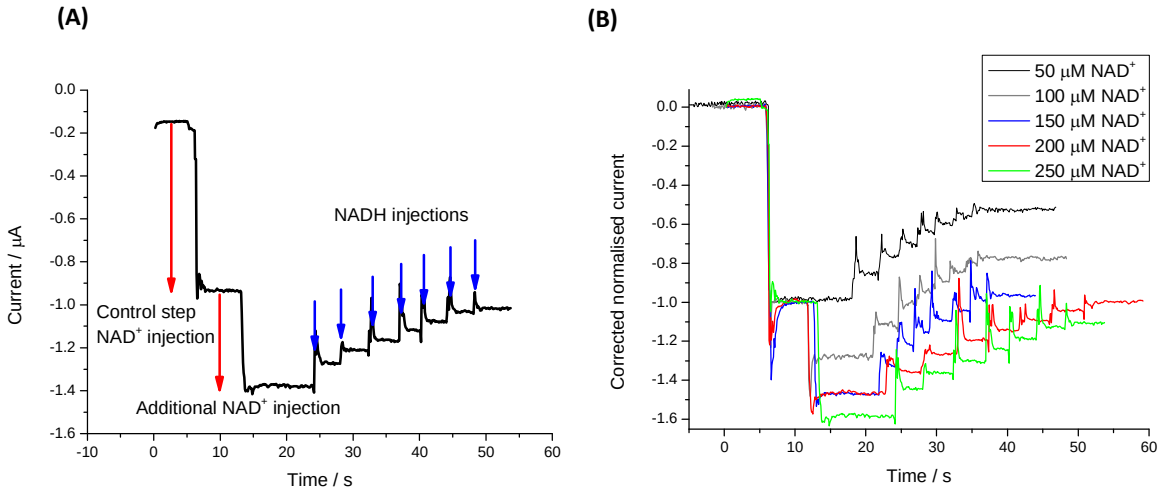


Figure 3-14: The determination of inhibition constant of NADH inhibition of NAD^+ reduction by wildtype *R.e* SH. (A) Chronoamperometry of NADH inhibition of NAD^+ reduction by wildtype *R.e* SH, the red arrows showed the two injections of NAD^+ solution into the electronic cell buffer, and the blue arrows showed the series of injection of NADH solution. (B) The overlay chronoamperometry of NADH inhibition of NAD^+ reduction by wildtype *R.e* SH with different concentration of NAD^+ injection, the y-axis is corrected normalised current.

According to Dixon equation, in order to determine the inhibition constant, plots of concentration of inhibitor NADH against the reciprocal of inhibited corrected normalised current for each test was made. Ideally, these plots should intersect at one single point which equals $-K_i$. However, in reality, due to experimental errors, these plots will intersect at different points. Therefore, no accurate inhibition constant value can be determined, but rather a range of inhibition constant value can be concluded at the region of plots intersection. In this case, the plots intersected between -0.3 mM to -0.5 mM. Therefore, the inhibition constant for NADH inhibition of NAD^+ reduction for the wildtype enzyme is between 0.3 to 0.5 mM (**Figure 3-15**).

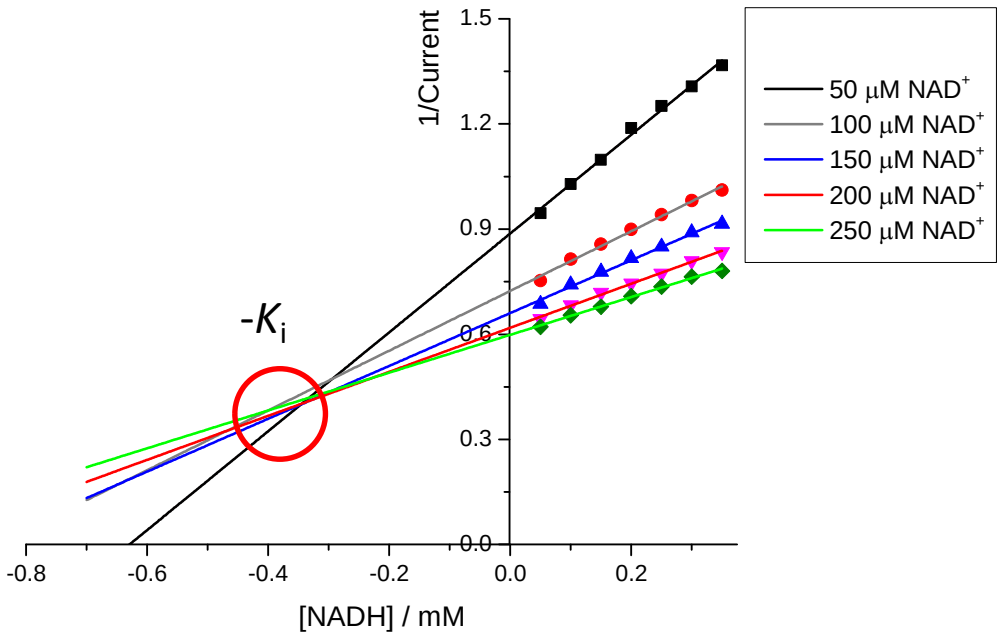


Figure 3-15: The Dixon plots of NADH inhibition of NAD^+ by wildtype *R.e* SH.

3.4.1 Inhibition constant for NADH inhibition of NAD^+ reduction for the variant $HoxF^{D467S}$

The procedure for determination of inhibition constant for NADH inhibition of NAD^+ reduction by $HoxF^{D467S}$ is the same as the wildtype *R.e* SH. First, the variant $HoxF^{D467S}$ was

immobilised on the electrode. And the electrode was posed at -0.57 V vs SHE favouring NAD^+ reduction. Then, a control step of 50 µM NAD^+ was injected into the electronic cell, and a corresponding catalytic current was observed. After the control step, a series of seven equal injection of final concentration 0.05 mM NADH were made into the electronic cell. Then, a series of additional four tests were carried out with similar procedure. First, a control step of 50 µM NAD^+ was injected. Then an additional 50 µM, 100 µM, 150 µM, or 200 µM NAD^+ was further injected into the system, thus making the final NAD^+ concentration of the five tests 50 µM, 100 µM, 150 µM, 200 µM, and 250 µM. After NAD^+ injections, a series of seven equal injection of final concentration 0.05 mM NADH were made into the electronic cell. Then the current plots were further corrected and normalised (**Figure 3-16A**). According to Dixon equation, in order to determine the inhibition constant, plots of concentration of inhibitor NADH against the reciprocal of inhibited corrected normalised current for each test was made. In this case, the plots intersected between -0.15 mM to -0.35 mM. Therefore, the inhibition constant for NADH inhibition of NAD^+ reduction for the wildtype enzyme is between 0.15 to 0.35 mM (**Figure 3-16B**).

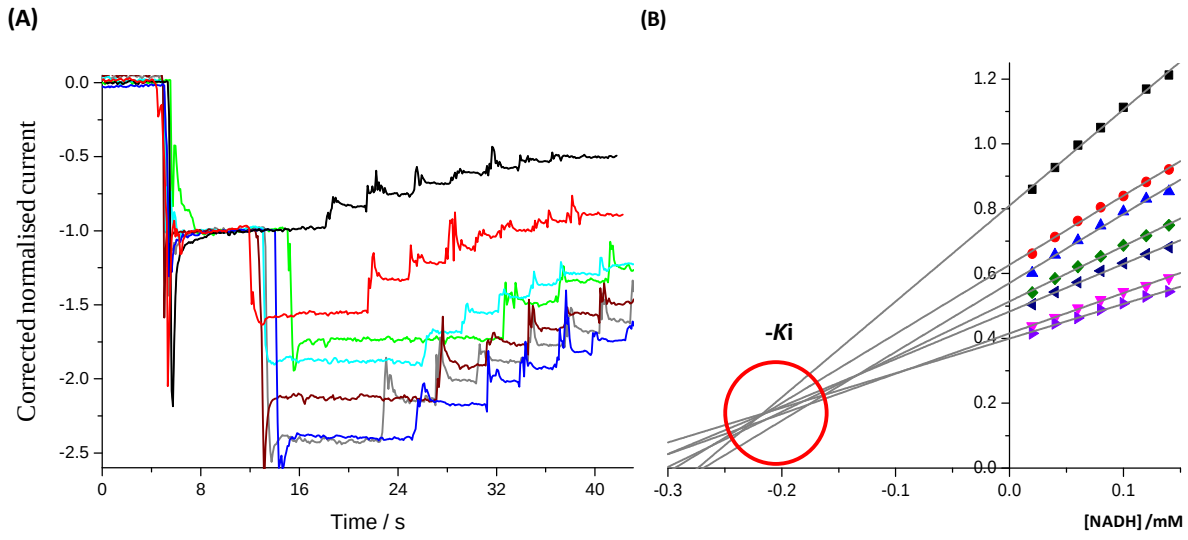


Figure 3-16: The determination of inhibition constant of NADH inhibition of NAD^+ reduction by variant $HoxF^{D467S}$. (A) The overlay chronoamperometry of NADH inhibition of NAD^+ reduction by variant $HoxF^{D467S}$ with different concentration

of NAD^+ injection, the y-axis is corrected normalised current. (B) The Dixon plots of NADH inhibition of NAD^+ by variant $HoxF^{D467S}$.

3.5 Electrochemical characterisation of *R.e* SH variant $HoxF^{E341A, S342R}$

After all the four enzymes were characterised, the general conclusion was that variant $HoxF^{E341A, D467S}$ had the highest activity and affinity for $NADP^+$, so it was the best candidate for the new NADPH regeneration system. However, there were still some drawbacks for this variant. Its activity was still not ideal, as its activity for $NADP^+$ reduction was less than 10% of the activity for wildtype enzyme catalysing NAD^+ reduction. This might lead to the overall activity for the new NADPH regeneration system when incorporated with variant $HoxF^{E341A, D467S}$ much less lower than the current NADH regeneration system containing the wildtype enzyme. The chronoamperometry of $NADP^+$ reduction catalysed by $HoxF^{E341A, D467S}$ also indicated that this variant had low stability. There were still plenty of residues can be targeted for mutagenesis in order to produce more robust $NADP^+$ reductase variants. Thus far only three variants were produced. In this way, a new *R.e* SH double variant $HoxF^{E341A, S342R}$ was produced based on rational design strategy and site-direct mutagenesis approach. This variant kept the mutation on Glu341 as the previous data indicated that this is crucial for $NADP^+$ binding. This variant also introduced a brand new mutation at the neighbouring residue Ser342 to arginine. This new variant was then characterised electrochemically to determine its activity and affinity for NAD^+, NADH, and $NADP^+$ in the hope of finding a better candidate than the previous double variant $HoxF^{E341A, D467S}$ for the new NADPH regeneration system.

3.5.1 The electro-catalytic behaviour of $HoxF^{E341A, S342R}$

The electro-catalytic behaviour of $HoxF^{E341A, S342R}$ was determined by cyclic voltammetry. The procedure was the same as cyclic voltammetry for the other enzymes. First, cyclic voltammetry was carried out at 5 mM NAD^+. At high potential, no current is observed. When the potential reached -0.3 V, catalytic current was observed, and as the potential went lower, the current increased significantly. When the potential reached -0.46 V vs SHE, the catalytic current was around -0.75 μA. The result showed that $HoxF^{E341A, S342R}$ had low activity for NAD^+ reduction, and its activity were

similar with HoxF^{E341A}. Then, cyclic voltammetry was carried out at 5 mM NADP$^+$. The catalytic current was -0.25 μA at -0.46 V vs SHE (**Figure 3-17**).

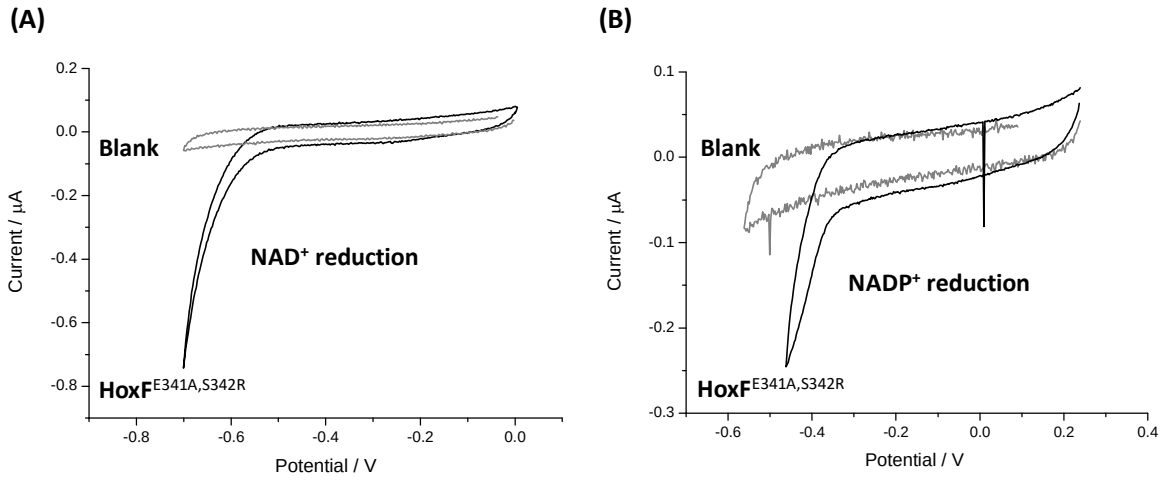


Figure 3-17: (A)The cyclic voltammetry of 5 mM NAD$^+$ reduction by variant HoxF$^{E341A/S342R}$, and the CV with a blank electrode with no NAD$^+$ addition as control. (B)The cyclic voltammetry of 5 mM NADP$^+$ reduction by variant HoxF$^{E341A/S342R}$, and the CV with a blank electrode with no NADP$^+$ addition as control.

3.5.2 The affinity constant of HoxF$^{E341A, S342R}$

The affinity constants of NAD$^+$, NADH, and NADP$^+$ for HoxF$^{E341A, S342R}$ were determined by chronoamperometry according to the same procedure as the other enzymes (**Figure 3-18**). Its affinity constant for NAD$^+$ was 648±234 μM, and its affinity constant for NADH was 59±17 μM. Due to the low activity for both NADH and NAD$^+$, the signal to noise ratio was low. Thus it was hard to determine the accurate current data point. The Michaelis-Menten fittings showed a less than 0.99 R^2 value. And the variation for different K_M values was large, leading to high standard deviations. Most importantly, the affinity constant for NADP$^+$ was determined. The affinity constant for NADP$^+$ was 353±105 μM. This was much lower than that of HoxF$^{E341A, D467S}$. And from the chronoamperometry, there was no obvious current decrease, which indicated that HoxF$^{E341A, S342R}$ was more stable than HoxF$^{E341A, D467S}$. However, it was worth noticed that only four K_M data for NADP$^+$ reduction of HoxF$^{E341A, S342R}$ were determined, and one of them was significantly deviated from the rest three data. Thus this figure was discarded, and the final K_M data was the average value for three data points.

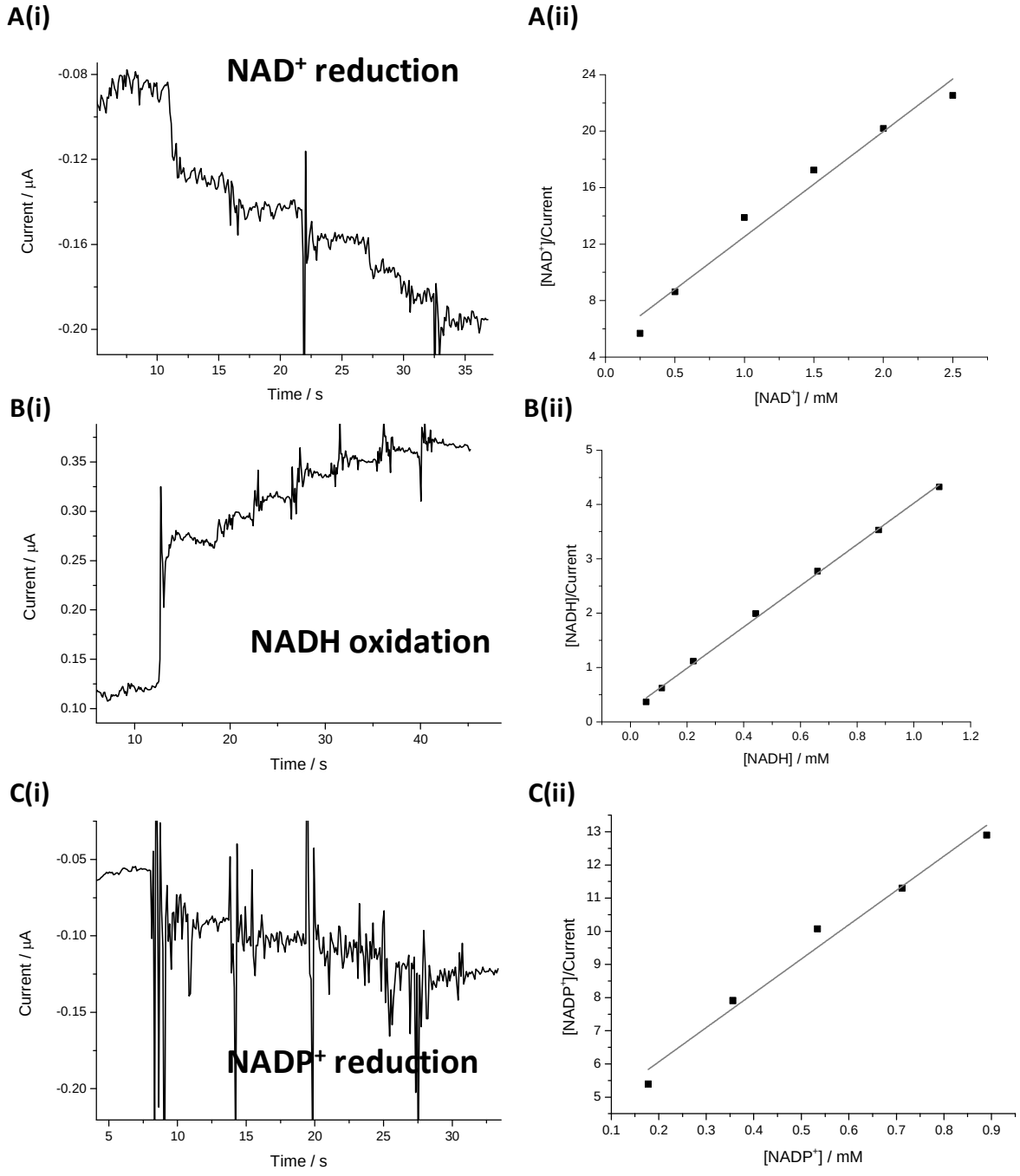


Figure 3-18: The determination of affinity constants for variant HoxF$^{E341A, S342R}$. A(i) Chronoamperometry of NAD^+ reduction. A(ii) The corresponding Michaelis-Menten plot. B(i) Chronoamperometry of NADH oxidation. C(ii) The corresponding Michaelis-Menten plot. C(i) Chronoamperometry of $NADP^+$ reduction. C(ii) The corresponding Michaelis-Menten plot.

3.6 Summary of kinetic data for $NADP^+$ reductase variants

In this chapter, five enzymes (*R.e* SH, and its variants HoxF^{E341A}, HoxF^{D467S}, HoxF$^{E341A, D467S}$, and HoxF$^{E341A, S342R}$) were characterised electrochemically. Their electro-catalytic behaviours and affinity constants for a range of substrate including NAD^+, $NADP^+$ and NADH were determined (**Table 3-1**). Among these characterisations, their behaviours towards $NADP^+$ were most crucial as they determined whether an enzyme would be suitable to incorporate into the new NADPH regeneration system. Additionally, the stability of the enzymes was also an importance factor to be taken into consideration, as the NADPH regeneration system requires the enzyme functioning normally as long as possible in order to maximise the turnover number. The wildtype enzyme was inert to $NADP^+$. It exhibited hardly any activity towards $NADP^+$ reduction, and the affinity constant for $NADP^+$ was over 5mM. The variant HoxF^{D467S} showed very similar behaviours with the wildtype enzyme. It also had low activity and high affinity constant for $NADP^+$, leaving it undesirable for the NADPH regeneration system. The variant HoxF^{E341A} has a much lower affinity constant for $NADP^+$, at about 1.3 mM. However, its electro-catalytic behaviour for $NADP^+$ reduction indicated that its activity for $NADP^+$ was still low, and undesirable for NADPH regeneration. The double variant HoxF$^{E341A, D467S}$ which contained both mutations for the two single variants, had a better behaviour compare with the two single variants. It also had a low affinity constant at around 1.0 mM. This indicated that this variant was desirable for the new NADPH regeneration system. However, the chronoamperometry of this variant showed its low stability at minute time scale. In order to pursuit more robust enzyme for $NADP^+$ reduction, an additional double variant HoxF$^{E341A, S342R}$ was produced and characterised. This variant also showed high activity for $NADP^+$ reduction as that of Hox$^{E341A, D467S}$. It had a more desirable affinity constant for $NADP^+$ at 0.35 mM; almost three times lower than that of HoxF$^{E341A, D467S}$. Most importantly, this variant had a higher stability than HoxF$^{E341A, D467S}$. After a comparison for all the enzymes, the double variant HoxF$^{E341A, S342R}$ had high stability, high activity for $NADP^+$ reduction, and lowest affinity constant for $NADP^+$. Thus this variant was the best candidate for the new NADPH regeneration system. In the following chapters of this thesis, the variant HoxF$^{E341A, S342R}$ was used for NADPH regeneration.

Table 3-1: Summary of affinity constants for all enzymes with NAD^+, NADH, and $NADP^+$

	K_M^{NAD+} / µM	K_M^{NADH} / µM	K_M^{NADP+} / µM
Wildtype	118±13	192±28	>5000
$HoxF^{E341A}$	379±104	86±25	1322±361
$HoxF^{D467S}$	106±12	229±51	3695±326
$HoxF^{E341A,D467S}$	1357±836	85±31	1116±287
$HoxF^{E341A,S342R}$	648±234	59±17	353±105

3.7 The Comparison of biochemical determined affinity constants and electrochemical determined affinity constants

In this work, all the enzyme variants were characterised both electrochemically and biochemically. The biochemical data were obtained by Janina Preissler in Lenz Group. The affinity constants determined biochemically were different from the affinity constants determined electrochemically (**Table 3-2**). One possible explanation for this observation is that the environment of the enzymes was different. In the biochemical assays, enzymes move freely in the solution, while in the electrochemical assays, all functional enzymes are immobilised on the electrode surface. In this project, the enzymes need to be immobilised on the carbon particle, which resembles the situation of the electrochemical assays. Therefore, the affinity constant determined by electrochemical assays is more relevant in this project.

Table 3-2: Comparison between electrochemical determined affinity constants and biochemical determined affinity constants for different enzymes.

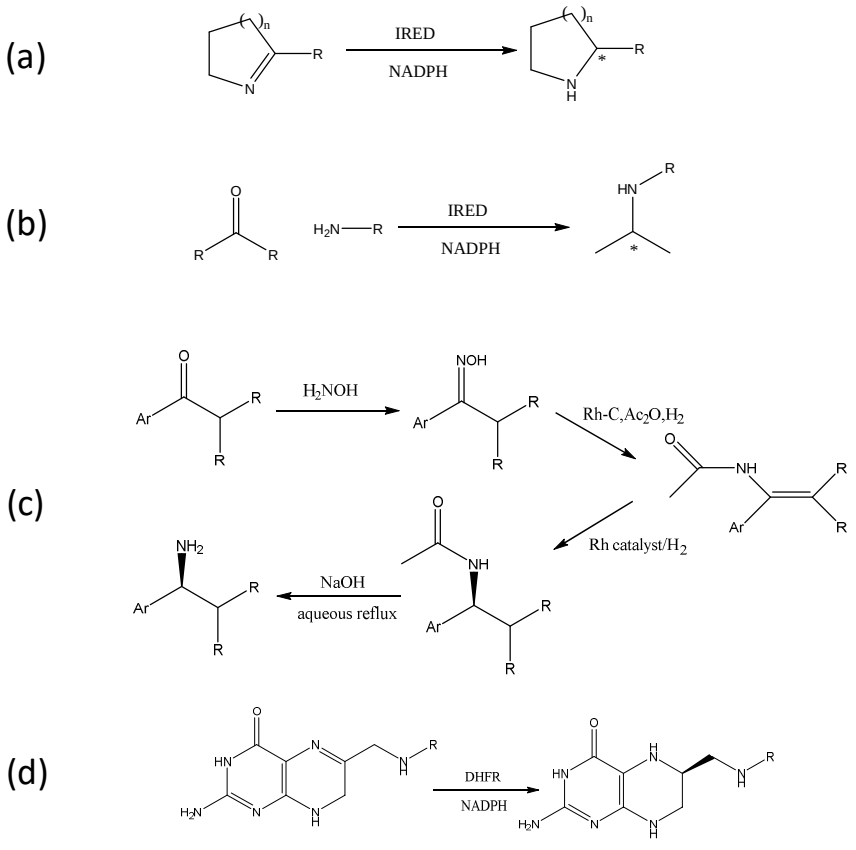
	K_M^{NAD+} / mM		K_M^{NADP+} / mM	
SH varaints	Electrochemical	Biochemical	Electrochemical	biochemical
Wildtype	0.12±0.01	0.055±0.08	>50	>50
E341A	0.38±0.1	0.061±0.11	1.32±0.36	4.83±1.7
D467S	0.11±0.01	0.066±0.18	3.70±0.33	3.39±0.98
E341A+D467S	1.36±0.84	0.065±0.18	1.12±0.29	2.25±1.05
E341A+S342R	0.65±0.23	1.32±0.69	0.35±0.11	0.60±0.33

Chapter Four: Demonstration of NADPH recycling coupled to NADPH dependent enzymes

In order to test the feasibility and robustness of the new NADPH regeneration system, two NADPH dependent enzymes were coupled with this new system: Imine reductase, and P450 monooxygenase. There are a number of NADPH-dependent enzymes which are of interest for different industries. P450 monooxygenase is a crucial NADPH dependent enzyme able to catalyse the hydroxylation of C-H bonds[50]. Imine reductases are another typical NADPH dependent enzyme with huge application potential to catalyse the reduction of C=N bonds, or the reductive amination of ketones[137]. In this chapter, the new NADPH recycling system will be coupled with these enzymes to demonstrate their feasibility. Part of the work involving P450 was carried out in collaboration with Dr. Koji Urata and Professor Luet L. Wong. Part of the work involving imine reductase was carried out with assistance from supervision of Jake Nicholson in the Vincent group.

4.1 Introduction to imine reductases

Imine reductases (IREDs) are NADPH-dependent oxidoreductases catalysing the asymmetric reduction of the C=N bond of pro-chiral imines to the corresponding chiral amines[138]. IREDs are also able to catalyse the asymmetric reductive amination of ketones to generate chiral 2° and 3° amines[56] (Scheme 1a, b). Chiral amines are crucial building blocks for active pharmaceutical ingredients, fine chemicals and other amine products in agricultural industries[139]. Therefore, IREDs are extremely useful in a variety of areas, as producing single chiral amines is challenging using traditional organic synthetic approaches. For instance, the well-established N-Acetylenamide strategy of producing primary chiral amines requires at least four steps from the starting material, and involving complicated Rhodium complex as catalyst, as well as extreme temperature and pH conditions[140] (Scheme 1c). On the contrary, imine reductase enzymatic approaches enjoy the general advantages for biocatalysis, such as mild condition, and fewer steps. Dihydrofolate reductase (DHFR) belongs to the super family of imine reductase, it catalyses the NADPH dependent reduction of 7, 8-dihydrofolate to 5, 6, 7, 8- tetrahydrofolate (Scheme 1d). Compared with the traditional organic synthesis approaches, this reaction occurs at neutral pH, room temperature, and only requires NADPH as its sole co-substrate.



Scheme 4-1 Asymmetric reduction of amines with different approaches.

However, most IREDs have very narrow substrate scope, limiting their application. Recently, Mitsukura and co-workers reported two new IREDs, (*R*)-IRED from *Streptomyces* sp. GF3587, and (*S*)-IRED from *Streptomyces* sp. GF3546[59]. Their native substrate is 2-methylpyrroline, but these two enzymes have a broad range of substrates, and are therefore particularly useful in a variety of asymmetric reductions of imines and iminium ions. Since their discovery, these enzymes and a number of their homologues have been studied and characterised both functionally and structurally. (*R*)-IRED from *Streptomyces* sp. GF3587 has been purified and crystallised by Muller and co-workers, and its crystal structure has been solved (**Figure 4-1**)[141].

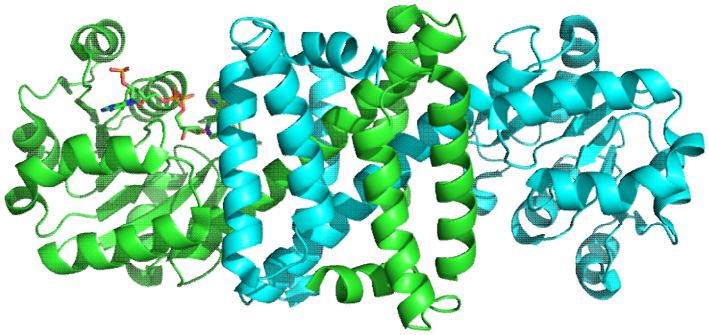


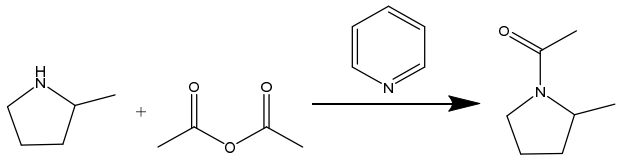
Figure 4-1 Crystal structure of (*R*)-IRED from Streptomyces sp. GF3587 PDB: 4OQY, PyMOL

This protein is a homodimer of two 31 kDa subunits. The binding of the two monomers relies on the α-helix secondary structure at the C-terminus, while the N-terminal domain forming a unique Rossmann fold is responsible for the binding of NADPH. The protein undergoes a conformational change when binding to the cofactor NADPH[47].

4.1.1 NADPH recycling system coupled with imine reductase

The imine reductase used in this work was the commercially available IRED (046) from Prozomix, a homologue of (*S*)-IRED from *Streptomyces* sp. GF3546. IRED (046) strictly uses NADPH as its redox equivalent, and is thus ideal for coupling with the new NADPH regeneration system to demonstrate its robustness. IRED (046) natively catalyse the reduction of 2-methylpyrroline to (*S*)-2-methylpyrrolidine with over 99% *ee*.

Before the reaction, a GC-FID method was developed to detect and quantitatively calculate the substrate and product. The product and the substrate were not separable by GC. Therefore, the compounds need to be derivatised in order to be separated on a GC column. First, the substrate and the product need to be basified by addition of NaOH before extraction into ethyl acetate; otherwise the substrate and the product cannot be extracted into the organic phase. Before testing by GC, the sample in ethyl acetate was treated with acetic anhydride and pyridine for N-acetylation the substrate and the product (**Scheme 4-2**), to enable the compounds to detected by the GC FID detector. The N-acetylated compound could be separate by CP-Chirasil-Dex CB GC column.



Scheme 4-2 The N-acetylation of the substrate 2-methylpyrroline

As discussed in chapter two, the GC instrument used in this work is TRACE™ 1310 Gas Chromatograph from Thermo Scientific™. The GC column used was CP-Chirasil-Dex CB from Agilent. The column was 25 m in length, 0.25 mm diameter, and 0.25 µm film thickness, fitted with a guard of 10 m undeactivated fused silica of the same diameter. The carrier gas was He (CP grade), and the flow rate was 2 mL/min. The inlet temperature was 200 °C. The injection volume was 0.1 µL, and the injection condition was splitless with split flow of 60 mL/min, splitless time 0.8 min, and purge 5 mL/min. The detection was Flame ionization detector (FID) at 200 °C. The detection gas was H_2 (35 mL/min), air (350 mL/min), and N_2 (40 mL/min). The method used to separate each compound was: hold at 70 °C for 5 min, then ramp to 180 °C at a rate of 5 °C/min, and lastly hold at 180 °C for 2 min. Following this protocol, the substrate methylpyrroline was detected at the retention time of 21.62 min. (*S*)-2-methylpyrrolidine was detected at the retention time of 17.45 min, and (*R*)-2-methylpyrrolidine at 17.19 min (**Figure 4-2**).

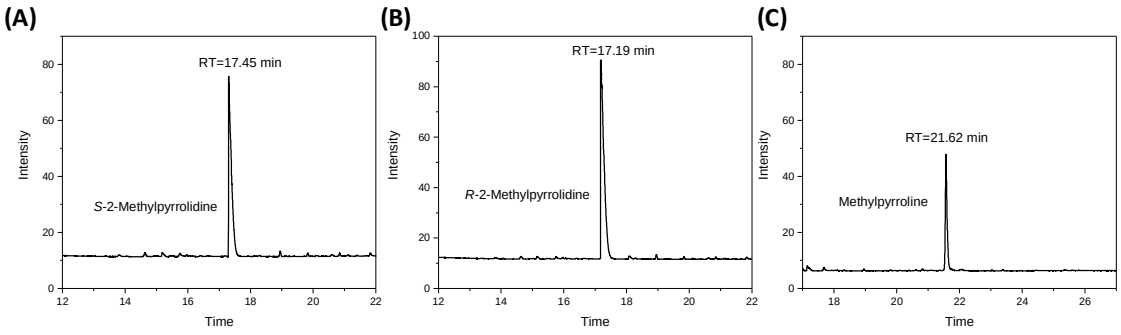


Figure 4-2 The GC standard results for (*S*)-2-methylpyrrolidine (A), (*R*)-2-methylpyrrolidine (B), and methylpyrroline (C). (RT: Retention Time)

Preliminary work on the characterisation of IRED (046) was carried out by Jake Nicholson in the Vincent research group. The reaction of imine reductase catalysed reduction of 2-methyl-1-pyrroline directly using NADPH was first carried out as a positive control reaction. The reaction condition was as followeds: methylpyrroline (10 mM), cofactor: NADPH (10-20 mM) or NADH 20 mM, imine reductase (1 mg), Tris buffer (50 mM pH 7.5), 1 mL scale in Eppendorf tubes, 24 hrs, 32°C, shaking at 300 rpm. The result was detected by GC (**Figure 4-3**). Upon adding 20 mM NADH, no product was detected, this confirmed that the imine reductase were not able to utilise NADH as its redox equivalent to sustain the reduction of methylpyrroline. Upon adding 10 mM NADPH (1:1 ratio of cofactor and substrate), the product, (*S*)-2-methylpyrrolidine was detected, and the conversion rate was about 50%. This indicated that a 1:1 ration of NADPH and substrate was not able to push the reduction reaction to 100% conversion, while the reaction reaches equilibrium when about 50% of the substrate being reduced. When adding 20 mM NADPH, the conversion rate reached over 90%, indicating that excessive of NADPH pushed the reaction equilibrium to the direction of producing (*S*)-2-methylpyrrolidine and $NADP^+$.

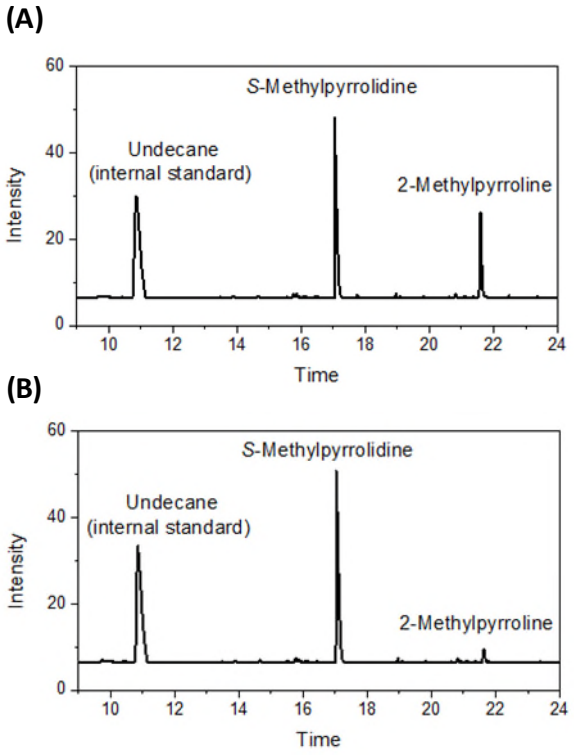


Figure 4-3 GC results for the positive control of imine reductase catalysed reduction of Methylpyrroline with different amount of NADPH supply: (A) 10mM NADPH, and (B) 20 mM NADPH.

After determining the viability of IRED, the enzyme was then ready to be coupled with the new NADPH regeneration system based on soluble hydrogenase variants. This new system was discussed in detail in chapter three. The soluble hydrogenase HoxHYFU from *Ralstonia eutropha* was used previously in H_2 driven NADH regeneration, and proved to be robust. A number of mutations were introduced around the cofactor binding pocket of the HoxF subunit of hydrogenase, in the hope of changing the cofactor specificity. Four variants were prepared, and their affinity for NAD^+ and $NADP^+$ were determined electrochemically. One of the variants, $HoxF^{E341A/S342R}$, had the highest activity and affinity towards $NADP^+$. Therefore it was the best candidate to be incorporated into the new NADPH regeneration system. Since then, a new variant $HoxF^{E341A/S342R/D467S}$ was obtained, and a preliminary study indicated that it was also promising for recycling NADPH. Therefore, in this set of experiments, both the two variants, $HoxF^{E341A/S342R}$ and $HoxF^{E341A/S342R/D467S}$ were coupled with IRED. Wild-type SH was also used as a negative control for these experiments, because it has been chosen to bave a very low affinity for $NADP^+$. This group of experiments were carried out under the

following conditions: substrate 15 mM, cofactor (NAD^+ or $NADP^+$) 1 mM, hydrogenase variants 0.1 mg/mL, IRED from Prozomix 1 mg/mL in Tris buffer (100 mM, pH 8.0). The reactions were carried out at 1 mL scale at the bottom of 10 mL round bottom flasks. Prior to the reaction, the Tris buffer was saturated with H_2 by bubbling H_2 for one hour. A magnetic stirrer bar was stirring at 300 rpm throughout the reaction time, and in the meantime, H_2 was constantly flowing through the head space of the flask. After 16 hours reaction at room temperature, the reaction outcome was analysed by GC and ^{1}H NMR.

Table 4-1 A summary of the conversion, cofactor turnover number, and the enzyme total turnover number of different *R.e* SH variant with $NADP^+$ and NAD^+.

R.e SH variant	Cofactor	Conversion	Cofactor TN	SH TTN
$HoxF^{E3421A/S342R}$	NAD^+	0	0	0
$HoxF^{WT}$	NAD^+	0.8	0.12	250
$HoxF^{WT}$	$NADP^+$	<1	<0.1	79
$HoxF^{E3421A/S342R}$	$NADP^+$	32	8	11000
$HoxF^{E3421A/S342R/D467S}$	$NADP^+$	18	4.5	9500

The results are summarised in **Table 4-1**. In the control reaction, $HoxF^{WT}$ was used in the system. As discussed before, $NADP^+$/NADPH were not able to bind with $HoxF^{WT}$. Therefore when adding a catalytic amount of $NADP^+$, hardly any product was detected, as the wildtype hydrogenase was not capable of reducing $NADP^+$ to NADPH and sustaining the IRED for the reduction of methylpyrroline. The trace amount of (*S*)-2-methylpyrrolidine produced was hypothesised to be due to a small amount of NADPH contamination in $NADP^+$. When adding NAD^+ to the system containing wildtype SH, although the hydrogenase was able to reduce NAD^+ to NADH by oxidising H_2, IRED was not able to take the reducing NADH as its redox equivalent to reduce the substrate. Therefore, still only trace amount of product was detected by GC. Then $HoxF^{E341A/S342R}$ was incorporated into the system. When NAD^+ was added, still no conversion was observed. Although the $HoxF^{E341A/S342R}$ was able to reduce NAD^+ to NADH with decreased activity compared with the wildtype enzyme, the reduced NADH was not able to be used by IRED. These control reactions

clearly indicated that the wildtype hydrogenase was not able to recycle $NADP^+$ to sustain the downstream reaction catalysed by IRED. When $NADP^+$ was added into the system, both the two variants showed considerable conversion of substrate, indicating that the new NADPH regeneration system with these two variants was successful. The system with $HoxF^{E341A/S342R}$ achieved 32% conversion after 16 hours of reaction time, and the turnover number for the enzyme $HoxF^{E341A/S342R}$ was 11000. The system with the new variant $HoxF^{E341A/S342R/D467S}$ only achieved 18% conversion under the same reaction condition, and the turnover number was 9500. This is consistent with the electrochemical data which also indicated that $HoxF^{E341A/S342R}$ was more robust and active than the new variant $HoxF^{E341A/S342R/D467S}$. Therefore $HoxF^{E341A/S342R}$ is still the best candidate for the new NADPH regeneration system.

Although $SH^{E341A/S342R}$ was determined to be the best candidate enzyme for the new NADPH regeneration system, in the previous experiments, the conversion was only 32%. To achieve a higher conversion, the reaction condition still needs to be optimised. A group of preliminary experiments carried out indicated that the IRED achieved its highest activity at pH 7.5 solution and under 32 °C. Therefore, the following experiments were then all carried out under these conditions. The H_2 driven 2-methyl-1-pyrroline reduction reaction was carried out in Tris buffer (50 mM pH7.5). The reaction was carried out in a stainless steel pressure vessel (Tinyclave steel, Buchi AG), and 15-25 mM 2-methyl-1-pyrroline, 0.1-1 mM $NADP^+$, 1 mg IRED (046), and 1 mg $SH^{E341A/S342R}$ were added into 1 mL Tris buffer (50 mM, pH 7.5) at the bottom of a 50 mL glass insert within the pressure vessel. Then the pressure vessel was pressurised at 2 bar H_2. The pressure vessel was then immersed in a water bath at 32 °C. The reaction mixture in the pressure vessel was stirred at 300 rpm by a magnetic stirrer bar. In order to optimise the condition for the H_2 driven methylpyrroline reduction by IRED, four parallel reactions with different conditions were carried out (**Table 4-2**). After the reaction, GC was applied to determine the conversion rate of each reaction. When 15 mM substrate and 1 mM NADPH were added to the mixture, the reaction achieved an over 99% conversion after 16 hours. The cofactor turnover number was 15, and the $SH^{E341A/S342R}$ turnover number was 24000. However, when the substrate concentration from 15 mM to 25 mM, and other conditions remained the same,

only 67% conversion was achieved after 16 hours. Even if a similar the reaction was kept running for another 24 hours, the conversion would increase to 88%, but it was still not possible to achieve full conversion. On the other hand, the turnover number for cofactor and the enzyme both increased. The turnover number for cofactor increased from 15 to 22, while the turnover number for $HoxF^{E341A/S342R}$ increased from 24000 to 35000. However, when adding 15 mM substrate with only 0.1 mM NADPH, the conversion was only 34% after 40 hours, and although the cofactor turnover number was higher due to the lower cofactor to substrate ration, the SH turnover number was low. This is unsurprising because the K_M $NADP^+$ for $HoxF^{E341A/S342R}$ is over 1 mM, so 0.1 mM $NADP^+$ is far below the K_M value at which the enzyme reaches half of its maximum speed. Therefore, under these conditions the regeneration of NADPH was very slow and greatly limited the overall conversion.

Table 4-2 Summary of variant $HoxF^{E341A/S342R}$ catalysed reduction of methylpyrroline under different conditions

Entry	[Substrate]/mM	[cofactor]/mM	Hours	Conversion	[Product]/ $g \cdot L^{-1}$	Cofactor TN	Hydrogenase TN
1	15	1	16	99	1.3	15	24000
2	25	1	16	67	1.4	17	27000
3	25	1	40	88	2.0	22	35000
4	15	0.1	40	34	0.4	51	8000

To conclude, the new NADPH regeneration system coupled with IRED had its best performance with respect to productivity when the substrate concentration was at 25 mM, and $NADP^+$ at 1 mM. Under these conditions, the system achieved 67% conversion within 16 hours, and 88% within 40 hurs, and had high turnover number for both the enzyme, and the cofactor. This indicated that the new H_2 driven NADPH regeneration system was able to be successfully coupled with IRED to sustain the reduction from imine to amine with high enantio-selectivity, and high conversion rate, providing that a reasonably high cofactor concentration is used. However, compared with the traditional way of using glucose and glucose dehydrogenase as NADPH regeneration system, the overall turnover number for both cofactor and the enzyme were still low. Therefore, the system requires further optimisation. One possible approach to increase the overall activity of the system is

to immobilise the imine reductase and the SH variant together on carbon particles. As described before, co-immobilised enzymes can enjoy a substrate channelling effect, which allows the regenerating NADPH to interact directly with the downstream enzyme (in this case IRED), before diffusion into the solution. This is the direction to be explored in the future.

4.2 Introduction to Cytochrome P450 mono-oxygenase

Cytochrome P450 (CYP, or P450) belongs to a large protein superfamily of haemproteins, containing a haem group within their active site[142]. P450s exist in most living organisms and are involved in crucial metabolism processes. This enzyme has a spectrophotometric wavelength absorption peak at 450 nm when bound with CO, hence the name P450. P450s catalyse a variety of reactions such as oxidative dehalogenation, oxidative C-C bond cleavage, as well as alcohol and aldehyde oxidation. The most attractive reaction catalysed by P450 is the hydroxylation of C-H bonds[143].

$$RH + O_2 + NADPH + H^+ \xrightarrow{P450} ROH + H_2O + NADP^+$$

P450 is also a promiscuous enzyme whose native substrates are fatty acids, terpenes and gaseous alkanes. Thus P450 is a crucial enzyme in biotechnology, as P450 is able to functionalise C-H bonds, which are complicated to activate using traditional organic synthesis approaches. Also, the introduction of a hydroxyl group potentially alters the property of a compound, such as its solubility, and toxicity. P450s are structurally very diverse[144]. Most P450 enzymes only contain the haem domain but not a diaphorase domain. Therefore they rely on other enzymes such as ferredoxin and ferredoxin $NADP^+$ reductase, or NADPH-P450 reductase to oxidase NADPH and transfer the electrons to the haem centre. These P450s are not ideal for *in vitro* enzymatic catalysis, as they require additional enzymes like NADPH-P450 reductase to assist them for the catalysis. One type of P450 have both the haem domain and the diaphorase domain connected by a linker, enabling the internal transfer of the electrons from NADPH to the haem centre within the protein. This is

particularly advantageous for *in vitro* biocatalysis, as it requires no co-expression of other enzymes to assist the electron transfer. CYP102A1 is one such P450. As the third P450 isolated from *B. megaterium*, CYP102A1 was designated $P450_{BM3}$. $P450_{BM3}$ is a soluble enzyme easy to express in the well-established *E. coli* expression system with high yield[145].

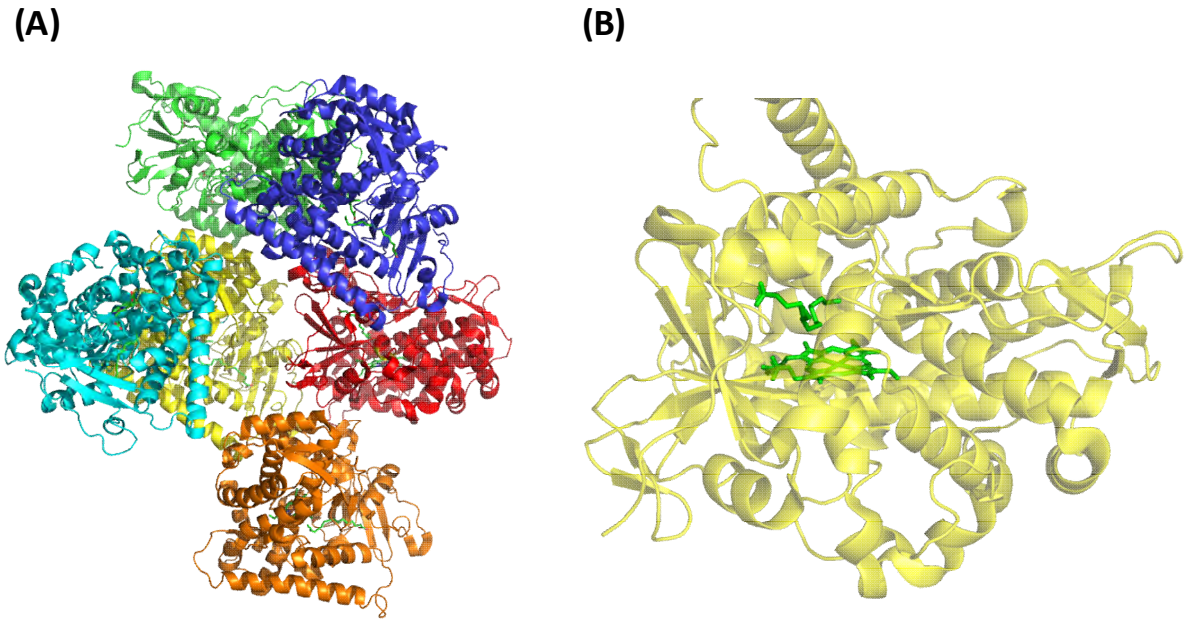


Figure 4-4 The crystal structure of $P450_{BM3}$ CYP102A1. (PDB:3QI8, PyMOL)

$P450_{BM3}$ is a relatively large protein with the molecular weight of 120 kDa, containing a 55 kDa haem domain (BMP) for hydroxylation of C-H bonds, and a 65 kDa $NADP^+$ reductase domain (BMR) with two prosthetic flavin cofacotrs, FAD and FMN, for the oxidation of NADPH (**Figure 4-**). The BMR domain shares high sequence similarity with the mammalian cytochrome P450 reductase. The two domains are connected by a linker, crucial for maintaining the functionality of the entire enzyme. Unlike hydrogenases, which rely on FeS clusters as electron transfer relays, P450s directly transfer electrons from the flavin group of BMR to the haem catalytic centre of BMP[146].

4.2.1 An NADPH regeneration system coupled with a P450 BM3 variant

The P450 used in this work was $P450_{BM3}$ (CYP102A1) from *Bacillus megaterium*. The P450 enzyme was heterogeneously expressed in *E. coli* BL21 (DE3) and crudely purified by ammonia chloride precipitation. Previous work has demonstrated that P450 BM3 oxidises octane to octanol with high turnover using GDH and glucose as the NADPH regeneration system. In this work, the *R.e* SH variant was used as NADPH recycling enzyme with H_2 bubbling. The effectiveness of this new NADPH regeneration system was characterised and compared with the traditional GDH/glucose system. To conduct the experiment, 0.5 μM P450 enzyme, together with 0.5 μM *R.e* $SH^{E341A/S342R}$ enzyme solution, 1 mM $NADP^+$, and 20 μg/mL catalase were mixed in 1.5 mL phosphate buffer (100 mM, pH 7.4) in a 6 mL glass vial in the glovebox. P450 produces H_2O_2 was by product during the catalysis process, and decreases the activity of the system. Therefore catalase is used to get rid of the H_2O_2. Before the experiment, the buffer was bubbled with N_2 overnight to remove O_2, and then bubbled with H_2 for 30 minutes to saturate the buffer with H_2. Then the glass vial was bubbled with H_2 for another 30 seconds to allow the H_2 to fill the head space of the vial. At last, 5 mM octane in DMSO solution was added into the system by gas-tight syringe. The glass vial was then injected with 10% air to the solution mixture as well as the head space. The reaction mixture was stirred for 2 hours at room temperature.

The reaction mixture was tested by GC (**Figure 4-**). An aliquot of 1 mL reaction mixture was removed from the system and put into a separate Eppendorf tube, mixed and vortex with 300 μL ethyl acetate to extract octane and octanol from the aqueous phase. For GC test, a TRACE GC instrument from ThermoFinnegan with a SPB-1 fused silica capillary column and flame ionisation detection were used. The following GC procedure was applied to analyse the sample: Injector temperature: 230 ºC, FID temperature: 250 ºC Oven temperature: 100 ºC for 40 mins.

The retention time for reactant and products were as followed: 3-octanone: 34.4 min 2-octanone: 35.2 min 4-octanol: 35.8 min 3-octanol 37.3 min 2-octanol: 38.1 min

Besides, a group of control experiments were also carried out. The same reaction was carried out with GDH/glucose as $NADP^+$ regeneration system. In this reaction, 10 U/mL GDH and 200 mM

glucose were added to the system to replace *R.e* SH variant and H_2. Another experiment with the same condition using *R.e* SH variant but without addition of $NADP^+$ was also carried out as negative control. The GC result clearly showed that without addition of $NADP^+$ no product peak observed. This indicated that the cofactor is crucial for P450 to be functional. The GC result for P450 coupled with GDH/glucose NADPH recycling system showed that five products were generated from the reaction, 3-octanone, 2-octanone, 4-octanol, 3-octanol, and 2-octanol. The product with highest yield is 2-octanol. The GC graph for *R. e* SH variant/H_2 system showed almost the same results. All the five products were observed with very similar yields. This indicated that the new H_2 driven NADPH recycling system is at least as efficient as the conventional GDH/glucose system.

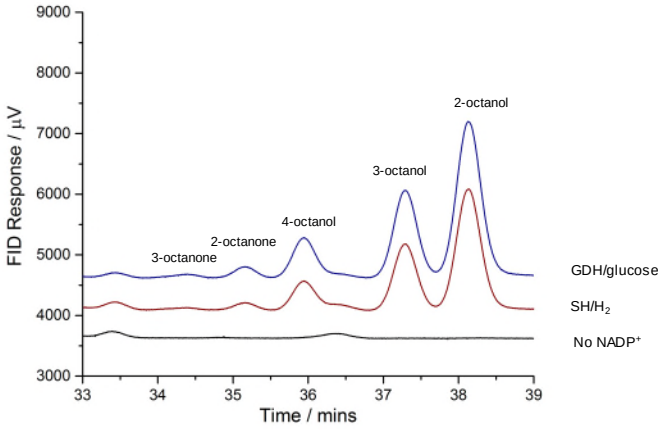


Figure 4-5 The GC results for P450 catalysed oxidation of 3-octanone with the H_2 driven NADPH regeneration system.

Although the new H_2 driven NADPH system had promising results when coupled with P450, there are a number of limitations and drawbacks hampering the further development of it for P450 reactions. P450 loses its activity when binding to a carbon particle, making immobilisation on the particle system unfeasible in this circumstance. Whole SH variant from *R. e* has to be used to both oxidise H_2 and to reduce $NADP^+$. As discussed previously, the whole SH HoxHYFU is not very stable, and it is less active than hyd-1 from *E. coli.* Also, *R.e* SH variant and P450 moving freely in the buffer, with no substrate channelling effect, makes it less effective as in the particle system when the enzymes are immobilised together. On the other hand, unlike other oxidoreductases, P450 uses

NADPH and O_2 together to catalyse the reaction. Therefore, a constant supply of air or pure O_2 is inevitable. However, the H_2 driven NADPH recycling system requires supply of H_2 as driving force. A combined supply of H_2 and O_2 mixture has a potential explosion risk, and thus is not feasible for industrial use. In this way, P450 is not yet an ideal NADPH-dependent enzyme to be incorporated into the new H_2 driven NADPH regeneration system. This work is a proof of concept showcase to demonstrate that the new NADPH recycling system is active and has a potential to be incorporated with useful redox enzymes.

Chapter Five: Expression and application of soluble transhydrogenase UdhA

5.1 Introduction

Transhydrogenation is the process of either transferring a proton from NADH to $NADP^+$ forming NADPH and NAD^+, or transferring a proton from NADPH to NAD^+ forming NADH and $NADP^+$. Transhydrogenation does not happen uncatalysed. In living organisms, a group of enzymes called transhydrogenases are in charge of carrying out this reaction and keep the equilibrium of the nicotinamide cofactors in the cell within set limits. Transhydrogenases are divided into two categories, the energy dependent membrane-bound transhydrogenase and the energy independent soluble transhydrogenase[112]. The energy dependent transhydrogenase requires constant ATP supply and is hard to purify as these proteins are membrane bound, making them undesirable for enzymatic catalysis applications. Soluble transhydrogenase, on the other hand, is more useful both in academia and industry. Pyridine soluble transhydrogenase UdhA from *E. coli* has been well studied and characterised, and shows great potential for catalysing transhydrogenation reactions. Previous work has demonstrated UdhA coupled with other NADH cofactor regeneration enzymes to recycle NADPH and sustain NADPH-dependent enzymes[111].

Transhydrogenation is one approach to achieve NADPH regeneration system based on the current H_2 driven NADH regeneration system. In this chapter, soluble transhydrogenase UdhA is expressed and isolated from *E. coli*. The isolated UdhA is then characterised to examine its activity for converting NAD^+ to $NADP^+$, and coupled with the current NADH recycling system to examine whether it enables the system to recycle NADPH.

As discussed in chapter one, one of the approaches to transform the current NADH regeneration system to a novel NADPH system is using soluble transhydrogenase UdhA for the transhydrogenation of cofactors. Transhydrogenation of cofactors means transfer of a hydride from NADH to $NADP^+$, or from NADPH to NAD^+. When UdhA is coupled with the current system, only a catalytic amount of NAD^+ and $NADP^+$ is needed for a new NADPH system.

5.2 Molecular cloning of soluble transhydrogenase UdhA

The molecular cloning procedure of UdhA is similar to that of nuo genes. udhA is located in the genome of *E. coli* DH5α strain. This gene was amplified with NcoI and XhoI restriction sites introduced by PCR using the following primers (the restriction sites were underlined):

Forward primer:

5’ AGTGTAGCCATGGCACATTCCTACGATTACGATG

Reverse Primer:

5’ ATCCGCTCGAGAAACAGGCGGTTTAAACC

The PCR DNA fragment was digested by endonucleases NcoI and XhoI, and ligated into pET28a vector digested with the same pair of endonuclases. The resulting vector was verified by DNA sequencing provided by Source BioScience, and denoted as pETUdhA. Subsequently, the resulting vector was transformed into BL21 (DE3) *E. coli* competent cells for protein expression (**Figure 5-1**).

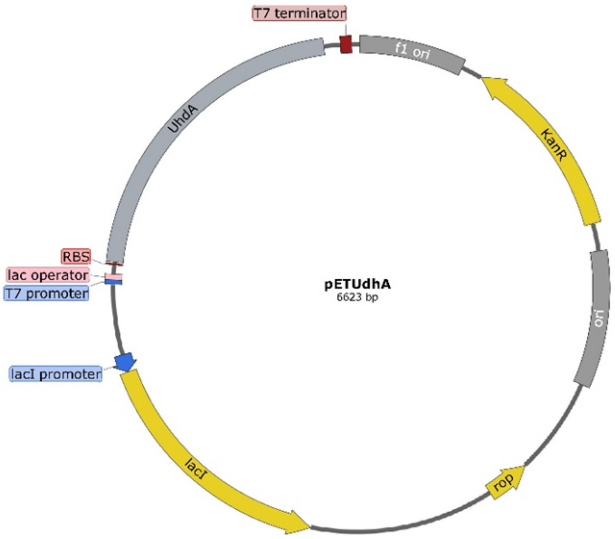


Figure 5-1 The plasmid map of the constructed pETUdhA.

5.3 Expression and isolation of UdhA

First, the soluble transhydrogenase UdhA was cloned into pET28a vector and overexpressed in *E. coil*. The protocol of cloning, expression and purification of UdhA is discussed chapter two. The SDS-PAGE result (**Figure 5-2**) of crude cell lysate of *E. coli* bearing pET28a vector with UdhA showed an enhanced band at around 50 kDa, which is correlated with the apparent molecular weight of UdhA (52 kDa). This indicated that soluble transhydrogenase UdhA was successfully overexpressed in *E. coli*. The next step is to purify the target protein UdhA. The purification process was also discussed in general in chapter two. According to the SDS-PAGE result, the purification process was not very successful, as the 'purified protein' still contained a lot of impurities. The reason remains to be explored, but on possible explanation is that the histag of the target protein UdhA is not fully exposed. Therefore, the target protein is not able to bind to the column very tightly and would be washed away by low concentration of imidazole buffer, when other impurity proteins would also come out.

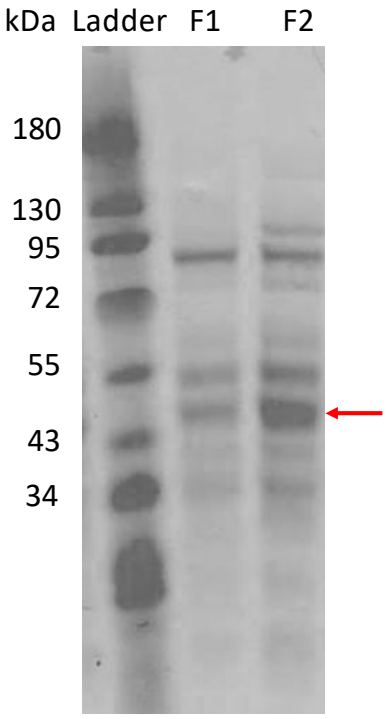


Figure 5-2 The SDS-PAGE result for UdhA expression and purification. F1: crude extract of cell overexpressed UdhA. F2: fraction went through Ni-NTA HisTrap column and washed with high concentration of imidazole. The red arrow indicates the target protein.

5.4 Cofactor stability

Before carrying on with transhydrogenation experiments, the stability of cofactors needed to be scrutinised. Previous work has illustrated that the stability of cofactors varied from different buffer and different pH. In this work, cofactors are mixed together with enzymes and particles in solution, and sometimes with shaking for a long period of time. As cofactors are not very stable, they might degrade, oxidised, or interact with each other during the reactions. As the stability of cofactors might affect the outcome of transhydrogenation experiments, it is important to carry out a cofactor stability test before the transhydrogenation experiments. To detect cofactors, HPLC methods are applied as discussed in Chapter two. As all the cofactors have a distinct absorption peak at 260 nm, the UV detector in HPLC is positioned to monitor 260 nm for cofactors. Meanwhile, the reduced

cofactors, NADH and NADPH, also has an additional distinct absorption peak at 340 nm, a second UV detector in HPLC is positioned to monitor 340 nm for NADH and NADPH.

5.4.1 Single cofactor stability

The stability of each cofactor was tested individually. NAD^+, NADH, $NADP^+$, and NADPH solution (5 mM cofactor in 1 mL deionised water) were put at ambient temperature overnight, with normal light condition. The starting samples and the overnight samples are examined by HPLC, using the method discussed in Chapter two. The oxidised form NAD^+ and $NADP^+$ were most stable as overnight result had a very similar peak area of the cofactor, and no other detectable peaks appeared. This indicated that hardly any NAD^+ or $NADP^+$ undergoes decomposition overnight (**Figure 5-3**).

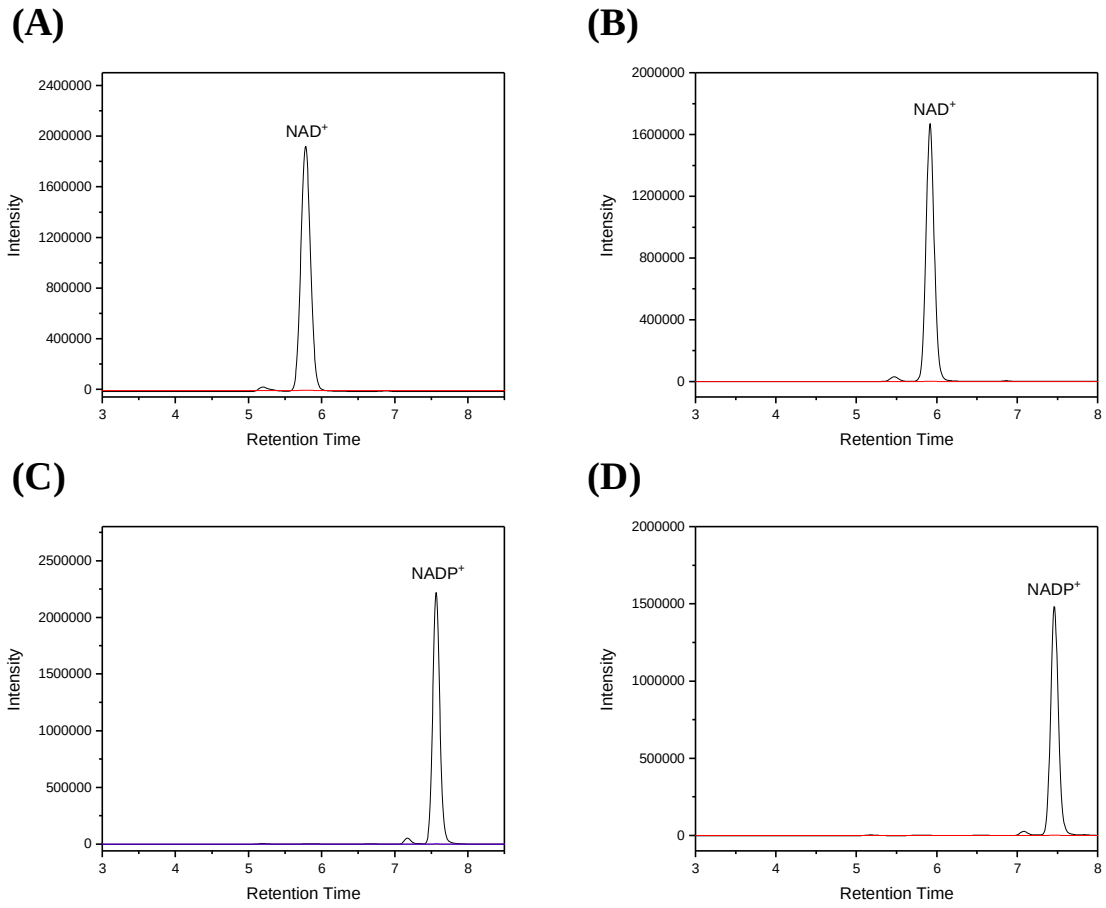


Figure 5-3 HPLC results for single cofactor NAD^+ and $NADP^+$ stability test. The figures showed the initial cofactor samples NAD^+ (A), and $NADP^+$ (B), as well as the overnight cofactor samples NAD^+ (C), and $NADP^+$ (D).

NADH and NADPH were less stable in comparison (**Figure 5-4**). First it is worth noting that the sample of NADH and NADPH contain some impurities (NAD^+ in NADH sample, and $NADP^+$ in NADPH sample), so the initial HPLC results for NADH and NADPH already contained the peaks corresponding to $NADP^+$ and NAD^+. The overnight sample of NADH showed a diminished NADH peak and a slightly increased NAD^+ peak, which suggests some of the NADH has been oxidised to NAD^+. No other impurity peak was observed from the HPLC results showing that NADH does not undergo any other form of degradation or decomposition overnight, nor it did interact with the buffer system. The situation for NADPH was similar to NADH. Part of the NADPH was reduced to $NADP^+$, and no other

observable side reactions happened. The oxidation of NADH and NADPH were most possibly due to the O_2 in the buffer, or on the head space of the tube.

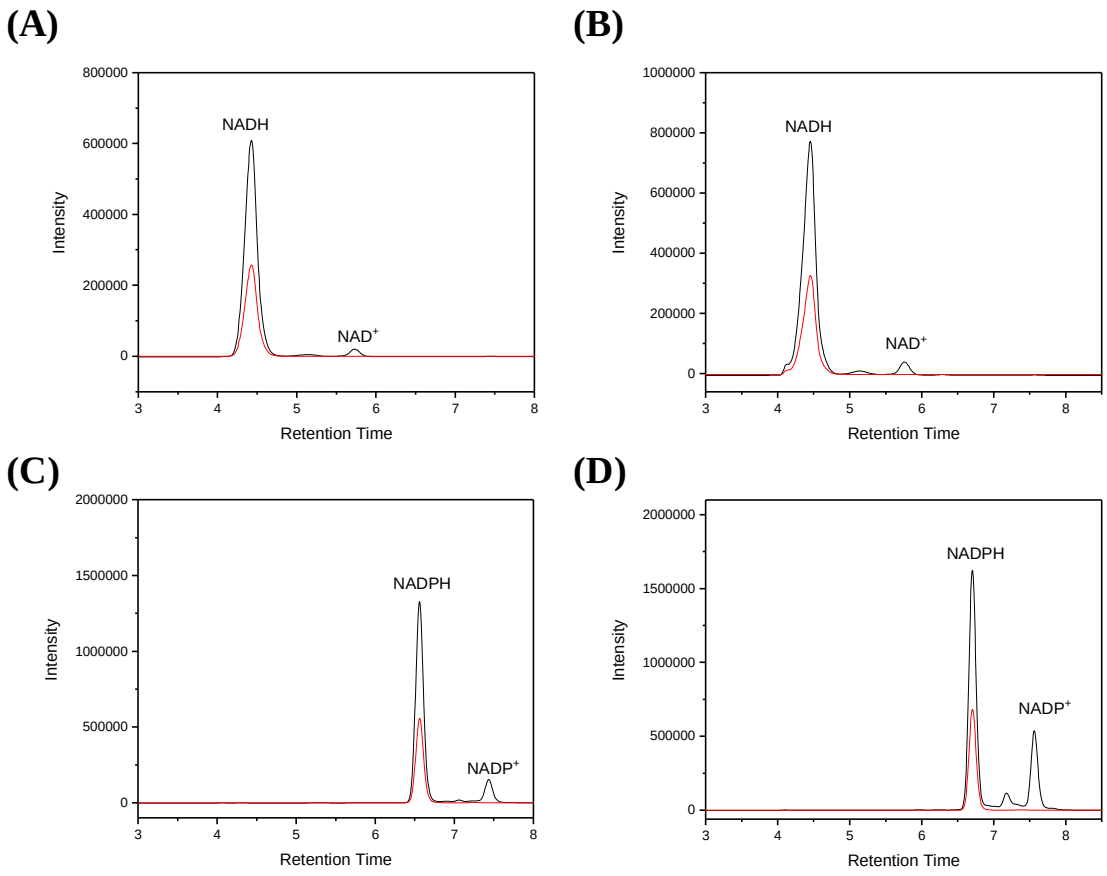


Figure 5-4 HPLC results for single cofactor NADH and NADPH stability test. The figures showed the initial cofactor samples NADH (A), and NADPH (B), as well as the overnight cofactor samples NADH (C), and NADPH (D).

5.4.2 Cofactor mixture stability

As transhydrogenation experiments require a mixture of cofactors (NAD^+/NADPH, or $NADP^+$/NADH), and the expected results are mixture of all four cofactors, it is important to also examine the stability of cofactor mixtures. First, all four cofactors are mixed (5mM NAD^+, 5 mM NADH, 5 mM $NADP^+$, 5 mM NADPH in 1 ml deionised water), and stay overnight at ambient temperature. The starting sample and the overnight sample are both tested on HPLC (**Figure 5-5**). The HPLC result for the starting sample shows clearly four

distinctive peaks for the related cofactors, and there are some minor peaks for unknown impurities. The overnight HPLC result showed that all the 340 nm peaks for NADH and NADPH disappeared, which indicated that these two cofactors were fully decomposed. Also, a lot of other peaks appears, and cannot identify if the NAD^+ and $NADP^+$ peaks still existed. This clearly indicated that the cofactors interacted with each other, and undergone some unknown side reactions.

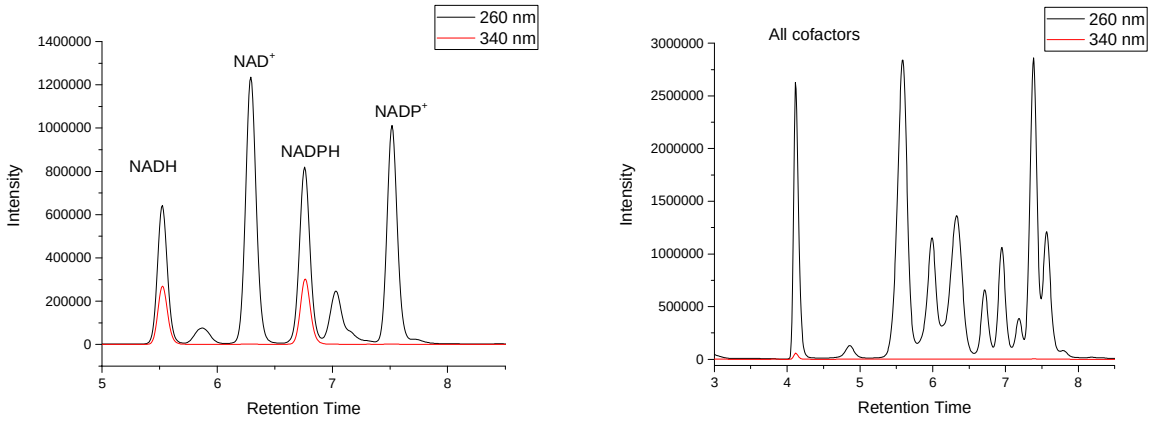


Figure 5-5 HPLC results for all four cofactors mixture stability test. (A) the initial sample of all four cofactors, and (B) the overnight cofactor samples.

According to the cofactor stability results. Although the individual cofactors were reasonably stable, the cofactor mixture was quite unstable. This was due to the interaction between different cofactors. In the UdhA meditated NADPH regeneration system, all the four cofactors would be present, therefore the instability of the cofactors would potentially hinder the robustness of the system. In this case, to avoid the interaction and decomposition of cofactors, all the reaction time for UdhA meditated cofactor transhydrogenation reactions would be limited to four hours.

5.5 Transhydrogenation using UdhA

The crudely purified UdhA enzyme was first used to test the transhydrogenation activity. The enzyme sample was dissolved in Tris buffer (100 mM, pH7.5), and concentrated 5 times

by vivaspin centrifuging at 10000 x g for 10 min. Then, 50 µL concentrated soluble lysate was added into 1 mL Tris buffer (100 mM, pH7.5) with either 5 mM NAD^+ and 5 mM NADPH, or 5 mM $NADP^+$ and 5 mM NADH. The reaction mixtures were left for four hours at ambient temperature. Then the reaction mixture was filtered in order to get rid of any components that could potentially block the HPLC columns. The filtered sample was then tested by HPLC. In order to prevent any oxidation of reduced cofactor by oxygen in the environment, the Tris buffer used is degassed prior to the experiment, and all the operations are carried out in N_2 glovebox.

The HPLC results for the two experiments were consistent (**Figure 5-6**). When NADH and $NADP^+$ were mixed and incubated for four hours by UdhA, NAD^+ and NADPH were detected by HPLC, this indicated that UdhA indeed mediated the transhydrogenation process of transferring the proton from NADH to $NADP^+$, producing NAD+ and NADPH. When NADPH and NAD^+ were mixed, the situation was the same. UdhA was also able to mediate the reverse, transferring a hydride from NADPH to NAD^+. In order to exclude to possibility that other cellular components catalysed the hydride transfer, a control reaction was carried out. A cell lysate without vector containing *udhA* gene was obtained. Therefore, the cell lysate would not contain overexpressed UdhA enzyme. The cofactor group either NAD^+/ NADPH or $NADP^+$/NADH, were incubated together with cell lysate without overexpressed UdhA under the same condition. The HPLC results indicated that no transhydrogenation observed. These data was sufficient to demonstrate that UdhA was activity and feasible to be incorporated into the current NADH recycling system and transform it into a new NADPH recycling system.

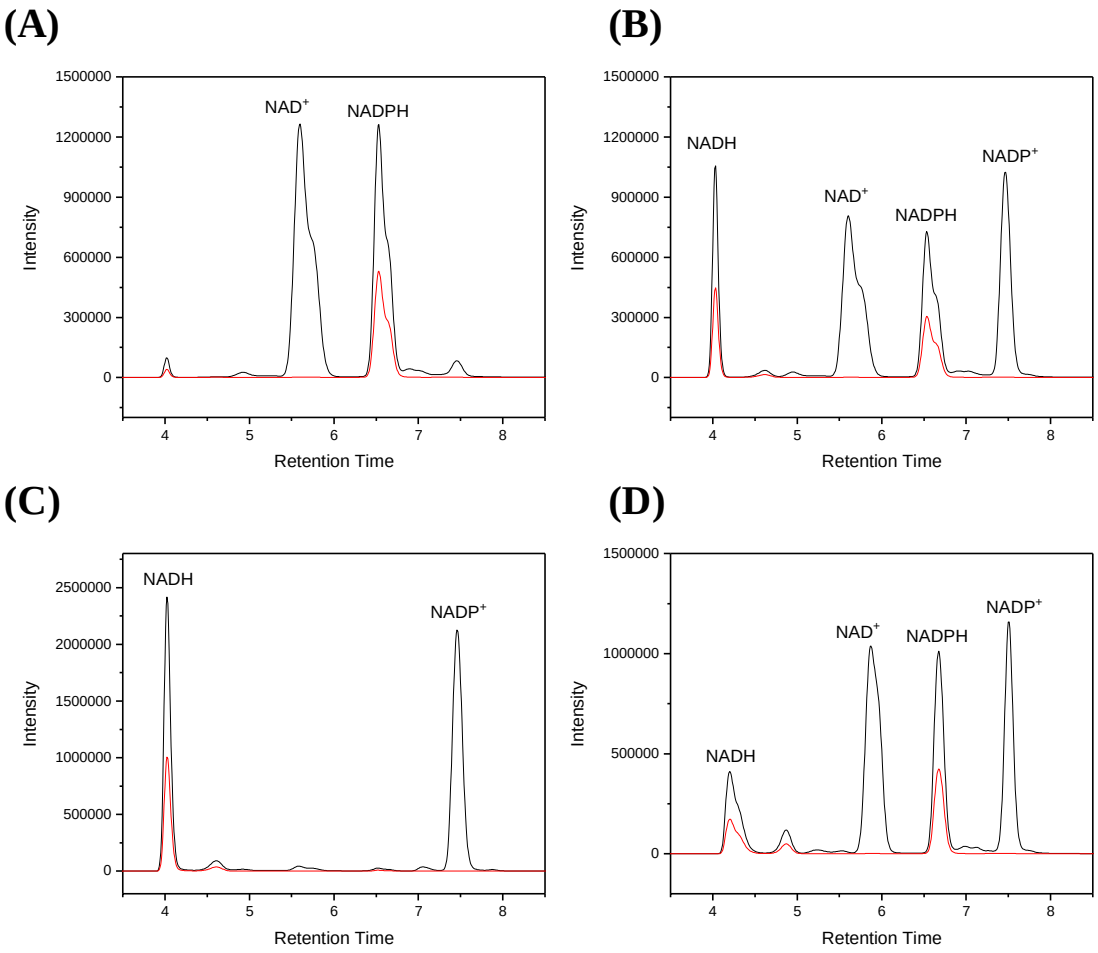


Figure 5-6 HPLC results for transhydrogenation mediated by UdhA. (A) the initial sample of NAD^+ and NADPH, and (B) the reaction mixture of NAD^+ and NADPH after four hours. (C) the initial sample of $NADP^+$ and NADH, and (B) the reaction mixture of $NADP^+$ and NADH after four hours.

5.6 Artificial transhydrogenation

Inspired by the mechanism of soluble transhydrogenase, an alternative approach for transhydrogenation is proposed via using a two enzyme particle system, called artificial transhydrogenation system, as discussed at the beginning of this chapter (**Figure 5-7**). One enzyme is the wildtype *R.e* SH which has been discussed in Chapter one and the characterisation of which was discussed in chapter three. This enzyme is a native enzyme in *Ralstonia eutropha* capable of converting between NAD^+ and NADH, and has no activity at all for $NADP^+$ or NADPH. The other enzyme is the new double variant *R.e* SH, $HoxF^{E341A/S342R}$, which has the highest activity for converting between $NADP^+$ and NADPH

among all the *R.e* SH variants, detail of which was also discussed in chapter three. This enzyme also has activity for NAD^+ and NADH, but much lower than the native enzyme. In the case of transferring of proton from NADH to $NADP^+$, the native ATP-independent transhydrogenase first oxidases NADH and releases NAD^+ and proton to the bulk solution, while the FMN molecule is reduced and retains the electron obtained from oxidising the cofactor. Then the $NADP^+$ would bind to the enzyme activity site, and the reduced FMN would transfer the electron to the cofactor and reduce it to NADPH. The proposed mechanism for this artificial transhydrogenation system is similar to that of the native transhydrogenase. Also in the case of transferring proton from NADH to NADPH by the artificial transhydrogenation system, the NADH is first oxidised by the wildtype *Re* SH, and the electron would transfer via the carbon bead to $HoxF^{E341A/S342R}$. The latter would take up the electron and reduce $NADP^+$ to NADPH.

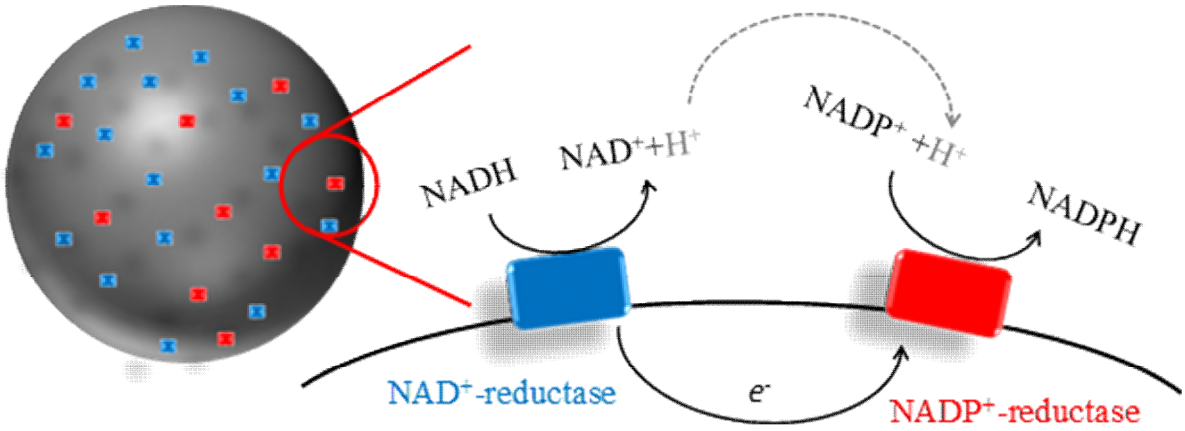


Figure 5-7 The illustrated figure showing the proposed mechanism of artificial transhydrogenase.

To characterise the proposed artificial transhydrogenation system, the two enzymes are co-immobilised on carbon particle BP2000, and cofactor couple NAD^+/NADPH or $NADP^+$/NADH are supplied. To carry out the experiment, 20 mg BP2000 is dissolved in 1 mL degassed Bis-Tris buffer (50 mM, pH 6.0) and sonicated for 20 min. Then 10 µL native

R.e SH (1-3 mg·mL^{-1}), 10 μL *R.e* SH variant HoxF$^{E341A/S342R}$ (1-3 mg·mL^{-1}), and 10 μL BP2000 suspension (10 mg·mL^{-1}) are mixed and incubated for 1 hour, during which the mixture was flipped a few times every 15 or 20 min. The enzyme particle mixture was then transferred to 1 mL degassed Bis-Tris buffer (50 mM, pH6.0) with 5 mM $NADP^+$ and 5 mM NADH. The previous cofactor stability experiments have showed that reduced cofactors NADH and NADPH are easily oxidised by O_2 in the environment, so all the operations were carried out in glovebox to avoid O_2. Since the cofactor mixtures are unstable overnight, the reaction mixture was incubated for only 4 hours under ambient temperature.

The cofactor mixture was then tested by HPLC before and after the experiment (**Figure 5-8**). After the experiments, the reaction mixture was filtered using a PALL Life Sciences GHP Acrodisc® 13 mm syringe filter with 0.2 μm GHP membrane prior to injecting into the HPLC, in order to get rid of particles and enzymes and to prevent blocking the HPLC columns. First, $NADP^+$ and NADH cofactor mixture is tested. The HPLC result for the starting mixture of $NADP^+$ and NADH showed clearly $NADP^+$ peak and NADH peaks. The HPLC result for the reaction mixture after incubating for 4 hours showed that all four cofactors can be detected. The NADH and $NADP^+$ peaks are smaller compared with the starting sample, indicating that some of the starting materials are consumed, and the NAD^+ and NADH has emerged. This suggested that the transhydrogenation reaction happens, and the hydride from NADH has transferred to $NADP^+$ to form NADPH and NAD^+ with the help of the enzyme particle system.

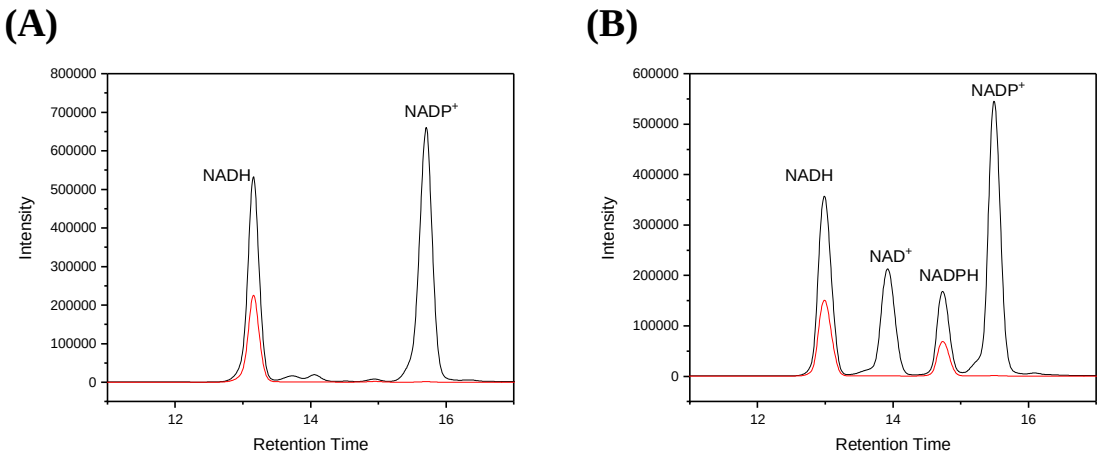


Figure 5-8 HPLC results for transhydrogenation mediated by artificial transhydrogenase. (A) the initial sample of NADH and $NADP^+$, and (B) the reaction mixture of NADH and $NADP^+$ after four hours.

To carry out a group of control reaction, the sole enzyme wildtype *Re* SH or the variant $HoxF^{E341A/S342R}$ was used. To carry out the control experiments, 10 uL wildtype *Re* SH or variant $HoxF^{E341A/S342R}$ was added into 1 mL degassed Bis-Tris buffer (50 mM, pH6.0) with 5 mM NAD^+ and 5 mM NADPH. The reaction mixture is incubated for four hours under ambient temperature. All the operations are carried out in glovebox to avoid oxygen. The cofactor mixture was then tested on HPLC before and after the experiment, following the same protocol as discussed in the last paragraph (**Figure 5-9**).

The result for the wildtype *Re* SH showed hardly any formation of NADPH, indicating that the enzyme had hardly any transhydrogenation activity. The small amount of NAD^+ was probably due to the oxidation of NADH. However, the control reaction for variant $HoxF^{E341A/S342R}$ showed an unexpected result: considerable amount of NADPH was produced. This indicated that variant $HoxF^{E341A/S342R}$ itself had the activity for transhydrogenation, and the activity of which was similar compared with the particle transhydrogenation system. One possible explanation for this surprising finding was proposed. Since the mutations on the *Re* SH had changed the cofactor specificity, the variant

HoxF$^{E341A/S342R}$ was able to take both NAD^+ and $NADP^+$. In addition to that, the variant also contains a FMN molecule in this catalytic centre. Therefore, the variant is likely to work as a transhydrogenase in the presence of NADH/$NADP^+$ couple.

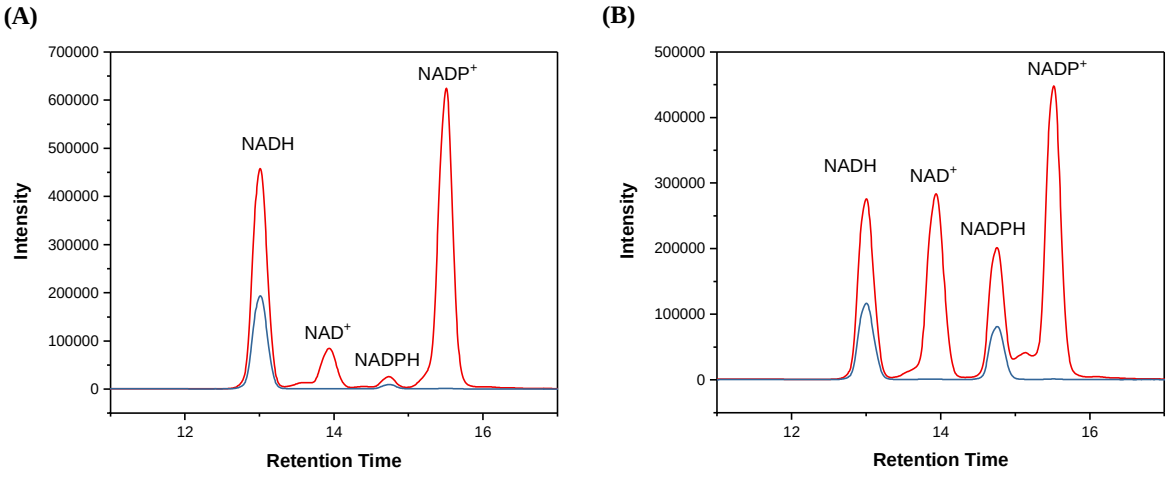


Figure 5-9 HPLC results for control reaction of transhydrogenation mediated by wildtype *R.e* SH (A), and the variant HoxF$^{E341A/S342R}$ (B).

5.7 Summary

This chapter mainly discussed about the soluble transhydrogenase, including its expression and purification strategy, its characterization process, as well as its feasibility to be incorporated into the NADH regeneration system to transform it to a novel NADPH regeneration system. The expression and purification process was not very successful, the expression level was not very high, and the purified sample still contained a lot of other proteins according to the SDS-PAGE result. Therefore the expression and purification process requires further optimization in the future. However, the characterization results showed that although the expression and purification was not that successful, the enzyme sample still exhibited high transhydrogenation activity. Hence it has the potential to be incorporated into the cofactor regeneration system. Before that, more experiments are required to quantitatively characterise the transhydrogenase, such as its K_M and K_{cat}.

Another discovery is that the variant HoxF$^{E341A/S342R}$ has transhydrogenation activity. The detailed mechanism remains to be explored. The applications for the new function of the variant HoxF$^{E341A/S342R}$ are also open to discussion.

Chapter Six: Other approaches for NADH and NADPH regeneration

As discussed in the previous chapters, a number of H_2 driven NADH and NADPH regeneration systems have been established and examined for feasibility, activity, and robustness in this work. In those systems, the NAD^+ or $NADP^+$ reductases play the central role. They receive electrons from hydrogenase splitting H_2, and protons from solution, to reduce NAD^+ or $NADP^+$. The resulting NADH or NADPH will sustain the cofactor dependent enzymes for the desired redox reactions. Previously the HoxFU subunits of soluble hydrogenase (SH) from *Ralstonia eutropha* were used as NAD^+ reductases and variants were used as $NADP^+$ reductases in these systems. However, *Ralstonia eutropha* is not a model organism and slow growth for SH expression. This microorganism is initially grown in medium with its preferred carbon source fructose in order for it to grow fast and enter the exponential phase, but this kind of heterotrophic condition suppresses the expression of hydrogenases. Therefore, the microorganism has to be switched to the less-preferred substrate glycerol upon fructose exhaustion to de-repress the expression of SH. This procedure is complicated and time consuming, with growth usually taking seven days before harvesting the cells. Also, plasmids are not able to be directly transferred into *Ralstonia eutropha*, but instead are reansferred using a much complicated and time-consuming process called bacterial conjugation. Therefore it is not easy to harvest enzymes or to carry out mutagenesis on its target genes. This does not only make the regeneration system costly, but also means that a directed evolution is tedious and time consuming. A number of approaches have been proposed to bypass *Ralstonia eutropha* to overcome these difficulties. First, the gene fragment of HoxFU subunits of soluble hydrogenase from *Ralstonia eutropha* was amplified and reconstructed in *E. coli*, a model organism much easier to handle. Second, another NAD^+ reductase part of the homologous soluble hydrogenase from a thermophile was also reconstructed in *E. coli*. Third, the NAD^+-reductase subunits of bacterial respiratory Complex I were overexpressed in *E. coli*. To construct an expression system in *E. coli* makes the process for enzyme expression and purification shorter, and makes it easier to make site-directed mutagenesis. Therefore, it would be potentially easier for directed evolution.

In this chapter, only the NAD^+-reductase domain of respiratory Complex I from *E.coli*, will be discussed in detail, including how the enzyme was expressed, purified, handled and characterised.

6.1 NAD^+-reductase domain of respiratory Complex I from *E. coli*

As discussed in Chapter Two, respiratory Complex I (NADH:uniquinone oxidoreductase) is a membrane protein complex involved in the cell respiration process. Complex I is a most conserved protein complex preserved in most living organisms including bacteria, plants and animals. It is a membrane protein complex that binds to either the inner cell membrane of prokaryote, or the mitochondria membrane in eukaryotic organisms. Complex I is in charge of oxidising NADH to NAD^+ and transferring the electrons to the other protein complexes involved in the respiration chain. Since Complex I has the activity to convert between NAD^+ and NADH, it is a potential candidate to be incorporated into the hydrogen driven NADH regeneration to replace the current NAD^+-reductase, HoxFU subunits from *Ralstonia eutropha*. Complex I from *E. coli* contains 14 subunits, namely NuoA to NuoN, and forms an L-shape complex. The hydrophobic arm is buried in the membrane, while the hydrophilic arm protrudes into the cytoplasm. It is the first subunit at the top of hydrophilic arm, NuoF subunit that in charge of oxidising NADH to NAD^+. Therefore nuoF subunit was isolated and expressed in *E. coli*.

6.1.1 Molecular cloning of NuoF and NuoEF from *E. coli* Complex I

Respiratory Complex I of *E. coli* consists of 24 nuo genes, seven of which present as duplications and two as triplications117. The nuoF gene was amplified directly from the E coli DH5α genome and included NcoI and XhoI restriction sites at the 5’ and 3’ ends, respectively, using the following pair of primers (the restriction sites were underlined):

Forward Primer:

5’ CATGCCATGGAAAACATTATCCGTAC TCCC

Reverse Prime:

5’ CCGCTCGAGCCAGC GCTCTTTCAG CAGGTT

The PCR DNA fragment was then digested by NcoI and XhoI, and ligated into pET28a vector previously digested with the same enzymes. The resulting vector was verified by DNA sequencing provided by Source BioScience, and denoted as pETnuoF (Figure 2-1). The resulting vector was transformed into BL21 (DE3) (New England Biolabs) E. coli strain competent cells for protein expression.

Figure 2 1 The graphic structure of plasmid pETnuoF. The green arrow shows the inserted nuoF gene, which is under control of T7 promoter.

Similarly, for the amplification of the DNA eoncoding the adjacent nuoE and nuoF genes together as well as to introduce NcoI and BamHI restriction sites, the following pair of primers was used during the PCR reaction (the restriction sites were underlined).

Forward Primer:

5’ ATGCATGCCATGG ACGAGA ATCAACAACC ACAA

Reverse Primer:

5’ CGC GGATCCTTAGTGCCAGCGCTCTTTCAGCAGGT

The amplified DNA fragment was digested by NcoI and BamHI, and ligated into pET28a vector previously digested with NcoI and BamHI. The resulting vector was verified by DNA sequencing provided by Source BioScience, and denoted as pETnuoEF (Figure 2-2). The resulting vector wastransformed into BL21 (DE3) E. coli competent cells. It is worth mentioning that the nuoE and nuoF genes belong to a polycistronic mRNA and overlap by four nucleotides. Since the nuoF and nuoE genes were amplified by PCR together, this overlapping was inherited in the plasmid, and the expression of nuoF is dependent on the native ribosomal binding site (RBS).

6.2 Expression and purification of NuoF subunit of Complex I

The nuoF gene was first amplified from *E. coli* genome using cell culture PCR. In the meantime NcoI restriction site was added to the 5' terminal, and XhoI restriction site was added to the 3' terminal of the gene. The PCR amplified DNA sequence was verified by DNA electrophoresis. Then, the nuoF DNA fragments, together with pET28a vector containing Kanamycin resistant gene were digested by NcoI and XhoI endonucleases. Both products were electrophoresis and collected by gel extraction kits. Finally, the DNA segment of Complex I gene fragments and the digested pET28a vector were connected together by T4 DNA ligase, and the product was verified by both electrophoresis and DNA sequencing. This new plasmid was denoted pETnuoF for further reference. pETnuoF was transferred into *E. coli* Dh5α strain for long term preservation and into BL21(DE3) strain for further gene expression and purification experiments.

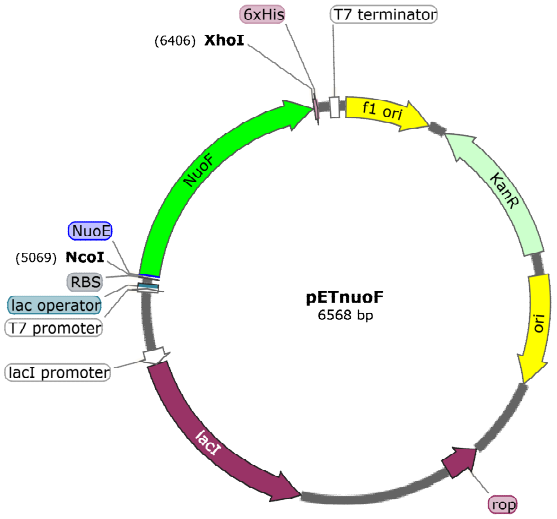


Figure 6-1 The graphic structure of plasmid pETnuoF. The green arrow shows the inserted *nuoF* gene, which is under control of the T7 promoter.

To express the target protein, *E. coli* strain BL21 (DE3) bearing pETnuoF plasmid was cultured in LB media with 50 mM kanamycin. A 2 μL stock culture of *E. coli* strain BL21 (DE3) bearing pETnuoF plasmid was inoculated into a 50 mL falcon tube containing 15 mL LB media as seed culture. Then the seed culture was put into shaker, shaking at 120 rpm under 37 ºC until the OD_{600} reached 0.8. The seed culture was then diluted into a 2 L flask containing 1 L new LB media with

50 mM kanamycin at the ratio of 1:100. The new culture was incubated in the shaker, shaking at the same speed and temperature until OD_{600} reached 0.6. Then 0.1 mM final concentration of IPTG was added into the flask, and the temperature was lowered to 16 ºC, shaking at the same speed overnight.

To purify the protein, the culture was first centrifuged and the harvested cells were re-suspended in Tris buffer (50 mM pH 8.0). The cells were broken open by sonication, and centrifuged again to separate cell debris and supernatant. The supernatant was loaded onto a HisTrap column of an AKTA protein purification system (HPLC). The column was washed by a gradient concentration of imidazole from 0 mM to 500 mM, and the fragments were analysed by SDS-PAGE.

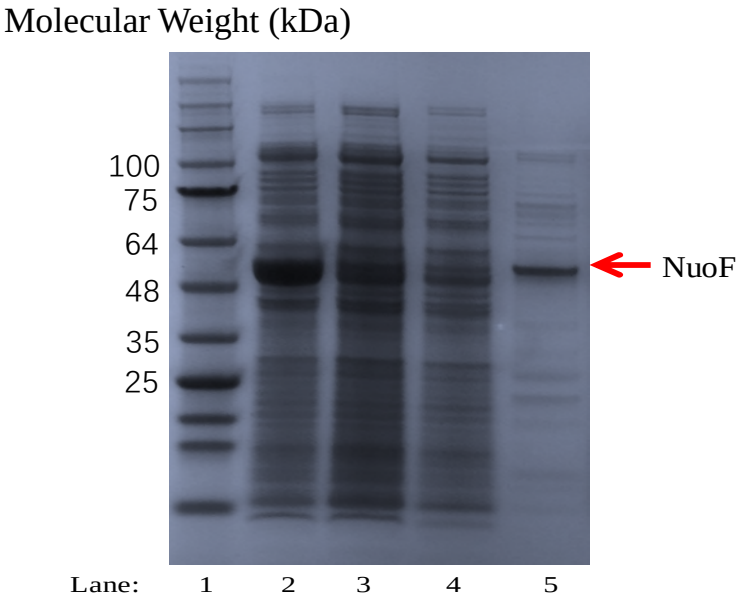


Figure 6-2 The SDS-PAGE chart of NuoF expression and purification. Lane1: marker. Lane 2: the whole cell lysate of E. coli cells overexpressing NuoF. Lane 3: the supernatant Lane 4: the supernatant flowing through the HisTrap column. Lane5: the collected fraction washed by ahigh concentration of imidazole buffer.

The SDS-PAGE results (**Figure 6-2**) clearly showed there was an enriched band with the right molecular weight for the NuoF subunit (around 52 kDa) in the whole cell lysate and the supernatant. This indicated that the NuoF subunit had been successfully overexpressed and the expression level was high. However, comparing lane 2 and lane 3, the targeting protein band is relatively smaller in lane 2 compared with that in lane 1. This may indicate that part of the protein formed an insoluble body and precipitated with the cell debris. Yet most of the protein was soluble. The flow through

from the HisTrap column did not have an enhanced band at the molecular weight of NuoF, indicating that most of the targeting protein was bound to the column. The fraction washed with a high concentration of imidazole buffer showed a clear band for the target protein. Although there were some impurities of other proteins, the amount was relatively low compared with the targeting protein. Therefore, the impurities would not have considerable impact on the downstream reactions.

To conclude, the NuoF subunit of Complex I was successfully overexpressed in *E. coli*. The target protein was purified by HisTrap column, though some of the targeting protein precipitated during the process. The purified protein was buffer exchanged to get rid of the high concentration of imidazole which may impair the stability of the protein, and stored at 4 ºC freeze for further treatment.

6.2.1 Characterization of NuoF subunit

To further characterise the activity of the NuoF subunit, both chemical and electrochemical approaches were applied. Benzyl viologen (BV) is frequently used as a colourimetric reagent for biochemical redox reactions. Oxidised benzyl viologen is colourless while reduced benzyl viologen is purple. NuoF catalysed oxidation of NADH provides electrons for reduction of oxidised BV through its FeS cluster. Benzyl viologen upon receiving the electron from NuoF is reduced and becomes purple (**Figure 6-2**).

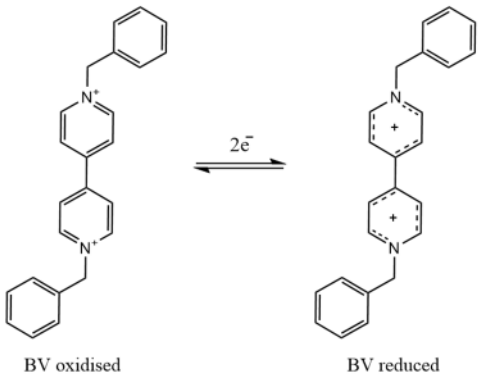
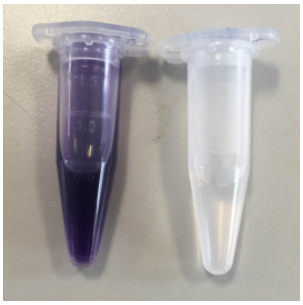


Figure 6-2 The oxidised benzyl viologen receives two electrons from a donor and becomes reduced.

To examine whether NuoF can catalyse the oxidation of NADH, a benzyl viologen assay was carried out. 5 mM NADH and 5 mM benzyl viologen were added to 1 mL of Tris buffer (50 mM Tris, pH 7.5). Then 5 μL NuoF protein stock solution was added to the mixture to start the reaction. The system was left shaking gently at room temperature for 10 minutes. A control mixture of 5 mM NADH and 5 mM benzyl viologen without NuoF was used as a negative control. After a reaction time of 10 minutes, the mixture containing NuoF turned purple, while the control reaction remained colourless (**Figure 6-3**). This indicated that NuoF can catalyse the oxidation of NADH and reduction of benzyl viologen. The reduced form of benzyl viologen is prone to be oxidised back and loses its colouration by the O_2 in the air. Therefore, all the procedures were carried out in a glovebox filled with N_2, and the buffer used was pre-purged with N_2 to avoid contact with O_2.



1 2

Figure 6-3 The benzyl viologencolourimetric assay for NuoF. (1) 5 mM NADH, 5 mM benzyl viologen containing nuoF. (2) 5 mM NADH, 5 benzyl viologen containing no nuoF.

As shown in fig 6-2 lane 5, the purified NuoF contains impurities of trace amount of other proteins. Therefore, there is a possibility that it was actually other impurity proteins which catalysed the reaction. To exclude this possibility, another control experiment was carried out: 5 mM NADH and 5 mM benzyl viologen were mixed, and 5 μL cell lysate from cells containing no overexpressed NuoF was added to the system. The same reaction condition was applied for 10 minutes. However, the result showed that the mixture also turned purple after 10 minutes. This indicated that there are indeed some other components in the cell other than NuoF which can mediate the oxidation of NADH and the reduction of benzyl viologen. The benzyl viologen assay itself was not specific enough to show that NuoF catalysed the conversion between NADH and NAD^+.

To further characterise the activity of NuoF, an electrochemical approach was applied. The procedure was the same as used in Chapter Four for characterising HoxFU and its variants. A 2 μL aliquot of concentrated cell supernatant containing the overexpressed NuoF protein was spotted on the carbon electrode to prepare a protein film. The electrochemical cell contained 5 mL potassium phosphate buffer (50 mM, pH 7.5) together with 1 mM NAD^+, and the water bath surrounding the electrochemical cell was set to 30 ºC. The working electrode was rotated at a speed of 2000 rpm. A cyclic voltammogram was recorded over a potential range between +0.14 V and -0.46V (vs SHE) at the scan rate of 0.1 V/s. A control experiment was also performed with cell free extract containing no NuoF on the electrode.

In the cyclic voltammetry experiment, NuoF showed high activity towards the reduction of NAD^+. When the potential reached -0.3 V (vs SHE), catalytic current of NAD^+ reduction was observed, and the catalytic current reached around 1 μA when the potential reached -0.5 V (vs SHE). This indicated that NuoF had a high activity towards reduction of NAD^+. The cell free extract containing no NuoF showed no catalytic current for NAD^+ reduction (**Figure 6-4**). This excluded that possibility that other cell components catalysed the reduction of NAD^+ on the electrode.

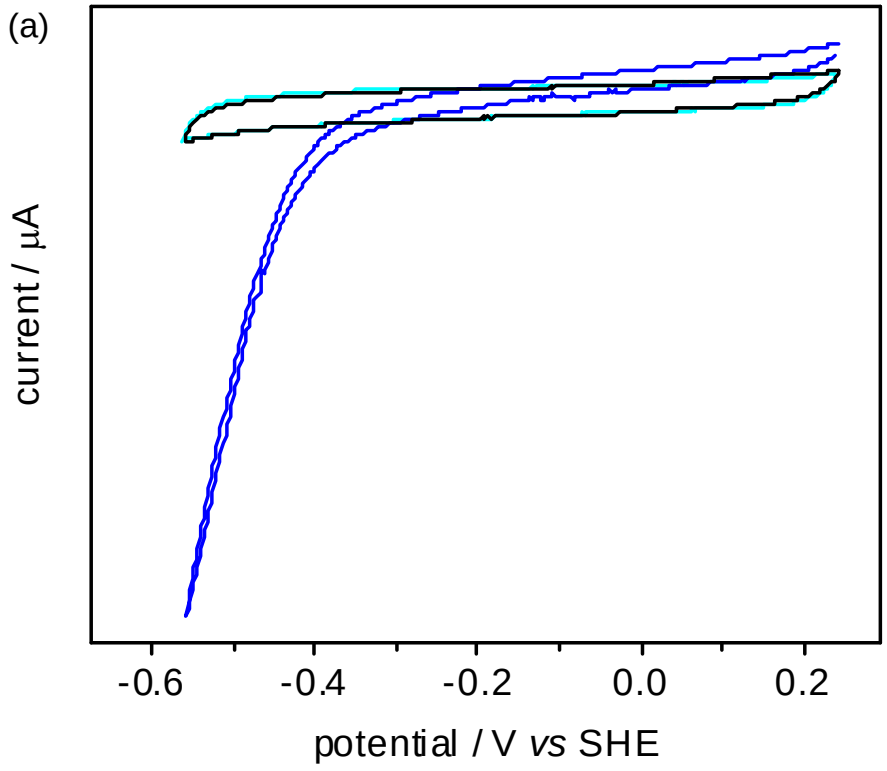


Figure 6-4 Cyclic voltammograms of protein film electrochemistry using a pyrolytic graphite edge (PGE) rotating disc electrode showing a blank electrode (Black), electrode modified with cell free extract containing NuoF subunit (blue), and electrode modified with cell free extract containing no NuoF subunit (cyan).

In addition to the previous characterisations, to study the dynamic of nuoF, synchrotron IR microspectroscopy combined with protein film electrochemistry was also applied. This part of work was done in the Diamond Light Source, UK by Dr. Philip A. Ash in Vincent group. The cell free extract of nuoF was first immobilised on carbon particle Black Pearls 2000 from Cabot Corporation. The experiment was carried out in a reflection−absorption electrochemical cell mounted on an IR microscope. The microspectroscopy experiments were carried out on the MIRIAM beamline using a Vertex 80 V FT-IR spectrometer and a Hyperion 3000 IR microscope from Bruker, together with a high-sensitivity photovoltaic mercury cadmium telluride detector at the temperature of 77 K. By applying a 36× objective and 25×25 μm^2 aperture, the spectra were acquired in reflection mode. The data were analysed by the 7.0 version of Bruker Optik's OPUS software. **Figure 6-5** shows an oxidised (+0.242 V) minus reduced (-0.558 V) difference spectrum for electrode-adsorbed NuoF.

The data were collected in the microspectroscopy cell. The 1540 cm^{-1} positive peak is correlated with the characteristic spectrum of oxidised flavin, and the 1522 cm^{-1} positive peak is correlated with the isoalloxazine ring of oxidised flavin. The 1556 and 1551 cm^{-1} negative peaks are consistent with the reduced form of FMN. The spectrum clearly shows the FMN in the catalytic site of NuoF being oxidised and reduced at the relevant poteintals.

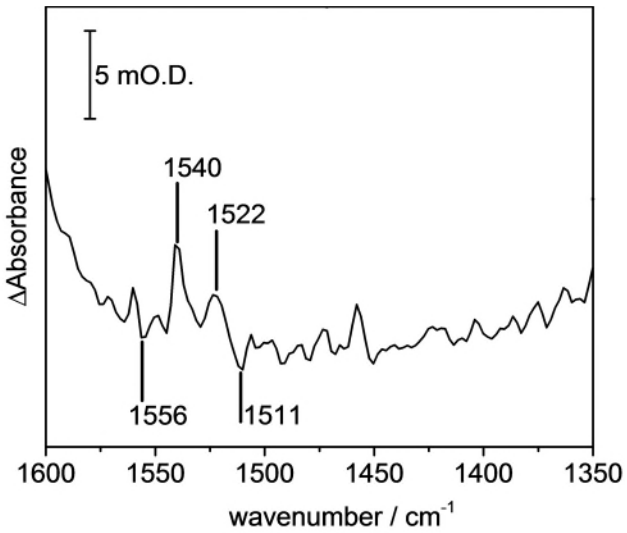


Figure 6-5 Spectroelectrochemistry of cell free extract containing NuoF subunit adsorbed on carbon black particles. Oxidised (+0.242 V) minus reduced (+0.558 V) difference spectrum recorded in the microspectroscopy cell. The difference spectrum was calculated an average of 1024 interferograms.

6.2.2 Discussion of NuoF

Although the NuoF subunit of Complex I exhibited promising activity for NAD^+ reduction, its stability remains the biggest problem for it to be incorporated into the cofactor regeneration system. During the expression process, though the majority of NuoF was soluble, there were already some of the NuoF forming an insoluble body and precipitating with the cell debris. The precipitation was more obvious during the purification process. The purified NuoF became cloudy, and precipitated protein was visible in less than an hour. The purified protein solution was then spotted on an electrode for electrochemical test again, and showed no catalytic current for NAD^+ reduction or NADH oxidation. This indicated that most of the isolated protein had precipitated and was not functional

anymore. Therefore, the electrochemical characterisation was carried out with cell free extract containing NuoF, which exhibited a longer lifetime for NuoF. The other proteins and cell components may play a role in helping to stabilise NuoF. Even when NuoF was in the form of cell extract, the protein was still unstable, and its activity was totally lost after remaining at room temperature for four hours. In this circumstance, NuoF is not yet an ideal candidate to be incorporated into the H_2 driven NADH/NADPH regeneration system, as the NAD^+ reductase was not stable. It was also not feasible to immobilise the cell free extract containing NuoF directly on particles, as the particle surface would be mostly occupied by irrelevant cell components, and would have far less space for the hydrogenase, and oxidoreductase to be immobilised on. Also, other cell components are likely to lead to other side reactions and by-products, and thus lower the overall selectivity and robustness of the system.

From the perspective of protein structural biology, the instability of NuoF was probably caused by the hydrophobic surface area. In the structure of Complex I, although NuoF is at the top of the hydrophilic arm, it binds to the nearby NuoE and NuoG subunits. It is hypothesised that NuoF contains a Substantial hydrophobic area for the binding of the other two subunits, as in some protein complexes, the binding between each subunit relies on the hydrophobic interaction. However, the hydrophobic area of NuoF might lead to its instability and tendency to precipitate. Hirst and co-workers isolated the flavoprotein subcomplex of Complex I, which is set of the homologues of Nqo1 and Nqo2 from *Thermus thermophiles* HB-8, and the homologues of NuoF and nuoE from *E. coli*, from bovine heart mitochondria. This indicates that NuoE and NuoF bind tightly and hard to separate. Hirst and co-worker's work has shed lights upon the next step towarsa increasing the stability of NuoF subunit. Furthermore, NuoG is another subunit directly binding to NuoF. Unlike NuoE, NuoG is a relatively large protein with a molecular weight of 100 kDa, and containing 3 FeS clusters. All the three FeS clusters are involved in the electron transfer between NuoF to Quinone. Therefore, coexpression of NuoG together with NuoF, or NuoE and NuoF, might also contribute the stability of nuoF. On the other hand however, as NuoG is a large protein containing three FeS clusters, the resulting NuoEFG complex might be hard to express, purify, and handle. In this way,

NuoEF and NuoEFG subcomplexes were constructed and overexpressed, to examine their stability and activity.

6.3 Overexpression, purification, and characterisation of NuoEF subcomplex

In order to increase the stability of NuoF, it was co-expressed with the adjacent subunit NuoE. NuoE subunit is a 24 kDa polypeptide containing one FeS cluster. However, the chain of electron transfer through Complex I from NuoF to Quinone bypassed NuoE, even though it contains a FeS cluster. The function of NuoE is yet to be unveiled, but in this work, NuoE is only used to attempt to stabilise NuoF.

To overexpress NuoE and NuoF together, a new construct was made. Gene nuoE and nuoF were amplified at the same time from the *E. coli* genome. It is worth noticing that nuoE and nuoF were not expressed as a fusion gene with a linker. The two genes were expressed separately with the control of one promoter. In the *E. coli* genome, the genes were expressed natively in the same manner. All the 13 nuo genes formed an operon and are transcribed together in a long mRNA, and then translated to separate protein subunits by ribosomes. The DNA fragment of NuoEF was inserted into the pET28a vector in the same way as the construction of pETnuoF, and the resulting construct was denoted as pETnuoEF. Furthermore, pETnuoEFG was also constructed in the same way. The pETnuoEF system encodes one 6x Histag at the 5’ terminus of NuoF. And pETnuoEFG encodes one 6x Histag at the 5’ terminus of NuoG. The two constructs were then transferred into BL21 (DE3) *E. coli* competent cells for overexpression.

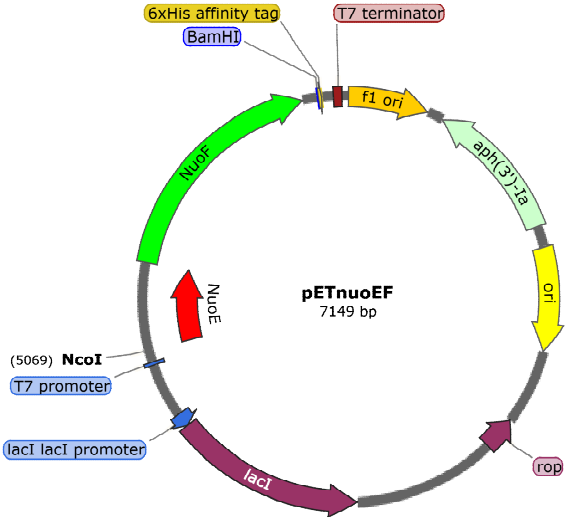


Figure 6-5 The structure of plasmid pETnuoEF. The green arrow shows the inserted *nuoF* gene, and the red arrow shows the *nuoE* gene, which are both under control of the T7 promoter.

To overexpress the NuoEF subcomplexes, the same procedures and conditions as for NuoF were applied. The purification process also relied on a HisTrap column. In the NuoEF subcomplex, only NuoF contained a Histag at 5' terminus, so the purification process relied on NuoE and NuoF subunits bound together, and then stick to the column. Isolated NuoE subunit was not able to bind to the column on its own, since it does not contain a Histag.

The cell strain containing pETnuoEF plasmid was grown at 37° C until the OD_{600} reached 0.8. Then the culture was grown at 16° C overnight, and 0.1 mM IPTG was added to induce the expression of NuoE and NuoF. The cell pellet was harvested by centrifugation and resuspended in 25 mL Tris buffer (50 mM Tris pH 8.0). The SDS-PAGE results of whole cell soluble lysate showed that there were two enhanced bands at around 50 kDa, and 18 kDa, which correlate with the molecular weight of NuoE and NuoF subunits, indicating that the two target subunits had successfully expressed (**Figure 6-6**). However, the downstream purification process was not successful. There was no target subunits observed in the imidazole washed fractions. This is probably due to the reason that when NuoE and NuoF bind together, the Histag is not properly exposed, stopping the complex from binding to the HisTrap column. Another possible reason is that the expression of two subunits NuoE

and NuoF together under one single promoter was problematic. Therefore, another strategy to co-express NuoE and NuoF subunits together, and to isolate them, had to be developed.

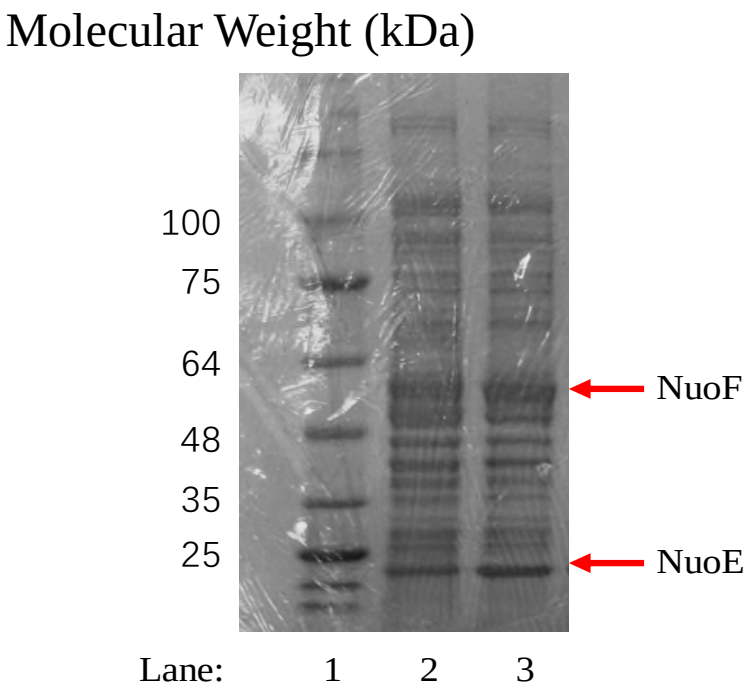


Figure 6-6 The SDS-PAGE chart of NuoEF expression and purification. Lane1: marker. Lane 2: the whole cell lysate of *E. coli* cells overexpressing NuoEF. Lane 3: the supernatant

6.4 Overexpression, purification, and characterisation of NuoEFG subcomplex

Given the expression of NuoEF was not successful, the new strategy was to co-express three adjacent subunits, namely NuoE, NuoF and NuoG. Part of this work was carried out by a technician in the Vincent group, Claudia Orbegozo Rubio. The molecular cloning process was very similar to that of NuoEF. All the three genes encoding NuoE, NuoF, and NuoG were amplified together by one pair of primers, and then ligated to the pACYCDuet vector. In this way, the three subunits were under the control of one single promoter, the T7 promoter. Therefore, the Histag was conjugated at the C-terminus of the NuoG subunits. The downstream purification process using a HisTrap column relied on the three subunits binding together and then binding to the column with the Histag of nuoG. If

the other two subunits NuoE, and NuoF do not bind with NuoG tightly after overexpressed in the cell, the purification process would then only be able to harvest the NuoG subunit alone, but not the other two subunits. The resulting plasmid containing NuoEFG gene sequence was denoted pACnuoEFG, and was then transferred into *E. coli* strain BL21 (DE3) for overexpression.

The overexpression procedure was also the same as that of NuoEF overexpression. First, the *E. coli* BL21 cells bearing the pACnuoEFG plasmid were incubated in 10 mL LB media overnight at 37 °C overnight, and then dilute 1:100 to 1 L LB media for continuing cultivation until OD_{600} reached 0.8. Then the cell culture was induced by adding 0.1 mM IPTG and kept growing at 16 °C overnight. The cell was then harvest by centrifugation, and resuspended in 40 mL Tris buffer (50 mM pH 8.0). The solution was subjected to sonication to break the cell membrane, and centrifugation again to separate the soluble lysate and insoluble cell debris. The soluble cell lysate is subjected to the next purification step.

The purification process was similar to that for NuoF and NuoEF. The AKTA and HisTrap Column were used. The cell soluble lysate was filtered with a 0.2 μm filter to prevent any insoluble cell components from blocking the column. Then the lysate was loaded into a pre-equilibrate HisTrap column and washed with Tris buffer until all cell components not binding to the column flowed through. The protein still bound to the column was clearly visible at the top part of the column, as it had a distinctive red colour.

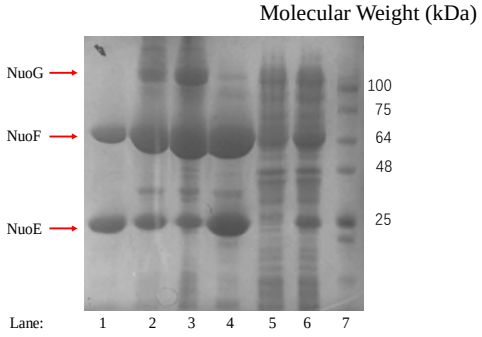


Figure 6-7 The SDS-PAGE chart of NuoEFG expression and purification. Lane1: precipitant. Lane 2 and 3: flowing through the HisTrap column. Lane 4: the collected fraction washed by a high concentration of imidazole buffer. Lane5: Supernatant. Lane 6: the whole cell lysate of *E. coli* cells overexpressing NuoEFG. Lane 7: Marker.

The SDS-PAGE result for NuoEFG expression indicated that all the three subunits had been successfully expressed (**Figure 6-7**). The soluble lysate clearly showed three enhanced bands at around 100 kDa, 50 kDa, and 20 kDa respectively, which were close to the molecular weight of the three subunits of NuoEFG. On the contrary, the flow-through did not show any of the three enhanced bands, which indicated that all the three subunits were bound to the HisTrap column. However, most of the NuoG subunit was insoluble and precipitated with the cell debris. The other two subunits NuoE and NuoF were both soluble and were able to be isolated by a high concentration imidazole wash. The SDS-PAGE for purified Complex I subunits showed that although all three subunits were successfully expressed, most NuoG precipitated and not bind with NuoE and NuoF. NuoE and NuoF were able to bind together and be isolated. The purified NuoEF was quite clean, as hardly any other protein bands were visualised from SDS-PAGE lane. The purified NuoEF had a very strong and distinctive red colouration resulting from the iron element of the FeS clusters.

The purified NuoEF subunits were first tested by benzyl viologen assays. The procedure was the same as previously described for NuoF subunit. Benzyl viologen turned into dark blue as soon as NuoEF subunit was added. Considering the purity of the enzyme was very high, this indicated that NuoEF subunits had a strong activity to reduce benzyl viologen by NADH. Then the enzyme was spotted on the electrode to test its electrochemical activity for NADH oxidation and NAD^+ reduction. The procedure was described in chapter four. However, NuoEF subunits did not show any activity towards NAD^+ reduction nor NADH oxidation. This was contradictory with the result for NuoF, which had high catalytic current for NAD^+ reduction. The reason was yet to be investigated. One hypothesis was that when the two subunits bind together, the protein was not able to be immobilised on the electrode surface properly, or the additional NuoE subunit hinders the transfer of electron from the catalytic site of NuoF to the surface of electrode. The NuoEF was also tested on carbon particle. Ten µL NuoEF aliquot was mixed with 10 µL hyd-1 enzyme and then mixed with 10 µL carbon particle BP2000 solution for one hour on ice. The enzyme particle mixture was then

transferred into 1 mL Tris buffer (50 mM, pH8.0) containing 1 mM NAD^+ pre-saturated with H_2. The reaction mixture was then transferred into a 1 mL glass cuvette to be monitored by UV-vis, while the H_2 kept flowing through the head space of the reaction mixture. No NADH formation was observed from the UV-vis spectrum after one hour. This indicated that NuoEF did not have the activity when immobilised on carbon particle. This is probably because NuoEF is hard to be immobilised.

6.5 Discussion of NAD^+ reducing subunits from Complex I

The results for Complex I subunits shed light upon the alternatives for replacing *R.e* HoxFU as the NAD^+ reductase in the cofactor regeneration system. However, there are still a number of barriers yet to be overcome. The purification of NuoF subunit was successful, and the NuoF subunit had high NAD^+ reducing activity on an electrode. However, NuoF was highly unstable, not suitable for directly incorporating into the current NADH regeneration system to replace *R.e* HoxFU. To increase the stability of NuoF, the adjacent subunits NuoE and NuoG were co-expressed with NuoF. The results for co-expressed subunits were not ideal. Although the stability was increased, when bound with the additional NuoE subunit, the NuoF subunit lost its activity for reducing NAD^+ using electrons supplied by a carbon surface.

The additional subunit NuoE may help improve the stability of NuoF by blocking the hydrophobic surface and preventing aggregation and precipitation, but at the same time, this may unfortunately affect the adsorption onto carbon or the electron transfer to carbon. Hydrophobic domains can be useful for attachment to carbon, so the same site that causes precipitation might be crucial for adsorption on carbon and electron transfer. This future scope will be discussed in detail in Chapter Seven.

Chapter Seven: Conclusions and outlook

7.1 Conclusions

This thesis mainly focused on the development and extension of a H_2 driven cofactor regeneration system, based on the previous one developed by Dr. Holly Reeve from the Vincent Group. Two directions for further development of this system were explained: one is to improve the activity and robustness of the current NADH regeneration system, and the other one is to extend to NADPH regeneration and couple to NADPH dependent enzymes. In this thesis, both directions have been extensively explored, with some positive achievements. However, there are still several obstacles to be overcome, and possible directions for future work are discussed.

7.1.1 Development towards a more robust NADH regeneration system

In the NADH regeneration system developed by Dr. Reeve, *R.e* HoxFU was used as the NAD^+ reductase, and thus played a central role in the system. However, as discussed before, *R.e* HoxFU has a number of disadvantages, and hinders the cost and overall activity of the system, because it must be expressed in the slow growing *R.e* cells. Therefore, a number of approaches were tested to address this problem. In this Thesis, the focus was to develop the NADH oxidase subunit NuoF of *E. coli* Complex I to replace the current *R.e* HoxFU. The NuoF subunit was successfully expressed and characterized electrochemically.The NuoF subunit had strong NAD^+ reducing activity on the electrode. However, The NuoF subunit was extremely unstable, and precipitated very fast after isolation, therefore it was not practical to be incorporated into the cofactor regeneration system. To improve its stability, the adjacent subunits NuoE and NuoG were co-expressed. In this way, although the stability improved, the activity for reducing NAD^+ on the electrode was totally lost. Therefore, currently the NADH oxidase of Complex I subunits is not suitable to be incorporated into

the NADH regeneration system and replace the *R.e* soluble hydrogenase HoxFU. The enzyme requires further engineering or other investigation in order to produce a stable and robust enzyme to recycle NADH on a carbon surface.

7.1.2 Development towards NADPH regeneration system

In order to develop a new NADPH regeneration system based on the H_2 driven NADH regeneration system, several possibilities were explored. First, an extra enzyme, soluble pyridine nucleotide transhydrogenase UdhA was introduced. UdhA is a soluble enzyme capable of transferring hydride between NAD^+ and NADPH, or NADH and $NADP^+$. Therefore, by incorporating this new enzyme to the current three enzyme NADH regeneration system, and adding a catalytic amount of both NAD^+ and $NADP^+$, the reduced NADH should be able to transfer its hydride to $NADP^+$ mediated by UdhA. Thus, the NADPH should be able to sustain the downstream redox reaction catalysed by an NADPH-dependent enzyme.

In chapter five, UdhA was expressed and crudely purified. The purification process was not very successful, so the target enzyme UdhA contained many other protein impurities. The preliminary results showed that the crude purified UdhA had strong transhydrogenation activity. Therefore, it was a promising enzyme to be incorporated into the new system for recycling NADPH. However, at the time this part of work was done, there was no suitable NADPH dependent enzyme available to test the system. Unlike other NADPH regeneration system, both NADH and NADPH presense in this system mediated by UdhA, therefore, to test if UhdA is functional, a strictly NADPH dependent enzyme is required. At that stage, most commercially available NADPH dependent enzymes can be incorporated into this system can also use NADH as their redox equivalent. And only recently, the strictly NADPH dependent enzyme imine reductase was commercially available.

Inspired by mechanism of UdhA, an artificial transhydrogenase was also designed as a proof of concept system to mimic the mechanism of UdhA. The wildtype *R.e* HoxFU and the variant $SH^{E341A/S342R}$ were co-immobilised on carbon particles of BP2000. It was expected that this artificial transhydrogenase was able to transfer proton from NADH to $NADP^+$ as UdhA did. However, the results of the control experiments showed that the variant $SH^{E341A/S342R}$ itself already had transhydrogenation activity, because it retains enough NAD^+ reduction activity to work reversibly on both NAD^+ and $NADP^+$ and hence to transfer hydride between them.

Another approach to develop an NADPH regeneration system was to mutate the NAD^+ reductase *R.e* HoxFU to allow it to accept $NADP^+$ as its substrate. This part of work was in collaboration with Dr. Oliver Lenz. Four variants of HoxHYFU whith altered residues in HoxF subunit were provided by Dr. Lenz generated by rational design. The four variants were tested electrochemically using protein film electrochemistry, and the affinity and apparent activity for all the variants were determined. Among all the variants, $SH^{E341A/S342R}$ exhibited the highest affinity towards $NADP^+$. Therefore, it was tested as a replacement for the wildtype NAD^+ reductase to establish a new NADPH recycling system. The new NADPH recycling system with $SH^{E341A/S342R}$ was then coupled with P450 monooxygenase and imine reductase to demonstrate its feasibility. The results showed that the new NADPH regeneration system was robust and active enough to regenerate NADPH to sustain the downstream redox reactions of these enzymes.

The third approach proposed to develop a new NADPH regeneration system was to mutate the NAD^+ reductase subunit of Complex I subunit so that it would reduce $NADP^+$. However, the difficulties in obtaining a stable and soluble form of Complex I NADH oxidase which worked on a carbon surface meant that this aim was not feasible yet.

Overall, the $SH^{E341A/S342R}$ variant looks most promising for NADPH recycling. This enzyme could be used alone in solution for H_2 driven NADPH recycling, or immobilised on a carbon support with a more robust hydrogenase such as *E. coli* hyd-1. Unfortunately, *E. coli* expression of the *R.e* SH is not yet straightforward so this enzyme has to be prepared in *R.e* where cell growth takes approximately seven days. This is not feasible for commercial application, so further developments, either on SH expression or Complex I solubilisation will be crucial. Nevertheless, this thesis has demonstrated the feasibility of H_2 driven NADPH recycling *in vitro*. An interesting and unexpected discovery was that the $SH^{E341A/S342R}$ variant also functions as a transhydrogenase.

7.2 Outlook

One of the major future directions for this project is to increase the stability of the NuoF subunit of Complex I. As discussed in this Thesis, the previous work has illustrated that NuoF is capable of reduce NAD^+ to NADH with high activity on electrode. Also, NuoF subunit has a number of advantages over the *R.e* SH currently used in the H_2 driven NADH regeneration system. Therefore, NuoF is a potential candidate to replace *R.e* SH to develop a more robust and cheaper NADH regeneration system. However, as discussed in Chapter four, the NuoF subunit itself is highly unstable. Although several approaches have been tested to improve its stability, no big breakthrough obtained. In the future, one major task is to improve the stability of NuoF subunit and to make feasible to be incorporated into the NADH regeneration system.

One possible approach is to immobilise the purified NuoF subunit onto carbon particle immediately after the protein comes out of the purification column. Previous work finds out that the NuoF subunit is stable and functional in whole cell lysate. This is probably due to the interaction of NuoF with other protein and cell components may help stabilise the subunit itself. The isolated NuoF subunit tends to participate very quickly. This might due to the large hydrophobic surface area of the subunit, which is used to bind with the adjacent NuoE and NuoG subunits. In this way, if the isolated protein

was directly put into buffer with carbon particle, the carbon particle might help stabilise the subunit by binding with its hydrophobic surface, and prevent from its further degradation. The other two enzymes of the NADH regeneration system, hydrogenase, and NADH-dependent enzyme could be then immobilised onto the carbon particle. In the future, the isolated NuoF subunit could be first immobilised on carbon particle as soon as being purified. Then, the enzyme particle mixture could be tested on the electrode to examine whether it still retains its functionality. If the subunit is stably and active on the carbon particle, the other two enzymes could be incorporated as well to finalise the entire NADH regeneration.

Protein engineering is another approach to increase the stability of NuoF subunit. As the subunit has a large hydrophobic surface area might contribute to its instability, altering some key residues within this area may help increase its solubility and consequently improve its stability and prevent from precipitation. Compared with the first approach, this method requires much more workload. Identify key residues for surface stability is challenging. Mutagenesis of such residues might lead to collapse of the overall protein structure, or lower catalytic efficiency. The molecular cloning process is also tedious and time consuming. Therefore, the first approach should be prioritised, and if it turns out to be not feasible, then the second approach could be implemented.

Interestingly, during the course of this project, the finding that $HoxF^{E341A/S342R}$ is a good $NADP^+$ reducing enzyme was taken up by collaborator Dr. Lars Lauterbach who demonstrated it in whole cell NADPH-dependent imine reduction.

Appendix

DNA sequence

NADH:quinone oxidoreductase subunits *Escherichia coli* str. K-12 sub str. MG1655

NuoE:

1 atgaaaaaca ttatccgtac tcccgaaacg catccgctga cctggcgtct gcgcgatgac

61 aaacagccag tgtggctgga cgaataccgc agcaaaaacg gttacgaagg cgcgcgtaag

121 gcgctgaccg ggctgtctcc ggacgaaatc gttaatcagg taaaagacgc tggtctgaaa

181 gggcgcggcg gcgcgggctt ctcgactggc ctgaaatgga gcctgatgcc gaaagacgaa

241 tccatgaaca tccgttacct gctgtgtaat gccgatgaaa tggagccggg cacctataaa

301 gaccgcctgt tgatggagca actgccgcac ctgctggtgg aaggtatgct catctccgcg

361 tttgcgctga aagcttaccg tggctacatc ttcctgcgtg gcgaatatat cgaagcggca

421 gttaatctgc gccgtgccat tgccgaagcc accgaagcgg gtctgcttgg caaaaacatt

481 atgggaacag gtttcgattt cgaactgttc gtccataccg gggcagggcg ctacatctgc

541 ggggaagaaa cagcgttaat caactccctg gaaggacgtc gtgctaaccc acgctcgaag

601 ccacccttcc cggcaacctc cggcgcatgg ggtaaaccga cctgtgtcaa caacgtcgaa

661 accctgtgta acgttccggc gatcctcgct aacggcgtgg agtggtatca gaacatctcg

721 aaaagtaaag atgctggcac caagctgatg ggcttctccg gtcgggtgaa aaatccggga

781 ctgtgggaac tgccgttcgg caccaccgca cgcgagatcc tcgaagatta cgccggtggt

841 atgcgtgatg gtctgaaatt taaagcctgg cagccaggcg gcgcggggac tgacttcctg

901 accgaagcgc accttgatct gccgatggaa ttcgaaagta tcggtaaagc gggcagccgt

961 ctgggtacgg cgctggcgat ggcggttgac catgagatca acatggtgtc gctggtgcgt

1021 aacctggaag agtttttcgc ccgtgagtcc tgcggctggt gtacgccgtg ccgcgacggt

1081 ctgccgtgga gcgtgaaaat tctgcgtgcg ctggagcgtg gtgaaggtca gccgggcgat

1141 atcgaaacac ttgagcaact gtgtcgattc ttaggcccgg gtaaaacttt ctgtgcccac

1201 gcacctggtg cagtggagcc gttacagagc gccatcaaat atttccgcga agaatttgag

1261 gcgggaatca aacagccgtt cagcaatacc catttgatta atgggattca gccgaacctg

1321 ctgaaagagc gctggtaa

NuoE:

1 atgcacgaga atcaacaacc acaaaccgag gcttttgagc tgagtgcggc agagcgtgaa

61 gcgatcgagc acgagatgca ccactacgaa gacccgcgtg cggcgtccat tgaagcgctg

121 aaaatcgttc agaagcagcg tggctgggtg ccggatggtg cgatccacgc gatcgccgat

181 gtgctgggta ttccggcaag cgacgtcgaa ggtgtggcaa cgttctacag tcagatcttc

241 cgccagccgg ttggtcgcca tgtgatccgt tattgtgaca gcgtggtctg tcatatcaac

301 ggttatcagg gtattcaggc ggcgctcgag aaaaagctga acatcaaacc agggcaaacg

361 acatttgatg gccgctttac gctgctgcca acttgctgcc tggggaactg tgataaaggg

421 ccaaacatga tgatcgatga ggacactcac gcgcatctga ccccggaagc gatccctgaa

481 ctgctggagc ggtataaatg a

NuoG:

1 atggctacaa ttcatgtaga cggcaaagaa tacgaggtca acggagcgga caacctgctg

61 gaagcttgtc tgtctctggg ccttgatatt ccttactttt gctggcatcc ggcgctggga

121 agtgtcggtg cttgccgcca gtgtgcggtg aagcaatacc aaaacgcgga agacacgcgt

181 ggtcgcctgg tgatgtcctg tatgacaccg gcttccgatg gcacctttat ttccattgac

241 gacgaagaag cgaaacagtt ccgtgaaagc gtggtcgagt ggttgatgac caaccacccg

301 cacgactgtc cggtatgtga agagggcggt aactgccatc ttcaggatat gactgtgatg

361 accggacaca gcttccgtcg ctaccgtttc accaaacgta cccaccgtaa tcaggatttg

421 gggccattca tctctcacga aatgaaccgc tgcatcgcct gctaccgctg tgtgcgttac

481 tacaaagatt acgctgacgg tacagatctg ggcgtttacg gtgcgcacga caacgtctac

541 ttcggtcgcc cggaagacgg cacgctggaa agcgaatttt ccggtaacct ggtcgaaatt

601 tgcccgaccg gcgtatttac cgacaaaacg cactccgagc gttacaaccg taaatgggat

661 atgcagtttg cgccgagcat ctgccagcaa tgttccatcg gctgtaacat cagccccggt

721 gaacgttacg gcgaactgcg tcgtatcgaa aaccgttaca acggtacggt aaaccactac

781 ttcctctgcg accgtggtcg tttcggttac ggttacgtca acctgaagga tcgtccgcgt

841 cagccagtac agcgtcgtgg cgatgatttc attaccctca acgccgaaca ggcaatgcag

901 ggcgcggcag atattctgcg tcagtcgaag aaagtgatcg gtattggttc tccgcgtgcc

961 agcgtggaaa gcaactttgc gctgcgtgaa ctggtgggcg aagaaaactt ctacaccggt

1021 atcgctcacg gtgagcagga acgtctgcaa ctggcgctga aagtgctgcg tgaaggcggc

1081 atttatactc cggctctgcg cgaaatcgaa tcttacgatg cggtactggt gctgggcgaa

1141 gacgttaccc agaccggcgc gcgcgtcgcg ctggcagtgc gtcaggctgt gaaaggtaaa

1201 gcgcgcgaaa tggcggcagc acagaaagtg gctgactggc agattgcggc aatcctcaac

1261 atcggtcaac gtgcgaagca tccgctgttt gttaccaacg ttgatgacac ccgtctggat

1321 gatatcgcgg cgtggactta ccgcgcaccg gttgaagatc aggcgcgttt aggttttgcc

1381 atcgcccatg cgctggataa ctctgcacca gcggttgacg gtatcgaacc tgagctgcaa

1441 agcaaaatcg acgtcatcgt gcaggcactg gcaggtgcga agaaaccgtt gattatctcc

1501 gggacgaacg ccggtagctt agaggtgatt caggcggcgg ctaacgtcgc gaaagccctg

1561 aaaggtcgcg gcgctgacgt cggtatcacc atgattgccc gttccgtcaa cagcatgggg

1621 ctgggcatta tgggtggcgg ttcgcttgaa gaagcgttaa ccgaactgga aaccggacgc

1681 gccgacgcgg tggtggtgtt ggaaaacgat ctgcatcgtc acgcttctgc tatccgcgtg

1741 aatgctgcgc tggctaaagc accgctggtg atggtggttg atcatcaacg cacagcgatt

1801 atggaaaacg cccatctggt actttctgct gccagctttg ctgaaagcga cggtacggtg

1861 atcaacaacg aaggccgcgc ccaacgtttc ttccaggttt acgatcctgc ttattacgac

1921 agcaaaactg tcatgctgga aagctggcgc tggttacact cgctgcacag caccctgctg

1981 agccgtgaag tggactggac gcagctcgac catgtgattg acgctgttgt ggcgaaaatc

2041 ccggaactgg caggtatcaa agatgctgcg ccggatgcga cattccgtat tcgtgggcag

2101 aaactggccc gtgaaccgca ccgttacagc ggtcgtaccg ccatgcgcgc caatatcagc

2161 gttcatgagc cgcgtcagcc gcaggatatt gacaccatgt tcaccttctc gatggaaggt

2221 aacaaccagc cgactgcgca ccgttcgcaa gtgccgtttg cctgggcgcc gggctggaac

2281 tccccgcagg cgtggaacaa attccaggac gaagtgggcg gcaaactgcg ctttggcgat

2341 ccgggcgtgc gtctgtttga aaccagcgaa aatggtctgg attacttcac cagcgtaccg

2401 gcacgcttcc agccgcagga cgggaaatgg cgtatcgcgc cgtattacca cctgtttggc

2461 agcgatgaat tgtcacagcg tgctccggtc ttccagagcc gtatgccgca gccgtacatc

2521 aaactcaacc cagcggatgc cgcgaagttg ggtgtgaacg caggtacacg cgtctccttt

2581 agttacgatg gcaacacggt cacgctgccg gttgaaatcg ccgaaggact gacggcaggg

2641 caggtgggct tgccgatggg tatgtccggc attgctccgg tgctggctgg cgcgcatctt

2701 gaggatctca aggaggcaca acaatga

DNA sequence

Soluble pyridine nucleotide transhydrogenase *Escherichia coli* str. K-12 sub str. MG1655:

1 atgccacatt cctacgatta cgatgccata gtaataggtt ccggccccgg cggcgaaggc

61 gctgcaatgg gcctggttaa gcaaggtgcg cgcgtcgcag ttatcgagcg ttatcaaaat

121 gttggcggcg gttgcaccca ctggggcacc atcccgtcga aagctctccg tcacgccgtc

181 agccgcatta tagaattcaa tcaaaaccca ctttacagcg accattcccg actgctccgc

241 tcttcttttg ccgatatcct taaccatgcc gataacgtga ttaatcaaca aacgcgcatg

301 cgtcagggat tttacgaacg taatcactgt gaaatattgc agggaaacgc tcgctttgtt

361 gacgagcata cgttggcgct ggattgcccg gacggcagcg ttgaaacact aaccgctgaa

421 aaatttgtta ttgcctgcgg ctctcgtcca tatcatccaa cagatgttga tttcacccat

481 ccacgcattt acgacagcga ctcaattctc agcatgcacc acgaaccgcg ccatgtactt

541 atctatggtg ctggagtgat cggctgtgaa tatgcgtcga tcttccgcgg tatggatgta

601 aaagtggatc tgatcaacac ccgcgatcgc ctgctggcat ttctcgatca agagatgtca

661 gattctctct cctatcactt ctggaacagt ggcgtagtga ttcgtcacaa cgaagagtac

721 gagaagatcg aaggctgtga cgatggtgtg atcatgcatc tgaagtcggg taaaaaactg

781 aaagctgact gcctgctcta tgccaacggt cgcaccggta ataccgattc gctggcgtta

841 cagaacattg ggctagaaac tgacagccgc ggacagctga aggtcaacag catgtatcag

901 accgcacagc cacacgttta cgcggtgggc gacgtgattg gttatccgag cctggcgtcg

961 gcggcctatg accaggggcg cattgccgcg caggcgctgg taaaaggcga agccaccgca

1021 catctgattg aagatatccc taccggtatt tacaccatcc cggaaatcag ctctgtgggc

1081 aaaaccgaac agcagctgac cgcaatgaaa gtgccatatg aagtgggccg cgcccagttt

1141 aaacatctgg cacgcgcaca aatcgtcggc atgaacgtgg gcacgctgaa aattttgttc

1201 catcgggaaa caaaagagat tctgggtatt cactgctttg gcgagcgcgc tgccgaaatt

1261 attcatatcg gtcaggcgat tatggaacag aaaggtggcg gcaacactat tgagtacttc

1321 gtcaacacca cctttaacta cccgacgatg gcggaagcct atcgggtagc tgcgttaaac

1381 ggtttaaacc gcctgtttta a

Bibliography

1. Bornscheuer, U. T. & Bucholz, K. Highlights in biocatalysis - Historical landmarks and current trends. *Eng. Life Sci.* **5**, 309–323 (2005).

2. Schmid, A. *et al.* Industrial biocatalysis today and tomorrow. *Nature* **409**, 258–268 (2001).

3. Wandrey, C., Liese, A. & Kihumbu, D. Industrial Biocatalysis: Past, Present, and Future. *Org. Process Res. Dev.* **4**, 286–290 (2000).

4. Adrie, S. & Patrick, A. *Applied Biocatalysis*. (CRC Press, 2000).

5. Damerow, P. Sumerian Beer : The Origins of Brewing Technology in Ancient Mesopotamia *. *Cuneif. Digit. Libr. J.* (2012).

6. Liese, A., Karsten, S. & Wandrey, C. *Industrial Biotransformations*. (John Wiley & Sons, 2006).

7. Thomas, J. M. Turning Points in Catalysis. *Angew. Chemie Int. Ed. English* **33**, 913–937 (1994).

8. McDonald, A. G. & Tipton, K. F. Fifty-five years of enzyme classification: Advances and difficulties. *FEBS J.* **281**, 583–592 (2014).

9. De Carvalho, C. C. C. R. Enzymatic and whole cell catalysis: Finding new strategies for old processes. *Biotechnol. Adv.* **29**, 75–83 (2011).

10. Willson, R. C. & Ladisch, M. R. Large-Scale Protein Purification. in 1–13 (1990). doi:10.1021/bk-1990-0427.ch001

11. Pollard, D. J. & Woodley, J. M. Biocatalysis for pharmaceutical intermediates: the future is now. *Trends Biotechnol.* **25**, 66–73 (2007).

12. Le??n, R., Fernandes, P., Pinheiro, H. M. & Cabral, J. M. S. Whole-cell biocatalysis in organic media. *Enzyme Microb. Technol.* **23**, 483–500 (1998).

13. Fukuda, H., Hama, S., Tamalampudi, S. & Noda, H. Whole-cell biocatalysts for biodiesel fuel production. *Trends Biotechnol.* **26**, 668–673 (2008).

14. Ban, K., Kaieda, M., Matsumoto, T., Kondo, A. & Fukuda, H. Whole cell biocatalyst for biodiesel fuel production utilizing Rhizopus oryzae cells immobilized within biomass support particles. *Biochem. Eng. J.* **8**, 39–43 (2001).

15. Ni, Y. & Chen, R. R. Accelerating whole-cell biocatalysis by reducing outer membrane permeability barrier. *Biotechnol. Bioeng.* **87**, 804–811 (2004).

16. de Carvalho, C. C. C. R. Whole cell biocatalysts: Essential workers from Nature to the industry. *Microb. Biotechnol.* (2016). doi:10.1111/1751-7915.12363

17. Sheldon, R. A. & Van Pelt, S. Enzyme immobilisation in biocatalysis: why, what and how. *Chem. Soc. Rev.* **42**, 6223–6235 (2013).

18. Arnold, F. H. Directed evolution: Creating biocatalysts for the future. *Chemical Engineering Science* **51**, 5091–5102 (1996).

19. Kuchner, O. & Arnold, F. H. Directed evolution of enzyme catalysts. *Trends Biotechnol.* **15**, 523–530 (1997).

20. Tao, J. & Kazlauskas, R. J. *Biocatalysis for Green Chemistry and Chemical Process Development*. (John Wiley & Sons, 2011).

21. Noyori, R. *et al.* Asymmetric hydrogenation of beta-keto carboxylic esters. A practical, purely chemical access to b-hydroxy esters in high enantiomeric purity. *J. Am. Chem. Soc.* **109**, 5856–5858 (1987).

22. Hidemasa, T., Mashima, K., Matsumura, Y. & Kumobayashi, H. ref.5h Cationic BINAP-Ru(I1) Halide Complexes: Highly Efficient Catalysts for Stereoselective Asymmetric Hydrogenation of. *J. Org. Chem.* **59**, 3064–3076 (1994).

23. Gao, J.-X., Ikariya, T. & Noyori, R. A Ruthenium(II) Complex with a C 2 - Symmetric Diphosphine/Diamine Tetradentate Ligand for Asymmetric Transfer Hydrogenation of Aromatic Ketones †. *Organometallics* **15**, 1087–1089 (1996).

24. Zanotti-Gerosa, A., Hems, W., Groarke, M. & Hancock, F. Ruthenium-catalysed asymmetric reduction of ketones. *Platin. Met. Rev.* **49**, 158–165 (2005).

25. Noyori, R. & Hashiguchi, S. Asymmetric Transfer Hydrogenation Catalyzed by Chiral Ruthenium Complexes. *Acc. Chem. Res.* **30**, 97–102 (1997).

26. Woodley, J. M. New opportunities for biocatalysis: making pharmaceutical processes greener. *Trends Biotechnol.* **26**, 321–327 (2008).

27. Sheldon, R. a. The E Factor: fifteen years on. *Green Chem.* **9**, 1273 (2007).

28. Sheldon, R. a. E factors, green chemistry and catalysis: an odyssey. *Chem. Commun. (Camb).* 3352–3365 (2008). doi:10.1039/b803584a

29. Hammami, R., Nouira, I. & Frein, Y. Effects of Customers' Environmental Awareness and Environmental Regulations on the Emission Intensity and Price of a Product. *Decis. Sci.* **49**, 1116–1155 (2018).

30. Ajikumar, P. K. *et al.* Terpenoids: Opportunities for biosynthesis of natural product drugs using engineered microorganisms. *Mol. Pharm.* **5**, 167–190 (2008).

31. Ajikumar, P. K. *et al.* Isoprenoid pathway optimization for Taxol precursor overproduction in Escherichia coli. *Science (80-.).* **330**, 70–74 (2010).

32. Jarvis, W. R., Colbeck, J. C., Krebber, A., Fleitz, F. J. & Brands, J. Biocatalytic Asymmetric Synthesis of Sitagliptin Manufacture. *Science (80-.).* **329**, 305–310 (2010).

33. Li, T. *et al.* Efficient, chemoenzymatic process for manufacture of the boceprevir bicyclic [3.1.0]proline intermediate based on amine oxidase-catalyzed desymmetrization. *J. Am. Chem. Soc.* **134**, 6467–6472 (2012).

34. Kwo, P. Y. *et al.* Efficacy of boceprevir, an NS3 protease inhibitor, in combination with peginterferon alfa-2b and ribavirin in treatment-naive patients with genotype 1 hepatitis C infection (SPRINT-1): An open-label, randomised, multicentre phase 2 trial. *Lancet* **376**, 705–716 (2010).

35. Pollock, J. A. *et al.* A mild biosynthesis of lactones via enantioselective hydrolysis of hydroxynitriles. *Tetrahedron Asymmetry* **18**, 1888–1892 (2007).

36. Ma, S. K. *et al.* A green-by-design biocatalytic process for atorvastatin intermediate. *Green Chem.* **12**, 81–86 (2010).

37. Nelson, D. L. & Cox, M. M. *Principles of biochemistry*. (W.H. Freeman and Company, 2008).

38. Breaker, R. R. & Joyce, G. F. Self-Incorporation of coenzymes by ribozymes. *J. Mol. Evol.* **40**, 551–558 (1995).

39. Massey, V. The chemical and biological versatility of riboflavin. *Biochem. Soc. Trans.* **28**, 283–96 (2000).

40. Lienhart, W. D., Gudipati, V. & MacHeroux, P. The human flavoproteome. *Arch. Biochem. Biophys.* **535**, 150–162 (2013).

41. Rouault, T. A. & Tong, W. H. Iron-sulfur cluster biogenesis and human disease. *Trends Genet.* **24**, 398–407 (2008).

42. Bandyopadhyay, S., Chandramouli, K. & Johnson, M. K. Iron-sulfur cluster biosynthesis. *Biochem. Soc. Trans.* **36**, 1112–9 (2008).

43. Rouault, T. a & Tong, W.-H. Iron-sulphur cluster biogenesis and mitochondrial iron homeostasis. *Nat. Rev. Mol. Cell Biol.* **6**, 345–351 (2005).

44. Johnson, M. K. Iron-sulfur proteins: new roles for old clusters. *Curr. Opin. Chem. Biol.* **2**, 173–181 (1998).

45. Johnson, D. C., Dean, D. R., Smith, A. D. & Johnson, M. K. Structure, Function, and Formation of Biological Iron-Sulfur Clusters. *Annu. Rev. Biochem.* **74**, 247–281 (2005).

46. Ogino, H., Inomata, S. & Tobita, H. Abiological Iron−Sulfur Clusters. *Chem. Rev.* **98**, 2093–2122 (1998).

47. Whitehouse, C. J. C., Bell, S. G. & Wong, L.-L. P450 $_{BM3}$ (CYP102A1): connecting the dots. *Chem. Soc. Rev.* **41**, 1218–1260 (2012).

48. Jia, C., Kitamura, T. & Fujiwara, Y. Catalytic functionalization of arenes and alkanes via C-H bond activation. *Acc. Chem. Res.* **34**, 633–639 (2001).

49. Grogan, G. Cytochromes P450: Exploiting diversity and enabling application as biocatalysts. *Curr. Opin. Chem. Biol.* **15**, 241–248 (2011).

50. Bernhardt, R. Cytochromes P450 as versatile biocatalysts. *J. Biotechnol.* **124**, 128–145 (2006).

51. Wrighton, S. A. & Stevens, J. C. The human hepatic cytochromes p450 involved in drug metabolism. *Crit. Rev. Toxicol.* **22**, 1–21 (1992).

52. Zuber, R., Anzenbacherová, E. & Anzenbacher, P. Cytochromes P450 and experimental models of drug metabolism. *J. Cell. Mol. Med.* **6**, 189–98 (2002).

53. Kroutil, W., Mang, H., Edegger, K. & Faber, K. Recent advances in the biocatalytic reduction of ketones and oxidation of sec-alcohols. *Curr. Opin. Chem. Biol.* **8**, 120–126 (2004).

54. Goldberg, K., Schroer, K., Lütz, S. & Liese, A. Biocatalytic ketone reduction - A powerful tool for the production of chiral alcohols - Part II: Whole-cell reductions. *Appl. Microbiol. Biotechnol.* **76**, 249–255 (2007).

55. Weckbecker, A. & Hummel, W. Cloning, expression, and characterization of an (*R*)-specific alcohol dehydrogenase from *Lactobacillus kefir*. *Biocatal. Biotransformation* **24**, 380–389 (2006).

56. Leipold, F., Hussain, S., Ghislieri, D. & Turner, N. J. Asymmetric reduction of cyclic imines catalyzed by a whole-cell biocatalyst containing an (S)-imine reductase. *ChemCatChem* **5**, 3505–3508 (2013).

57. Mitsukura, K., Suzuki, M., Tada, K., Yoshida, T. & Nagasawa, T. Asymmetric synthesis of chiral cyclic amine from cyclic imine by bacterial whole-cell catalyst of enantioselective imine reductase. *Org. Biomol. Chem.* **8**, 4533–5 (2010).

58. Hussain, S. *et al.* An (R)-imine reductase biocatalyst for the asymmetric reduction of cyclic imines. *ChemCatChem* **7**, 579–583 (2015).

59. Mitsukura, K. *et al.* A NADPH-dependent (S)-imine reductase (SIR) from Streptomyces sp. GF3546 for asymmetric synthesis of optically active amines: purification, characterization, gene cloning, and expression. *Appl. Microbiol. Biotechnol.* **97**, 8079–8086 (2013).

60. Mitsukura, K. *et al.* Purification and Characterization of a Novel (R)-Imine Reductase from Streptomyces sp. GF3587. *Biosci. Biotechnol. Biochem.* **75**, 1778–1782 (2011).

61. Adalbjörnsson, B. V. *et al.* Biocatalysis with thermostable enzymes: Structure and properties of a thermophilic ’ene’-reductase related to old yellow enzyme. *ChemBioChem* **11**, 197–207 (2010).

62. Toogood, H. S. & Scrutton, N. S. New developments in 'ene'-reductase catalysed biological hydrogenations. *Curr. Opin. Chem. Biol.* **19**, 107–115 (2014).

63. Pietruszka, J. & Schölzel, M. Ene reductase-catalysed synthesis of (R)-profen derivatives. *Adv. Synth. Catal.* **354**, 751–756 (2012).

64. Mangan, D., Miskelly, I. & Moody, T. S. A three-enzyme system involving an ene-reductase for generating valuable chiral building blocks. *Adv. Synth. Catal.* **354**, 2185–2190 (2012).

65. Fu, Y., Hoelsch, K. & Weuster-Botz, D. A novel ene-reductase from Synechococcus sp. PCC 7942 for the asymmetric reduction of alkenes. *Process Biochem.* **47**, 1988–1997 (2012).

66. Wong, C.-H. & Whitesides, G. M. Enzyme-catalyzed organic synthesis: NAD(P)H cofactor regeneration by using glucose-6-phosphate and the glucose-5-phosphate dehydrogenase from Leuconostoc mesenteroides. *J. Am. Chem. Soc.* **103**, 4890–4899 (1981).

67. Duine, J. A., Frank, J. & van Zeeland, J. K. Glucose dehydrogenase from Acinetobacter calcoaceticus. *FEBS Lett.* **108**, 3–6 (1979).

68. Zhou, S., Shanmugam, K. T. & Ingram, L. O. Functional Replacement of the Escherichia coli D - (𝔵) -Lactate Dehydrogenase Gene (ldhA) with the L - (𝔰) - Lactate Dehydrogenase Gene (ldhL) from Pediococcus acidilactici †. *Society* **69**, 2237–2244 (2003).

69. Adam, W., Lazarus, M., Saha-M??ller, C. R. & Schreier, P. Quantitative transformation of racemic 2-hydroxy acids into (R)-2-hydroxy acids by

enantioselective oxidation with glycolate oxidase and subsequent reduction of 2-keto acids with D-lactate dehydrogenase. *Tetrahedron Asymmetry* **9**, 351–355 (1998).

70. Liu, W. & Wang, P. Cofactor regeneration for sustainable enzymatic biosynthesis. *Biotechnol. Adv.* **25**, 369–384 (2007).

71. Van Der Donk, W. A. & Zhao, H. Recent developments in pyridine nucleotide regeneration. *Curr. Opin. Biotechnol.* **14**, 421–426 (2003).

72. Zhao, H. & Van Der Donk, W. A. Regeneration of cofactors for use in biocatalysis. *Curr. Opin. Biotechnol.* **14**, 583–589 (2003).

73. Chenault, H. K., Simon, E. S. & Whitesides, G. M. Cofactor Regeneration for Enzyme-Catalysed Synthesis. *Biotechnol. Genet. Eng. Rev.* **6**, 221–270 (1988).

74. Kameda, A. *et al.* A novel ATP regeneration system using polyphosphate-AMP phosohotransferase and polyphosphate kinase. *J. Biosci. Bioeng.* **91**, 557–563 (2001).

75. Wong, C. H., Wang, R. & Ichikawa, Y. Regeneration of sugar nucleotide for enzymic oligosaccharide synthesis: use of Gal-1-phosphate uridyltransferase in the regeneration of UDP-galactose, UDP-2-deoxygalactose, and UDP-galactosamine. *J. Org. Chem.* **57**, 4343–4344 (1992).

76. Ichikawa, Y., Wang, R. & Wong, C. H. Regeneration of sugar nucleotide for enzymatic oligosaccharide synthesis. *Methods Enzymol.* **247**, 107–127 (1994).

77. Xu, Z., Jing, K., Liu, Y. & Cen, P. High-level expression of recombinant glucose dehydrogenase and its application in NADPH regeneration. *J. Ind. Microbiol. Biotechnol.* **34**, 83–90 (2007).

78. Ichinose, H., Kamiya, N. & Goto, M. Enzymatic redox cofactor regeneration in organic media: Functionalization and application of glycerol dehydrogenase and soluble transhydrogenase in reverse micelles. *Biotechnol. Prog.* **21**, 1192–1197 (2005).

79. Shaked, Z. & Whitesides, G. Enzyme-catalyzed organic synthesis: NADH regeneration by using formate dehydrogenase. *J. Am. Chem. Soc.* **102**, 7104–7105 (1980).

80. Hummel, W. & Kula, M.-R. Dehydrogenases in the Synthesis of Chiral Compounds. *Eur. J. Biochem.* **184**, 1–13 (1989).

81. Mutti, F. G., Breuer, M. & Turner, N. J. Re s ear ch | r e p o r t s. **224015**, (2015).

82. Gao, C. *et al.* Production of (3S)-acetoin from diacetyl by using stereoselective NADPH-dependent carbonyl reductase and glucose dehydrogenase. *Bioresour. Technol.* **137**, 111–115 (2013).

83. Kreuter, J. Nanoparticles and microparticles for drug and vaccine delivery. *J. Anat.* **189 (Pt 3**, 503–505 (1996).

84. Johannes, T. W., Woodyer, R. D. & Zhao, H. Directed Evolution of a Thermostable Phosphite Dehydrogenase for NAD (P) H Regeneration. *Society* **71**, 5728–5734 (2005).

85. McLachlan, M. J., Johannes, T. W. & Zhao, H. Further improvement of phosphite dehydrogenase thermostability by saturation mutagenesis. *Biotechnol. Bioeng.* **99**, 268–274 (2008).

86. Mertens, R., Greiner, L., Van Den Ban, E. C. D., Haaker, H. B. C. M. & Liese, A. Practical applications of hydrogenase I from Pyrococcus furiosus for NADPH generation and regeneration. *J. Mol. Catal. B Enzym.* **24**–**25**, 39–52 (2003).

87. Bryant, F. O. & Adams, M. W. W. Characterization of Hydrogenase from the Hyperthermophilic Arhaebacterium, Pyrococcus furiosus. *J. Biol. Chem.* **264**, 5070–5079 (1989).

88. Ma, K., Schicho, R. N., Kelly, R. M. & Adams, M. W. Hydrogenase of the hyperthermophile Pyrococcus furiosus is an elemental sulfur reductase or sulfhydrogenase: evidence for a sulfur-reducing hydrogenase ancestor. *Proc. Natl. Acad. Sci. U. S. A.* **90**, 5341–4 (1993).

89. Ma, K. & Adams, M. W. W. Zinc-Containing Alcohol Dehydrogenase from the Hyperthermophilic Archaeon Pyrococcus furiosus An Unusual Oxygen-Sensitive , Iron- and Zinc-Containing Alcohol Dehydrogenase from the Hyperthermophilic Archaeon Pyrococcus furiosus. **181**, 1163–1170 (1999).

90. Lonsdale, T. H. *et al.* H2-driven biotransformation of n-octane to 1-octanol by a recombinant Pseudomonas putida strain co-synthesizing an O2-tolerant hydrogenase and a P450 monooxygenase. *Chem. Commun.* **51**, 16173–16175 (2015).

91. Reeve, H. a., Lauterbach, L., Ash, P. a., Lenz, O. & Vincent, K. a. A modular system for regeneration of NADcofactors using graphite particles modified with hydrogenase and diaphorase moieties. *Chem. Commun.* **48**, 1589–1591 (2012).

92. Lauterbach, L., Lenz, O. & Vincent, K. A. H2-driven cofactor regeneration with NAD(P)+-reducing hydrogenases. *FEBS J.* **280**, 3058–3068 (2013).

93. Reeve, H. A. *et al.* Enzymes as modular catalysts for redox half reactions in H2-powered chemical synthesis: from biology to technology. *Biochem. J.* **in press**, 215–230 (2016).

94. Reeve, H. A., Lauterbach, L., Lenz, O. & Vincent, K. A. Enzyme-Modified Particles for Selective Biocatalytic Hydrogenation by Hydrogen-Driven NADH Recycling. *ChemCatChem* **7**, 3480–3487 (2015).

95. Lauterbach, L., Idris, Z., Vincent, K. a. & Lenz, O. Catalytic Properties of the Isolated Diaphorase Fragment of the NAD+-Reducing [NiFe]-Hydrogenase from Ralstonia eutropha. *PLoS One* **6**, e25939 (2011).

96. Fontecilla-camps, J. C., Volbeda, A., Cavazza, C., Nicolet, Y. & Fourier, J. Structure / Function Relationships of [NiFe] - and [FeFe] -Hydrogenases. (2007).

97. Berggren, G. *et al.* Biomimetic assembly and activation of [FeFe]-hydrogenases. *Nature* **499**, 66–69 (2013).

98. Burgdorf, T. *et al.* [NiFe]-hydrogenases of Ralstonia eutropha H16: Modular enzymes for oxygen-tolerant biological hydrogen oxidation. *J. Mol. Microbiol. Biotechnol.* **10**, 181–196 (2006).

99. Lukey, M. J. *et al.* How Escherichia coli is equipped to oxidize hydrogen under different redox conditions. *J. Biol. Chem.* **285**, 3928–3938 (2010).

100. Burgdorf, T., Burgdorf, T., Lacey, A. L. De & Lacey, A. L. De. Functional Analysis by Site-Directed Mutagenesis of the NAD. *J. Bacteriol.* **184**, 6280–6288 (2002).

101. Blair, P., Oda, T., Green, D., Silver, D. & Hackenbrock, C. R. Studies on the Electron Transfer System. LIV. Isolation of the Unit of Electron Transfer*. *Biochemistry* **2**, 756–64 (1963).

102. Matsushita, K., Ohnishi, T. & Kaback, H. R. NADH-ubiquinone oxidoreductases of the Escherichia coli aerobic respiratory chain. *Biochemistry* **26**, 7732–7737 (1987).

103. Brandt, U. Energy converting NADH:quinone oxidoreductase (complex I). *Annu. Rev. Biochem.* **75**, 69–92 (2006).

104. Rich, P. R. The molecular machinery of Keilin's respiratory chain. *Biochem. Soc. Trans.* **31**, 1095–1105 (2003).

105. Berrisford, J. M., Baradaran, R. & Sazanov, L. A. Biochimica et Biophysica Acta Structure of bacterial respiratory complex I ☆. *BBA - Bioenerg.* **1857**, 892–901 (2016).

106. Efremov, R. G. & Sazanov, L. A. Structure of the membrane domain of respiratory complex I. supplementary information. *Nature* **476**, 414–20 (2011).

107. Baradaran, R., Berrisford, J. M., Minhas, G. S. & Sazanov, L. a. Crystal structure of the entire respiratory complex I. *Nature* **494**, 443–448 (2013).

108. Zickermann, V. *et al.* Architecture of complex I and its implications for electron transfer and proton pumping. *Biochim. Biophys. Acta - Bioenerg.* **1787**, 574–583 (2009).

109. Auriol, C., Bestel-Corre, G., Claude, J.-B., Soucaille, P. & Meynial-Salles, I. Stress-induced evolution of Escherichia coli points to original concepts in respiratory cofactor selectivity. *Proc. Natl. Acad. Sci. U. S. A.* **108**, 1278–1283 (2011).

110. Morina, K. *et al.* Engineering the respiratory complex I to energy-converting NADPH:Ubiquinone oxidoreductase. *J. Biol. Chem.* **286**, 34627–34634 (2011).

111. Boonstra, B., French, C. E., Wainwright, I., Bruce, N. C. & Wainwright, I. a N. The udhA Gene of Escherichia coli Encodes a Soluble Pyridine Nucleotide Transhydrogenase The udhA Gene of Escherichia coli Encodes a Soluble Pyridine Nucleotide Transhydrogenase. **181**, 1030–1034 (1999).

112. Sauer, U., Canonaco, F., Heri, S., Perrenoud, A. & Fischer, E. The Soluble and Membrane-bound Transhydrogenases UdhA and PntAB Have Divergent Functions in NADPH Metabolism of Escherichia coli. *J. Biol. Chem.* **279**, 6613–6619 (2004).

113. Cao, Z., Song, P., Xu, Q., Su, R. & Zhu, G. Overexpression and biochemical characterization of soluble pyridine nucleotide transhydrogenase from Escherichia coli. *FEMS Microbiol. Lett.* **320**, 9–14 (2011).

114. Mouri, T., Shimizu, T., Kamiya, N., Goto, M. & Ichinose, H. Design of a cytochrome P450BM3 reaction system linked by two-step cofactor regeneration catalyzed by a soluble transhydrogenase and glycerol dehydrogenase. *Biotechnol. Prog.* **25**, 1372–1378 (2009).

115. Boonstra, B., Rathbone, D. A., French, C. E., Walker, E. H. & Bruce, N. C. Cofactor regeneration by a soluble pyridine nucleotide transhydrogenase for biological production of hydromorphone. *Appl. Environ. Microbiol.* **66**, 5161–5166 (2000).

116. Reeve, H. a., Lauterbach, L., Ash, P. a., Lenz, O. & Vincent, K. a. A modular system for regeneration of NAD cofactors using graphite particles modified with hydrogenase and diaphorase moieties. *Chem. Commun.* **48**, 1589 (2012).

117. Saiki, R. K. *et al.* Primer-directed enzymatic amplification of DNA with a thermostable DNA polymerase. *Science* **239**, 487–491 (1988).

118. Karaoglanoff, V. Z. Über Oxydations- und Reduktionsvorgänge bei der Elektrolyse von Eisensalzlösungen. *Zeitschrift für Elektrotechnik und Elektrochemie* **12**, 5–16 (1906).

119. Ramette, R. W. Outmoded terminology: The normal hydrogen electrode. *J. Chem. Educ.* **64**, 885 (1987).

120. BANUS, M. G. A DESIGN FOR A SATURATED CALOMEL ELECTRODE. *Science (80-.).* **93**, 601–602 (1941).

121. Hill, H. A. Novel Method for the Investigation of the Electrochemistry of Metalloproteins : Cytochrome c. *Chem. Commun.* 771–772 (1977).

122. Blanford, C. F. The birth of protein electrochemistry. *Chem. Commun.* **49**, 11130 (2013).

123. Banks, C. E. & Compton, R. G. Exploring the electrocatalytic sites of carbon nanotubes for NADH detection: an edge plane pyrolytic graphite electrode study. *Analyst* **130**, 1232 (2005).

124. Nicholson, R. S. & Shain, I. Stationary Electrode Polarography. *Anal. Chem.* **36**, 707 (1964).

125. Barsukov, V. Z., Khomenko, V. G., Chivikov, S. V & Barsukov, I. V. On the faradaic and non-faradaic mechanisms of electrochemical processes in conducting polymers and some other reversible systems with solid-phase reagents. *Electrochim. Actalectrochimica Acta* **46**, 4083–4094 (2001).

126. Mayerhöfer, T. G., Mutschke, H. & Popp, J. Employing Theories Far beyond Their Limits-The Case of the (Boguer-) Beer-Lambert Law. *ChemPhysChem* **17**, 1948–1955 (2016).

127. Schug, K. A. *et al.* Vacuum Ultraviolet Detector for Gas Chromatography. *Anal. Chem.* **86**, 8329–8335 (2014).

128. Karger, B. L. HPLC : Early and Recent Perspectives. *J. Chem. Educ.* **74**, 45–48 (1997).

129. Chen, W. W., Niepel, M. & Sorger, P. K. Classic and contemporary approaches to modeling biochemical reactions. *Genes Dev.* **24**, 1861–1875 (2010).

130. Lineweaver, H. & Burk, D. The Determination of Enzyme Dissociation Constants. *J. Am. Chem. Soc.* **56**, 658–666 (1934).

131. Charles, B. Y. & Hanes, S. AMYLASE OF GERMINATED BARLEY . *Biochem. J.* **26**, 1406–1421 (1932).

132. Cleland, W. W. THE KINETICS OF ENZY\IE-CATALYZED REACTIONS WITH TWO OR MORE SUBSTRATES OR PRODUCTS II. INHIBITION: NOMENCLATURE AND THEORY’. *Biochim. Biophys. Acta - Bioenerg.* **67**, 173–187 (1962).

133. Pandelia, M. E., Ogata, H., Currell, L. J., Flores, M. & Lubitz, W. Inhibition of the [NiFe] hydrogenase from Desulfovibrio vulgaris Miyazaki F by carbon monoxide: An FTIR and EPR spectroscopic study. *Biochim. Biophys. Acta - Bioenerg.* **1797**, 304–313 (2010).

134. Road, M. Biophysica acta bba 66742 t h e use of d i x o n plots to study enzyme i n h i b i t i o n 25i. *biochemica* **289**, 251–253 (1972).

135. Cornish-bowden, B. A. The Use of the Direct Linear Plot for. *Biochem. J.* 305–312 (1975).

136. Idris, Z. No Title. (University of oxford, 2012).

137. Scheller, P. N. *et al.* Enzyme Toolbox: Novel Enantiocomplementary Imine Reductases. *ChemBioChem* **15**, 2201–2204 (2014).

138. Wetzl, D. *et al.* Expanding the Imine Reductase Toolbox by Exploring the Bacterial Protein-Sequence Space. *ChemBioChem* (2015). doi:10.1002/cbic.201500218

139. Pérez-Venegas, M. & Juaristi, E. Mechanoenzymatic resolution of racemic chiral amines, a green technique for the synthesis of pharmaceutical building blocks. *Tetrahedron* **74**, 6453–6458 (2018).

140. Nugent, T. C. & El-Shazly, M. Chiral amine synthesis - Recent developments and trends for enamide reduction, reductive amination, and imine reduction. *Adv. Synth. Catal.* **352**, 753–819 (2010).

141. Huber, T. *et al.* Direct Reductive Amination of Ketones: Structure and Activity of S -Selective Imine Reductases from Streptomyces. *ChemCatChem* **6**, 2248–2252 (2014).

142. Gonzalez, F. J. & Gelboin, H. V. Human cytochromes P450: evolution and cDNA-directed expression. *Environ. Health Perspect.* **98**, 81–85 (1992).

143. P.B. Danielson, B. S. P. The Cytochrome P450 Superfamily: Biochemistry, Evolution and Drug Metabolism in Humans. *Curr. Drug Metab.* **3**, 561–597 (2002).

144. Manikandan, P. & Nagini, S. Cytochrome P450 Structure, Function and Clinical Significance: A Review. *Curr. Drug Targets* **19**, (2018).

145. Kang, J.-Y. *et al.* Characterization of diverse natural variants of CYP102A1 found within a species of Bacillus megaterium. *AMB Express* **1**, 1 (2011).

146. Warman, A. J. *et al.* Flavocytochrome P450 BM3: an update on structure and mechanism of a biotechnologically important enzyme. *Biochem. Soc. Trans.* **33**, 747–753 (2005).